

THE EFFECT OF SURFACE CONDITIONS
ON NUCLEATE POOL BOILING HEAT
TRANSFER TO SODIUM

by

PAUL JAMES MARTO

B.S., University of Notre Dame
(1960)

S.M., Massachusetts Institute of Technology
(1962)

SUBMITTED IN PARTIAL FULFILLMENT OF THE
REQUIREMENTS FOR THE DEGREE OF
DOCTOR OF SCIENCE

at the

MASSACHUSETTS INSTITUTE OF TECHNOLOGY

February, 1965

Signature of Author _____
Department of nuclear engineering, -
January 11, 1965

Certified by _____
Thesis Supervisor

Accepted by _____
Chairman, Departmental Committee on Graduate Students

THE EFFECT OF SURFACE CONDITIONS
ON NUCLEATE POOL BOILING HEAT TRANSFER TO SODIUM

by

PAUL JAMES MARTO

Submitted to the Department of Nuclear Engineering on January 11, 1965, in partial fulfillment of the requirements for the degree of Doctor of Science.

ABSTRACT

A simplified theoretical model for bubble nucleation stability has been proposed, and an approximate stability criterion has been developed. This criterion contains both fluid and surface properties, and it predicts that nucleation for sodium should be unstable.

Commercial grade sodium was boiled from a horizontal disc at pressures of 65 mm, 200 mm and 400 mm Hg absolute, with sodium temperatures ranging from 1200°F to 1500°F. Heat fluxes as high as 236,000 BTU/hr.ft.² were attained. Boiler surface finishes ranged from highly polished mirror finishes to coarse, porous coatings.

By following a prescribed cleaning and filling procedure, nucleate boiling results were generally reproducible for a given type surface. The effect of roughness as well as any aging and hysteresis effects were experimentally determined. Incipient nucleate boiling results are discussed as well as the effect of pressure and pool depth on the nucleate boiling curve.

The effect of surface material, chemical treatment, heat flux and cavity geometry on nucleation stability was measured, and the experimental results agreed with the predictions of the proposed stability model.

Thesis Supervisor: Warren M. Rohsenow

Title: Professor of Mechanical Engineering

ACKNOWLEDGEMENT

The author wishes to express his sincere gratitude to his thesis advisor, Professor Warren M. Rohsenow for initiating this research work and for making numerous valuable suggestions throughout this thesis.

Many thanks are also due to Professor Peter Griffith for his thought-provoking discussions and for his reviewings and suggestions for changes in the manuscript.

The author is deeply indebted to the many people who helped carry out this research. Mr. R.E. Helms of Oak Ridge National Laboratory, Mr. R.C. Noyes of Atomics International, and Dr. A.F. Sarofim of M.I.T. were particularly helpful during the initial design of the equipment. Most of the machining was done at Laboratory Associates, Belmont, Massachusetts. Mr. J.B. Keefe and the machine shop of the M.I.T. Research Laboratory of Electronics machined the test surfaces and fabricated the doubly re-entrant type cavities. Mr. F. Johnson and all the other personnel at the M.I.T. Engineering Projects Laboratory and Heat Transfer Laboratory assisted many times in the assembly, operation and repair of the equipment.

Financial aid for this project was received in part from the National Science Foundation under grant GP 1304, from the National Aeronautics and Space Administration under grant NSG 496

and from the Atomic Energy Commission under contract No. AT(30-1)-3357. The author is also grateful to the General Electric Foundation for providing a fellowship during the initial stages of this work.

Miss Sheila Scanlon typed out the final manuscript and Mrs. Nicki Suo handled all the many details of this project.

Finally, a special note of thanks goes to the author's wife, Ginger, for proof-reading the final manuscript, and for her continuous patience and encouragement during this effort.

TABLE OF CONTENTS

	<u>Page</u>
ABSTRACT	ii
ACKNOWLEDGEMENT	iii
LIST OF FIGURES	vii
1. INTRODUCTION	
1.1 Engineering Applications of Boiling Alkali Metals	1
1.2 Previous Alkali Metal Pool Boiling Investigations	2
1.3 Surface Variables Affecting Boiling Results	7
1.4 Objective of Research	9
2. THEORY OF BUBBLE NUCLEATION STABILITY	
2.1 Simplified Stability Model	12
2.2 Stability Criterion	13
2.3 Variables which Affect Nucleation Stability	23
3. DESCRIPTION OF EQUIPMENT	
3.1 Boiler-Condenser	26
3.2 Main Heater	30
3.3 High Vacuum System	33
3.4 Helium Cover Gas Line	34
3.5 Sodium Fill System	35
3.6 Containment and Safety Equipment	36
3.7 Safety Controls	37
3.8 Instrumentation	39

4.	EXPERIMENTAL PROCEDURE	
4.1	Preparation of Test Surfaces	42
4.2	Preparation of Equipment	50
4.3	Operational Details	54
4.4	Treatment of Data	57
5.	RESULTS AND DISCUSSION	
5.1	Characteristics of Sodium Nucleate Boiling	61
5.2	Reproducibility of Results	69
5.3	Effect of Roughness	70
5.4	Boiling Hysteresis and Aging Effects	72
5.5	Stability during Nucleation	73
5.6	Effect of Pool Depth	79
6.	SUMMARY WITH RECOMMENDATIONS	
6.1	Nucleate Boiling of Sodium	81
6.2	Recommendations	84
	NOMENCLATURE	85
	BIBLIOGRAPHY	88
	APPENDICES:	
A.	Solution of the Approximate Energy Equation in the Liquid, Eq. (5)	92
B.	Analysis to Estimate the Wall Temperature Response during Nucleation	97
C.	Tabulation of Results	103
D.	Sample Calculation with Error Analysis	118
E.	Sodium Technology	123
	BIOGRAPHICAL NOTE	168

LIST OF FIGURES

- Fig. 1 Diagram of Proposed Nucleation Cycle Showing Interface Position and Liquid Temperature Distribution.
- Fig. 2 Idealized Cavity Showing Interface Force Balance.
- Fig. 3 Doubly Re-Entrant Type Cavity.
- Fig. 4 Schematic Diagram of Apparatus.
- Fig. 5 Partial Assembly of Equipment.
- Fig. 6 Heater and Boiler Sectional Drawing.
- Fig. 7 Condenser Sectional Drawing.
- Fig. 8 General View of Heat Transfer Facility.
- Fig. 9 Exploded View of Boiler-Condenser Section.
- Fig. 10 Details of Boiler.
- Fig. 11 Overhead View of Main Heater.
- Fig. 12 Electrical Wiring Diagram for Control System.
- Fig. 13 Overhead View of Four Test Surfaces.
- Fig. 14 Photomicrographs of Cross-Sections of Porous Samples (100X).
- Fig. 15 Photomicrographs of Cross-Sections of Artificial Cavities (75X).
- Fig. 16 Coincidence of Noise Level and Wall Temperature during Unstable Nucleate Boiling of Sodium at $Q/A = 61,700 \text{ BTU/hr.ft.}^2$.
- Fig. 17 Coincidence of Noise Level and Wall Temperature during Unstable Nucleate Boiling of Sodium at $Q/A = 87,600 \text{ BTU/hr.ft.}^2$.
- Fig. 18 Coincidence of Noise Level and Wall Temperature during Stable Nucleate Boiling of Sodium at $Q/A = 135,000 \text{ BTU/hr.ft.}^2$.

- Fig. 19 Enlarged Photograph Showing Coincidence of Noise Level and Wall Temperature During "Bumping" (2.5X).
- Fig. 20 Sample Data with Experimental Error Limits Showing Data of Noyes for Comparison.
- Fig. 21 Initiation of Bubble Growth for Water and Sodium.
- Fig. 22 Effect of Pressure on Nucleate Pool Boiling of Sodium.
- Fig. 23 Reproducibility of Nucleate Boiling Results.
- Fig. 24 Reproducibility of Nucleate Boiling Results.
- Fig. 25 Reproducibility of Nucleate Boiling Results.
- Fig. 26 Effect of Roughness on Nucleate Pool Boiling of Sodium.
- Fig. 27 Effect of Roughness on Nucleate Pool Boiling of Sodium.
- Fig. 28 Effect of Aging on the Nucleate Boiling Curve of Sodium.
- Fig. 29 Effect of Aging on the Nucleate Boiling Curve of Sodium.
- Fig. 30 Effect of Aging on the Nucleate Boiling Curve of Sodium.
- Fig. 31 Temperature Trace of Thermocouple No. 4 for Stainless Steel 316, LAP A Surface.
- Fig. 32 Temperature Trace of Thermocouple No. 6 for "A" Nickel, Mirror Surface with Artificial Porous Welds.
- Fig. 33 Temperature Trace of Thermocouple No. 6 for "A" Nickel, Mirror Surface with no Internal Welds.
- Fig. 34 Temperature Trace of Thermocouple No. 6 for "A" Nickel, Mirror Surface with no Internal Welds, plus Ten Artificial Cylindrical Cavities.
- Fig. 35 Effect of Material on Nucleate Boiling Stability of Sodium.
- Fig. 36 Effect of Chemical Treatment on Nucleate Boiling Stability of Sodium.

- Fig. 37 Effect of Artificial Cylindrical Cavities, .004 in. Diameter, on Nucleate Boiling Stability of Sodium.
- Fig. 38 Effect of Porous Coating on Nucleate Boiling Stability of Sodium.
- Fig. 39 Effect of Pool Depth on the Nucleate Boiling Curve of Sodium.
- Fig. 40 Comprehensive Plot of Sodium Heat Transfer Data at an Average Pressure of 65 mm Hg.
- Fig. 41 Schematic Representation of the Local Surface Heat Flux and Local Surface Temperature during Bubble Growth from a Cavity.
- Fig. 42 Photographs Showing Sodium Leakage.

1. INTRODUCTION

1.1 Engineering Applications of Boiling Alkali Metals

As part of the Atomic Energy Commission's long range power reactor program, much emphasis is being placed on thermal reactors like HNPF and on fast breeder reactors similar to EBR II, FERMI and LAMPRE. These reactors all use sodium as a coolant.

Although boiling of sodium will not occur during normal operation of these reactors, as part of their overall safety analysis, consideration must be given to nucleation and net vapor generation during possible accidents like loss of coolant flow, or loss of reactor heat sink. In the final hazards report of HNPF (1)*, it is indicated that even when the reactor is shut down, the loss of operation of the steam generators may lead to sodium boiling in the core, and thus to a possible over-pressurization of the primary system with sodium vapor. Also, for an uncontrolled reactor excursion, sodium boiling plays a key role in the sequence of events leading to the ultimate shutdown of the reactor by core meltdown.

* The underlined numbers in parentheses refer to the Bibliography.

Compact nuclear reactors with alkali metal working fluids are also being considered for space auxiliary power systems, where boiling may take place during normal operation in an advanced Rankine cycle. Fuel cells using a potassium-mercury amalgam as the anode and mercury as the cathode have also been designed (2). During operation the mercury stream receives potassium from the amalgam stream through an ionic reaction, and in a closed cycle, the "contaminated" mercury stream must therefore be re-purified by a fractional distillation process. Finally, boiling alkali metals may occur as working fluids in MHD generators, as coolants in rocket nozzles, and as temperature control devices for high temperature chemical reactions.

1.2 Previous Alkali Metal Pool Boiling Investigations

Alkali metal pool boiling data is quite sparse. The small amount of available data scatters considerably, especially for heat fluxes less than $100,000 \text{ BTU/hr.ft.}^2$, so that good engineering designs of the above-mentioned systems are very difficult.

Lyon, Foust and Katz (3) were the first investigators in the United States to perform saturated pool boiling experiments with liquid metals. They boiled mercury, mercury with additives, sodium, sodium-potassium alloy (57 wt.%K) and cadmium using a horizontal stainless steel 316 cylindrical

heating section, 3/4 in. O.D. by 5 in. long. A silicon carbide electrical resistance element, inserted inside the tubular test section supplied a heat source up to 130,000 BTU/hr.ft.². The boiler surface temperature was determined by oxyacetylene welding chromel-alumel type thermocouples into grooves machined in the boiler wall. Their results for sodium and NaK at 1 atm. pressure gave nucleate boiling heat transfer coefficients as high as 15,000 BTU/hr.ft.²°F with wall superheats less than 10°F. The data for NaK was quite scattered, while the sodium data, plotted as the heat flux versus $(T_w - T_{sat})$, exhibited a very steep slope. They noted large temperature fluctuations in the low heat flux region when boiling was barely taking place, and attributed the scatter in their results to the difficulty in measuring temperatures while this phenomenon was occurring.

Madsen and Bonilla (4) boiled sodium-potassium alloy (44 wt.%K) from a horizontal, low carbon nickel plate, 3 in. diameter. Heat fluxes as high as 135,000 BTU/hr.ft.² were attained using molybdenum resistance wire wound around and electrically insulated from molybdenum fins brazed to the bottom of the boiler plate. They determined the surface temperature by measuring the temperature distribution across the boiler plate using three chromel-alumel thermocouples, and by

extrapolating this distribution to the boiler surface. Their results differed markedly from Lyon's results for NaK, with their superheats being about 5 times as large as Lyon's. They suggested that large temperature differences measured within their NaK pool, due to poor natural convection currents, may have caused this discrepancy. Madsen and Bonilla also reported temperature fluctuations in the boiler surface which were characterized by a sudden dip in wall temperature followed by a gradual recovery. At low heat fluxes the sudden temperature drops were frequently accompanied by audible "bumps".

Noyes (5) has obtained pool boiling sodium data with a horizontal cylindrical heating section, 3/8 in. O.D. by 5 in. long. Two types of heaters were fabricated. One employed molybdenum as the resistance heating element and aluminum oxide as the electrical insulation; the other employed graphite for heating and boron nitride for insulating. Sheath materials were either molybdenum-0.5% titanium or stainless steel 347. Heat fluxes as high as 840,000 BTU/hr.ft.² were attained. Sheathed chromel-alumel thermocouples were fitted between the boiler wall and the electrical insulation surrounding the heater, and the boiler surface temperature was determined by subtracting the wall temperature drop from the measured thermocouple reading. Noyes mentioned that "all data obtained at

heat fluxes below 100,000 BTU/hr.ft.² exhibited a great deal of scatter", and he attributed this scatter to poor thermal contact between the sheath wall and the thermocouple at low heat fluxes. A more recent report by Noyes (6) gave somewhat better results in that the mean nucleate boiling heat transfer coefficient increased as the pressure increased. He also showed that the heat transfer coefficient for the stainless steel boiler was higher than for the molybdenum boiler. Large temperature fluctuations were also observed. Variations in these temperature traces were attributed not only to changes in heat flux and pressure but also to different surface finishes and wetting properties.

Brooks (7) boiled potassium from a 3 in. diameter horizontal plate, of low carbon nickel, using a heater similar to Madsen and Bonilla's. The heat flux was varied up to 115,000 BTU/hr.ft.². Three chromel-alumel thermocouples were placed about 0.160 in. away from the boiling surface, and the surface temperature was determined by subtracting the temperature drop across the boiler from the average reading of these thermocouples. Comparison of his data to existing pool boiling correlations showed the data to have a steeper slope. The conclusion was drawn that the effect of roughness and surface metal must be incorporated into correlations before liquid metal boiling predictions can be made with confidence. No mention

was made of temperature fluctuations.

More recently, Colver (8) boiled potassium from a horizontal tube, 3/8 in. O.D. by 1 1/4 in. long, made of Haynes 25. Heat fluxes as high as 543,000 BTU/hr.ft.² were reached using a graphite rod as the heating element and a boron nitride sleeve as the insulator. Three chromel-alumel thermocouples were brazed into grooves machined in the sheath wall. Boiling surface temperatures were determined by averaging the thermocouple readings in the tube wall and extrapolating to the surface. His results showed a great deal of scatter, and large hysteresis effects were noted depending on whether the data was recorded for an increasing or decreasing heat flux cycle. Large temperature fluctuations were also observed, with more violent traces occurring below heat fluxes of 200,000 BTU/hr.ft.².

In summarizing, it is clear first of all, that liquid alkali metal pool boiling data is difficult to obtain, and secondly, previous liquid alkali metal boiling results are inconsistent. Part of the explanation for this lies in the fact that with these boiling systems high temperature measurements are necessary, large temperature fluctuations due to boiling instabilities may occur, and visualization of the test section is impossible.

1.3 Surface Variables Affecting Boiling Results

In addition to the different measuring techniques and the different geometries used in all the previously mentioned investigations, and in addition to the inherent experimental problems associated with alkali metal boiling, it is believed that inconsistencies in the previous boiling data are due to poor control of the surface variables of the test section. Thus, inconsistencies in surface physical roughness, surface material and surface treatment (including surface preparation and chemical cleaning) may alter alkali metal nucleate boiling results. The effect of these surface conditions on nucleate boiling results for ordinary fluids has received much experimental attention.

Effect of Roughness

Corty and Foust (9) were among the first to extensively study the effect of surface roughness on nucleate boiling heat transfer coefficients. They boiled Freon 113, diethyl ether and n-pentane off copper and nickel plates for different surface polishes, and found that not only the position of the boiling curve, but also the slope depends on the degree of surface polish. Later, Berenson (10) showed that for boiling of n-pentane off copper, nickel and inconel flat plates, the surface roughness can increase the heat transfer coefficient

by as much as 500%. More recently, Bonilla, Grady and Avery (11) found that by applying sharp parallel scratches onto the boiling surface, heat transfer coefficients for water increased by as much as 88% and for mercury with 0.1% sodium by as much as 116%.

Effect of Surface Material

Since different solid metals have varying grain structures which can alter the size and shape of microscopic cavities on the boiling surface, and also since they have different thermal diffusivities which can alter the frequency of bubble generation, we would expect that surface material would also affect the nucleate pool boiling curve. Both Stock (12) and Berenson (10) have shown that heat transfer coefficients increase by as much as 200% depending on the material used.

Effect of Wetting Characteristics

Other variables which affect the surface energy of a given liquid-solid combination (chemical contamination of the solid in the form of an oxide layer, chemical contamination of the liquid due to additives and impurities, the state of stress of the system, etc.) can alter the wetting characteristics of a boiling fluid and also cause changes in the nucleate boiling curve (13, 14, 15). Averin (16) showed that treating the

boiling surface with oil alters the slope of the nucleate boiling curve for water. Recently, Young and Hummel (17) presented a very interesting paper showing the effect of coating a stainless steel surface with Teflon during pool boiling of water. They found that by introducing Teflon on a roughened surface (which thus prevents water from wetting the cavities), they increased the heat transfer coefficient by a factor of 10.

Since the alkali metals appear to wet all metals at temperatures near their boiling points (18, 19), and since they are so chemically active with most materials, it seems reasonable to assume that surface variables may play a larger role in boiling of alkali metals than in boiling of ordinary fluids.

1.4 Objective of Research

The main purpose of this research program is to establish an experimental procedure for cleaning, evacuating and filling a piece of equipment which will yield reproducible nucleate pool boiling sodium data for a given set of boiler surface conditions.

The effect of surface physical roughness (including artificial cavities), surface material and surface treatment on the nucleate pool boiling curve of sodium will be investigated, as well as aging and hysteresis effects due to the past history of the boiler plate.

Since stability during alkali metal nucleate boiling is very important, resulting in rapid temperature fluctuations which can lead to thermal fatigue of boiler materials, and since stability is inherently associated with the problem of obtaining reproducible nucleate boiling data, then both an analytical and experimental study of nucleation stability will be made with emphasis on which surface variables effect and control this phenomenon.

2. THEORY OF BUBBLE NUCLEATION STABILITY

It is well known that in most experimental equipment, boiling takes place by heterogeneous nucleation (20, 21)-- that is, nucleation from a pre-existing vapor phase trapped within some cavity or crevice.

During nucleation, vapor bubbles form and grow from prescribed sites on the boiling surface, and we call these locations active sites. Those sites which cannot trap vapor within them are called inactive sites. Some cavities may be active for a period of time and then suddenly become inactive. This causes nucleate boiling instability.

For ordinary fluids, bubble nucleation is very stable and consequently little effort has been made in studying this phenomenon. However, for the liquid alkali metals, stability during nucleation is very poor and this problem becomes significant in engineering design (22).

We will therefore investigate the basic physics involved for a particular cavity during nucleation, with the ultimate objective being to establish an approximate stability criterion which contains the proper fluid and surface variables. To accomplish this we examine what happens to the liquid-vapor interface just after a bubble breaks away from a cavity.

2.1 Simplified Stability Model

After bubble departure, we assume that cold liquid at a temperature T_0 rushes down into the cavity mouth. At the same time we assume the surrounding wall of the cavity has cooled to a minimum temperature identical to this cold liquid temperature, T_0 . We also postulate that T_0 is slightly larger than the saturation temperature at the liquid pressure, but less than the saturation temperature at the pressure of the vapor within the cavity, and that it depends on the heat flux per unit area, the wall material, and bubble frequency.

Due to the acceleration of the liquid, the inertia forces may be large. However, after travelling a very short distance into the cavity, because of the small dimensions involved, we assume these inertia forces are damped out and can be neglected.

Because of the curvature of the liquid-vapor interface, the vapor trapped inside the cavity is at a higher pressure than the liquid pressure. Since T_0 is less than the saturation temperature of this vapor, condensation begins to occur. The interface recedes into the cavity, limited by the rate at which the latent heat of vaporization, supplied at the meniscus, can be conducted away by the liquid. As the liquid travels into the cavity it receives heat not only from the condensation of vapor but also by conduction from the cavity walls.

The interface continues to slow down as the temperature of the liquid increases, and at some point when the bulk liquid temperature equals the vapor temperature, condensation will stop, the bubble will begin to grow again, and the cavity will remain active. This nucleation cycle is shown schematically in Fig. 1. If, on the other hand, the bulk liquid temperature never reaches the vapor temperature, all the vapor will continue to condense, leading to complete collapse of the cavity.

The above mechanism is very approximate, containing many inherent assumptions. However, it does establish a physical model which can be analyzed in an attempt to explain nucleation stability.

2.2 Stability Criterion

The analysis is similar to the work of Bankoff (23). We assume for simplicity a right cylindrical cavity and examine the forces acting on the liquid-vapor interface, as shown in Fig. 2, and neglect both inertia and viscous effects.

A force balance on the interface yields

$$p_v - p_l = \frac{2\sigma \cos \theta}{R_c} \quad (1)$$

where θ is the dynamic contact angle, and where it is assumed that the liquid wets the cavity wall (i.e., $\theta < 90^\circ$).

The Clapeyron equation is now employed to give approximately

$$p_v - p_L \approx \frac{\rho_v h_{fg}}{T_{SAT}} (T_m - T_{SAT}) \quad (2)$$

where T_m is the meniscus (or interface) temperature which is assumed equal to the vapor temperature, Fig. 1. Substitution of Eq. (2) into Eq. (1) gives the well-known relation

$$T_m - T_{SAT} = \frac{T_{SAT}}{\rho_v h_{fg}} \left(\frac{2\sigma \cos \theta}{R_c} \right) . \quad (3)$$

The energy equation in the liquid for a plane interface is

$$\rho_L c_L \frac{\partial T_L(\lambda, t)}{\partial t} + \rho_L c_L V(t) \frac{\partial T_L(\lambda, t)}{\partial \lambda} = k_L \frac{\partial^2 T_L(\lambda, t)}{\partial \lambda^2} + Q(t) \quad (4)$$

where λ is the coordinate distance into the liquid, measured from the interface, $V(t)$ is the velocity of the interface, $Q(t)$ is a fictitious volumetric heat source used to include the effect of heat transferred from the cavity walls, and where we have neglected the temperature gradients perpendicular to the cavity axis (similar to the assumption made in analyzing heat conduction in fins) and also viscous dissipation.

It should be realized here that if one includes conduction of heat from the cavity walls, the energy equation necessarily becomes two-dimensional. However, in our approximate analysis,

we assume instead that this effect of the wall is felt directly within the liquid only as a time dependent heat source. This approximation may be questionable for ordinary fluids, but for the alkali metals with their high values of thermal conductivity, it may be reasonable.

The second term on the left-hand side of Eq. (4), representing the effect of interface motion, may be safely omitted, because this convective term acts like a heat source term in Eq. (4) since $V(t)$ is always positive and the temperature gradient is always negative during interface penetration. The presence of a heat source within the liquid would decrease the rate of vapor collapse as shown by Florschuetz and Chao (24), so that neglecting this convective term leads to an increased collapse rate, and a more stringent condition for stability.

The approximate energy equation with initial and boundary conditions is then

$$\frac{\partial T_L(\lambda, t)}{\partial t} = \alpha_L \frac{\partial^2 T_L(\lambda, t)}{\partial \lambda^2} + \frac{Q(t)}{\rho_L c_L} \quad (5)$$

$$\text{at } t = 0: \quad T_L(\lambda, 0) = T_0 \quad (6)$$

$$Q(0) = 0 \quad (7)$$

at $t > 0$:
$$A R_L \left. \frac{\partial T_L(\lambda, t)}{\partial \lambda} \right|_{\lambda=0} = \rho_V h_{fg} \frac{dV}{dt} \quad (8)$$

$$T_L(0, t) = T_m = T_V = \text{constant} \quad (9)$$

$$T_L(\infty, t) = T_w(t) \quad (10)$$

where A is the surface area of the meniscus, and $\frac{dV}{dt}$ is the vapor volume change. Note that the curvature of the interface is neglected in the energy equation, but is utilized in Eqs. (1) and (8). Note also that the previous assumption that the effect of the cavity walls is felt in the liquid as a fictitious volumetric heat source $Q(t)$, in conjunction with the assumed boundary condition given in Eq. (10), leads to a physical model in which the liquid temperature inside the cavity equals the local wall temperature for all points in the liquid far from the interface.

The above problem was analyzed by Fabric (25), and the solution at the interface ($\lambda = 0$), given in Appendix A, is

$$T_m - T_0 = T_w(t) - T_0 + K_L \int_0^t \frac{dX/d\tau}{\sqrt{t-\tau}} d\tau \quad (11)$$

where

$$K_L = \frac{\rho_V h_{fg}}{2 \sqrt{\pi R_L \rho_L c_L}} (1 + \sin \theta) \quad , \text{ and}$$

where $dX/d\tau$ is the interface velocity.

Recent results of Moore and Mesler (26), Bonnet, Macke and Morin (27), and Marcus (28) have shown that the wall temperature near a nucleating site rapidly drops to some minimum value during bubble growth, and then gradually rises during the bubble waiting period (i.e., while interface penetration occurs).

We may estimate the transient response of the wall during interface travel, which is shown in Appendix B, as follows:

$$T_w(t) - T_o = \frac{bQ_o}{\sqrt{\pi R_w \rho_w c_w}} \sqrt{t} \quad (12)$$

where

$$T_o = T_{SAT} + \left[1 - \left(1 + \frac{\epsilon}{2} \right) K \right] (T_m - T_{SAT}) \quad (13)$$

with

$$K = c \left[Q_o \sqrt{f/\alpha_w} \right]^{-a} \frac{Q_o}{R_w}$$

In Eq. (13), ϵ is an empirical coefficient, less than one, which is used to approximate the wall temperature rise during the bubble waiting period. If an arbitrary value of $\epsilon = 0.3$ is chosen and the values of K given in Appendix B are used, then Eq. (13) predicts that T_o is greater than T_{SAT} , but less than T_m for boiling of water, methyl alcohol, liquid nitrogen, or sodium off stainless

steel. This result is consistent with our original assumption in the proposed stability model.

Substituting Eqs. (12) and (13) into Eq. (11), solving for $T_m - T_{SAT}$, and using Eq. (3) in this result, leads to the following integral equation for $\chi(t)$, the interface position

$$A = B\sqrt{t} + C \int_0^t \frac{dx/d\tau}{\sqrt{t-\tau}} d\tau, \quad (14)$$

where

$$A \equiv \left(1 + \frac{\epsilon}{2}\right) K \frac{T_{SAT}}{\rho_v h_{fg}} \frac{2\sigma \cos\theta}{R_c},$$

$$B \equiv \frac{bQ_0}{\sqrt{\pi R_w \rho_w C_w}}, \quad \text{and}$$

$$C \equiv K_L \equiv \frac{\rho_v h_{fg}}{2\sqrt{\pi K_L \rho_L C_L}} (1 + \sin\theta).$$

The solution to Eq. (14) with the initial condition $\chi(0) = 0$ (i.e., we have neglected any penetration into the cavity from inertia forces) is readily found if we take the Laplace transform and solve for $\bar{\chi}(s)$ to get

$$\bar{\chi}(s) = \frac{A}{C\sqrt{\pi} s^{3/2}} - \frac{B}{2Cs^2} \quad (15)$$

Inverting into the time domain gives the desired result

$$\chi(t) = \frac{2}{\pi} \frac{A}{C} \sqrt{t} - \frac{B}{2C} t \quad (16)$$

From the form of Eq. (16) it is clear that $\chi(t)$ goes through a maximum value. Here the interface must stop, and reverse its direction. At this position χ^* , $v(t) = \frac{d\chi}{dt} = 0$ corresponding to $t = t^*$. Applying this condition to Eq. (16) gives

$$t^* = \left(\frac{2A}{\pi B} \right)^2 \quad (17)$$

so that

$$\chi^* = \chi(t^*) = \frac{2}{\pi^2} \frac{A^2}{BC} \quad (18)$$

Equation (18) gives the maximum penetration of the interface into the cavity during nucleation. We now define a condensate thickness, l , as that thickness of liquid that would result if all the vapor initially inside a cavity of length L and area A_c were to condense isothermally. Thus

$$A_c \rho_v L = A_c \rho_l l, \text{ or}$$

$$l = \left(\frac{\rho_v}{\rho_l} \right) L \quad (19)$$

For a cavity to remain active (with $\theta < 90^\circ$), it is clear that χ^* must be less than l , otherwise all the vapor will condense and the cavity will be deactivated. For stability, therefore, we must have

$$n^* = \frac{\chi^*}{l} < 1 \quad (20)$$

Upon substituting Eq. (18) (with the definitions of A, B and C), and also Eq. (19) into Eq. (20), we have

$$\frac{4}{\pi} \left(\frac{\rho_L}{\rho_V} \right) \left(\frac{T_{SAT}^2 \sqrt{R_L \rho_L C_L}}{\rho_V^3 \lambda g^3} \right) \left(\frac{2\sigma}{JR} \right)^2 \left(\frac{(1 + \frac{\epsilon}{2})^2 C^2}{b Q_0^{2a-1} f^a \alpha_w^{1-a} \sqrt{R_w \rho_w c_w}} \right) \frac{1}{L(1 + \sin \theta)} < 1 \quad (21)$$

with $a > 0$, and

where R is the radius of curvature of the liquid-vapor interface (which for a cylindrical cavity has the form $R = R_c / \cos \theta$) and J is the mechanical equivalent of heat. This relationship shows the pertinent fluid and surface variables which can affect the stability of a cavity.

For liquids that do not wet solids (i.e., $\theta > 90^\circ$), A is negative; hence Eq. (16) predicts $\chi(t) < 0$ for all time, suggesting there is no penetration due to condensation, and stability is insured. Of course, some penetration would occur because of the initial momentum of the liquid, which was neglected in this analysis.

It is stressed again that the above relationship, Eq. (21), should be used only in a qualitative sense due to the many simplifications in the proposed model. For instance, since inertia effects have been omitted, this approximate solution is inapplicable at the beginning of interface penetration, and it gives an initial velocity of infinity. In addition, the estimated form of the wall temperature response gives an initial temperature-time gradient of infinity. However, for order of magnitude purposes, we can utilize Eq. (21) to compare η^* for a few liquids to see how stability varies.

We consider boiling of a degassed liquid at 1 atm. pressure, from a stainless steel 316 boiler, which has an RMS roughness of 140 μ in. We assume a heat flux of 50,000 BTU/hr.ft.². We assume a cavity radius of 0.0012 inches and an L/D ratio for the cavity of 5. As given in Appendix B, we use an approximate value of $b \approx 20$. We use the results of Hsu and Schmidt (29) to obtain $a = 0.920$ and $c = 484.6$, and utilize the values of f as given in Appendix B, with an assumed value of $\epsilon = 0.3$. Substituting these constants along with the fluid variables into Eq. (21), we find some interesting approximate values for η^* .

<u>Liquid</u>	<u>Dynamic Contact Angle, θ</u>	<u>η^*</u>
Methyl Alcohol	46°, reference (31)	.0087
Liquid Nitrogen	0°, assumed	.023
Water	60°, clean, reference (32)	.248
Water	80°, paraffin coated, "	.028
Sodium	0°, assumed	17,500

As mentioned earlier, too much significance should not be attached to the exact numerical values listed in the above table. The magnitude of $\eta^* = 17,500$ for sodium is physically meaningless and is probably due to the neglect of inertia and viscous effects in the proposed model. However, the main point which should be emphasized here is that the η^* magnitude for sodium is so very much larger than unity and so very much larger than the η^* magnitudes for the four other cases, where stable boiling has been observed, that it should not be surprising if unstable boiling is observed for sodium on stainless steel. In addition, since the other alkali metals have physical properties similar to sodium, then their η^* magnitudes should also be very much larger than unity, suggesting that unstable boiling should occur for all the alkali metals on stainless steel.

2.3 Variables which Affect Nucleation Stability

The factors in Eq. (21) may be grouped into those involving fluid properties, those involving surface material properties, those involving surface heat flux, and those involving cavity geometry. We now examine the influence of these quantities on stability.

Fluid Properties

It is evident that as $\left(\frac{\rho_L}{\rho_V}\right)$, $\left(\frac{T_{SAT}^2 \sqrt{R_L \rho_L C_L}}{\rho_V^3 h_{fg}^3}\right)$ and $\frac{1}{(1 + \sin \theta)}$ increase, then instability becomes more pronounced. For the alkali metals, all these terms are large because the alkali metals have high saturation temperatures, high thermal conductivities, contact angles near zero, and small vapor densities. In addition, the bubble frequency for nucleate boiling of the alkali metals appears to be very low as given in Appendix B. Since η^* depends on f^{-a} , this lower bubble frequency also contributes to greater instability. It is interesting to note that as the pressure increases, both $\left(\frac{\rho_L}{\rho_V}\right)$ and $\left(\frac{T_{SAT}^2 \sqrt{R_L \rho_L C_L}}{\rho_V^3 h_{fg}^3}\right)$ decrease for sodium, which should improve stability.

Surface Material Properties

We also see that as the term $\left(\alpha_W^{-a} \sqrt{R_W \rho_W C_W}\right)$ increases, then stability improves since a appears to be near

0.7 most of the time, as verified by Hsu and Schmidt's results (29). Metals like copper, molybdenum and nickel should be more stable than stainless steel, Haynes 25 and Inconel for the same cavity size distribution.

Surface Heat Flux

Likewise, since η^* depends on Q_0^{1-2a} (with $a > 0.6$ from Hsu and Schmidt's results (29)), then as the heat flux per unit area increases, stability should improve.

Cavity Geometry

Cavity internal geometry plays a significant role in stability. If a cavity is deeper, that is if L increases, and also if $\left(\frac{2\sigma}{JR}\right)$ decreases, then stability improves. Therefore, a large radius of curvature of the interface should improve boiling stability. More specifically, as the contact angle approaches 90° , or if the cavity shape is such that the cavity radius increases with depth, we would expect better stability. Thus, cylindrical and conical type cavities should not be as stable as bell shaped cavities. Indeed, a doubly re-entrant type cavity, as shown in Fig. 3 should be very stable because the radius of curvature is forced to pass through infinity in order for the interface to penetrate deeper than the cavity mouth.

3. DESCRIPTION OF EQUIPMENT

In order to design the equipment, the following conditions were established:

1. The working fluid should be sodium because it is inexpensive, its physical properties are well tabulated, and because its corrosive capabilities are rather well known.
2. The boiling system should be a closed reflux capsule with no loop operation.
3. The boiler surface should be a horizontal flat plate because this is a simple, one-dimensional geometry to boil from, because a large amount of horizontal flat plate boiling data is available for comparison, and because it is the easiest geometry on which to regulate surface finish.
4. The boiler surface must be easily removable to allow for different surface polishes, surface materials, etc.
5. The system must be designed as simply, as safely and as flexibly as possible.

With these "parameters" in mind, the final design resulted in a system where sodium boiled off a horizontal flat disc; the vapors rose inside a vertical pipe, and condensed due to forced

convection of air. The apparatus is shown schematically in Fig. 4, and a photograph showing partial assembly of the equipment is given in Fig. 5. Figures 6 and 7 are sectional drawings of the primary boiling system, and Fig. 8 is a photograph of the entire heat transfer facility.

The main components are grouped into the boiler-condenser, main heater, high vacuum system, helium cover gas line, sodium fill system, containment and safety equipment, safety controls, and instrumentation. These main components are now described more fully.

3.1 Boiler-Condenser

Figure 9 is a photograph showing an exploded view of the boiler-condenser before assembly. The boiler was a 2 1/2 in. schedule 40, stainless steel 316 pipe, 1 ft. long. It passed through the center of the vacuum chamber cover and was heliarc welded directly to the bottom of the cover. This pipe was originally flanged 9 in. above the boiler surface to allow for easy dismantling. Each flange was 4 1/2 in. O.D. x 1/2 in. thick, and was machined from stainless steel 316. The upper flange had two concentric knife edges machined into its face. The lower flange was grooved to accommodate a metallic gasket, and in the middle of the groove a single knife edge was machined. When bolted together, these flanges pressed the three knife

edges against the metallic gasket to provide a tight seal.

However, during the first few operational runs, it was noticed that small quantities of sodium vapor had leaked out this boiler pipe flange into the vacuum system, and the vapor had deposited on the cold portions of the vacuum chamber.

(A more complete discussion of this problem is given in Appendix E.) Both copper and nickel gaskets were used, having thicknesses from .060 in. to .020 in. Neither metal proved effective in confining the sodium at high temperatures. It was decided to reduce each flange thickness to 1/8 in. and to heliarc weld them in place. This final design is shown in Fig. 6. The weld, having an approximate penetration of .040 in., was ground off each time it was desired to open the boiler section and change the boiler surface. This procedure definitely reduced the flexibility of the boiler section, but it proved to be quite reliable and stopped the leakage completely. About a dozen welds were obtained with each set of flanges.

Four horizontal thermocouple wells were installed through the pipe wall. These wells were stainless steel 316 tubes, 1/4 in. O.D. x 1/8 in. I.D., which were capped at one end. They were heliarc welded to the outside of the pipe wall and penetrated one inch into the sodium pool. Their centerlines were located 1/2 in., 1 in., 1 1/2 in. and 2 in. from the boiler surface, and they were circumferentially orientated 45

degrees from one another (Fig. 9). These wells housed thermocouples No. 7, 8, 9 and 10 respectively. However, before any quantitative experimental runs were made, they were replaced by a single vertical thermocouple probe which was a 1/4 in. O.D. x 1/8 in. I.D. stainless steel 316 tube, capped at one end. This well housed thermocouple No. 11, and could be moved vertically to monitor the temperature distribution within the sodium.

Boiling took place from a horizontal flat disc 2 9/16 in. dia. x 3/4 in. thick, which was made either of stainless steel 316 or nickel "A". A detailed drawing of the boiler test section is shown in Fig. 10. The disc was heliarc welded to the stainless steel pipe wall by means of .020 in. thick mating flanges. This method of attachment was decided upon because the weld could be ground off, leaving the boiler plate ready for re-finishing and for re-welding. Each set of flanges could be used about four times.

Six thermocouple wells, .0635 in. in diameter, were drilled at a number of axial and radial positions in the test plate (Fig. 10). Four of these wells penetrated radially to a depth of 1.0 in. and had centerline distances from the test surface of .090 in., .280 in., .470 in. and .660 in. They were circumferentially orientated 90 degrees apart to provide an

accurate temperature distribution within the plate. Two other wells, on the .090 in. plane, penetrated to a 1/2 in. depth and they were circumferentially orientated 120 degrees from themselves and from the well with the 1.0 in. depth.

In most of the later experiments a 2 1/2 in. schedule 40, nickel "A" pipe, 3 1/2 in. long was welded to the test plate. This piece of pipe was internally polished to a good quality mirror finish and had no horizontal thermocouple wells welded to it. This prevented "rogue" nucleation sites (i.e., nucleation sites not on the test surface) from appearing.

The condenser section was a vertical, 28 in. length of 2 1/2 in. schedule 40 stainless steel 316 pipe with 18 copper fins, 18 in. long x 1 1/4 in. wide x 1/16 in. thick, silver soldered on the outside. It was welded directly to the boiler pipe just above the vacuum chamber cover. An outer jacket of mild steel which had the dimensions 6 in. O.D. x 5 3/4 in. I.D. x 28 1/4 in. long was fitted over this condenser pipe to channel the air flow over the copper fins. A 120 CFM centrifugal type air blower was attached to the inlet of this condenser cover by a flexible connector. The air entered at the top of the condenser through a horizontal 4 in. dia. x 3 in. long mild steel tube and was preheated by a coil of Chromel "A" resistance wire wrapped around Transite insulation. The air passed over the copper fins and left at the bottom of the

condenser through a horizontal 4 in. dia. x 3 in. long mild steel tube which was attached by a flexible connector to a 6 in. galvanized duct that led to the main M.I.T. exhaust system. Flexible connectors between the air blower and condenser inlet, and between the galvanized duct and condenser outlet were made of asbestos cloth interwoven with aluminum thread.

3.2 Main Heater

In order to interchange boiler surfaces quickly and with relative ease, it was necessary that the main heater should not be an integral part of the boiler test plate; therefore, radiant type heating was decided upon. The heater consisted of three tantalum-10% tungsten filaments fastened in series between four tantalum clamps. The filaments were .010 in. thick x 1 in. wide x 4 in. long. They were fabricated by corrugating a .010 x 3 x 4 in. foil along the 4 in. axis with an internal angle of 30 degrees. This corrugation gave added strength at high temperatures, and also, according to Sparrow and Lin (33), increased the effective emissivity. An overhead photograph of the heater is shown in Fig. 11.

The filaments operated near 4000°F (the melting point of tantalum-10% tungsten is approximately 5300°F) and required the use of a high vacuum system to prevent complete oxidation during operation. In general, the heater was quite reliable,

but there were several occasions when one of the filaments cracked due to oxidation embrittlement caused by the coarse grain structure of tantalum. These failures usually took place after operation at high power levels in a poor vacuum (i.e., a vacuum greater than one micron). It has been shown by the National Research Corporation (34) that use of a stabilized grain size form of the tantalum-10% tungsten alloy would eliminate this oxidation problem to a considerable extent.

Each filament was held in place by pressing it between two 1/4 in. thick tantalum clamps which were machined to fit the filament corrugations. This assembly was riveted together by placing a piece of tantalum wire, 1/6 in. dia. x 5/8 in. long, through a .0635 in. diameter drilled hole, and by peening over the edges of the wire. This method of attachment insured a good electrical contact at all times, and facilitated dismantling.

The tantalum clamps were fastened to 1/8 in. thick molybdenum electrodes using No. 10-32 x 3/4 in. long tantalum screws with hex. hd. nuts. These molybdenum pieces were bolted to "L" shaped molybdenum electrodes with 3/8 in. dia. x 1 in. long stainless steel cap screws with hex. hd. nuts. The "L" shaped electrodes were slotted vertically to allow for adjustment of the overall height of the filaments, and were in turn bolted to 3/8 in. thick horizontal copper bus bars, as shown in Fig. 6.

Vertical copper electrodes were silver soldered to the underside of the horizontal bus bars. They were fabricated by silver soldering a 1/2 in. pipe inside a 1 in. pipe (Fig. 6). Cooling water from the laboratory supply line flowed up the inside of the 1/2 in. pipe and down and out the annulus. These electrodes were electrically insulated from the vacuum chamber base plate by means of Teflon collars which were pressed between stainless steel flanges, silver soldered to the electrodes, and between the base plate (Fig. 6). However, in order to prevent the Teflon from outgassing at high temperature operation, water cooled copper coils were locally installed within grooves machined in the underside of the base plate.

High temperature electrical insulators made of aluminum oxide and also of Lava were used to channel the current so that the three filaments were connected in series. A DC power supply rated at 1000 amps, 15 volts was connected through flexible copper leads to the vertical copper electrodes.

To increase the thermal efficiency of the heater as much as possible, eleven concentric radiation shields were used. They were 12 in. high with diameters varying on the half inch from 8 in. to 13 in. The innermost shield was made of .010 in. thick molybdenum while all the rest were made of .019 in. thick stainless steel 304. In addition, fifteen horizontal radiation shields of stainless steel 304, .019 in. thick x 3 in. wide

x 6 in. long, were placed beneath the filaments. All these shields were polished on the inside surface to a mirror finish.

3.3 High Vacuum System

The boiler and heater were contained within a 14 in. O.D. x 1/8 in. thick x 18 in. long stainless steel 316 vacuum chamber. This vessel was fabricated by heliarc welding 3/4 in. thick x 16 3/4 in. diameter flanges to the top and bottom of the cylinder and by bolting to these flanges 3/4 in. thick x 16 3/4 in. diameter plates. Twelve 1/2 in. dia. x 2 in. long stainless steel hex. hd. cap screws with hex. hd. nuts were used with each flange. A single 14 1/4 in. O.D. "O" ring, which was made either of aluminum or copper, provided a vacuum seal. The aluminum "O" rings were butt welded from .081 in. diameter wire while the copper "O" rings were silver soldered from .072 in. diameter wire. Three Conax multiple thermocouple glands with Lava sealants were used to provide vacuum seals for all the thermocouples in the test section. These glands were heliarc welded to the vacuum chamber cover at positions 90 degrees apart on an 11 1/2 in. diameter circle. The Teflon collars which were previously described provided excellent seals for the main heater copper electrodes. A vacuum better than 10^{-5} mm Hg was generally attainable with this system. The entire vacuum chamber was covered with

1 1/2 in. of Fiberfrax thermal insulation to cut down heat losses during operation, and the unit was raised and lowered using two hydraulic jacks, and a steel support ring.

The high vacuum line consisted of a horizontal, 4 in. schedule 40 stainless steel pipe welded to the wall of the vacuum chamber at a point eleven inches above the base plate. This pipe was bolted to a National Research Corporation 4 in. flexible connector which in turn was bolted to a 4 in. stainless steel 316 90 degree elbow. Both flanges used standard neoprene gaskets for vacuum seals. The elbow was bolted to a National Research Corporation, type HS4-750 diffusion pump using a neoprene "O" ring. A Welsh Duo-Seal type 1402 B mechanical pump, connected directly in series with the diffusion pump, was used as the roughing and backing pump. No cold trap or separate roughing lines were used.

3.4 Helium Cover Gas Line

In order to maintain the sodium as free of oxides as possible, helium was used as a cover gas. The helium was dried and filtered by flowing through a molecular sieve bed (1/16 in. diameter pellets of an alkali metal alumino silicate from Linde Co. were packed firmly within a 2 in. dia. x 10 in. long stainless steel 304 cylinder) at liquid nitrogen temperatures. The entire helium gas line was 1/4 in. stainless steel 316 tubing and all valves were Hoke type TY440.

A Cenco-Megavac mechanical vacuum pump was connected to this helium system through a standard ice trap where the 1/4 in. stainless steel pressure tubing was joined to a series of 1/4 in. copper coils.

A large stainless steel 316 pressure tank was attached to the helium system above the condenser section. It was an 8 in. schedule 5 pipe, 18 in. long, with welded caps at both ends. Six brass baffles were silver soldered on the inside of the tank, and water cooled copper coils were soft soldered on the outside. The tank was used both as a reservoir to damp any pressure fluctuations during boiling, and also as a cold trap for sodium vapors. All breakable joints utilized stainless steel Parker Triple-lok or Swagelok fittings, and all permanent joints utilized stainless steel Parker Braze-lok fittings.

3.5 Sodium Fill System

Sodium was stored in a stainless steel 316 tank, 4 1/2 in. O.D. x 6 in. high. This tank was flanged at the top and was sealed with a 4 1/2 in. I.D. x 0.139 in. thick Viton "O" ring. A steel sheathed, 0.260 diameter Calrod heater was wrapped around the tank, and was covered with a 1/2 in. thick coating of Thermon cement to provide a good thermal bond. This heater was rated at 1.25 KW and received power through a 1 KVA variac.

Thermal insulation consisted of a 1/2 in. thick inner layer of Fiberfrax alumina-silica fibers and a 1/2 in. thick outer layer of standard fiberglass strips. The tank assembly rested on a Cenco household scale which had a capacity of 25 lbs. x 1 oz.

The sodium fill line was fabricated entirely from 3/8 in. diameter stainless steel 316 tubing. This line went from the fill tank through a 3/8 in. dia. x 12 in. long Anaconda flexible stainless steel tubing, and into the vapor space through the condenser top. Bristle heating tapes were wrapped around the entire length of the line, and were covered with the same type of thermal insulation used on the fill tank. Sodium was filtered before entering the boiler by passing through a flanged stainless steel cup, 1 1/2 in. O.D. x 3 in. long, which was packed with fine grade stainless steel wool. This filter was kept at a temperature near 350°F. The fill line entered into the vapor space of the condenser by means of a Conax packing gland with a Lava sealant. All valves were Hoke type TY445, and all breakable joints utilized either Parker Triple-lok or Swagelok fittings.

3.6 Containment and Safety Equipment

Since the boiler section operated within the 14 in. O.D. vacuum chamber, this chamber acted as a primary source of

containment for any sodium leakage.

In addition, the entire heat transfer apparatus was enclosed inside a 5 x 5 x 8 ft. high enclosure shown in Figs. 5 and 8. This enclosure was fabricated by bolting 20 gage steel sheets to an all-welded framework of 1 1/2 x 1 1/2 x 3/16 in. angle irons (Fig. 5). Rubber weather stripping was used between the sheets and framework to provide a pressure tight seal in the event that an inert atmosphere was necessary. A plexiglass window, 22 x 16 x 1/4 in., was attached to the top half of the front side of the enclosure. Just beneath this window was a 5 x 4 1/2 ft. hinged door. All valve handles were extended through the enclosure skin to permit operation from the outside. The enclosure was vented through a 6 in. duct to exhaust any possible fumes.

Safety equipment included an Ansul MET-L-X fire extinguisher, a safety helmet, safety glasses, a methyl methacrylate face shield and asbestos lined leather gloves.

3.7 Safety Controls

In order to safely operate the apparatus, a semi-automatic control system was utilized. This system monitored the sodium level within the boiler, the condenser air flow rate, the main electrode cooling water flow rate, and the main vacuum system pressure. If the sodium level dropped beneath a prescribed

value, if there was a loss of air flow, loss of vacuum or loss of water circulation, then this system activated a buzzer and one of four control panel lights. The system was semi-automatic because although detection was automatic, control of the equipment was manual. A master stop button on the control panel was used to shut off the main power supply in the event of an emergency. An electrical wiring diagram for this control circuit is shown in Fig. 12.

Each sensing device operated an electrical relay which controlled a common buzzer and an individual light. The sensor for the air flow rate was a mercury switch attached to a butterfly valve inside the air duct. When the flow of air was turned on or off, the butterfly valve would open or close the mercury switch. The sensor for the sodium level utilized the vertical thermocouple probe described earlier. A 110 volt DC power supply was connected to this probe which was electrically insulated from the condenser by means of a Conax electrode gland with a Teflon sealant. The sodium level would act as a switch, making or breaking contact when the level was above or below the probe tip. The sensors for both the water flow rate and the high vacuum system utilized standard pressure diaphragms attached to micro-switches. As the water pressure (or vacuum) changed, the diaphragm would move, thereby opening or closing the micro-switch.

3.8 Instrumentation

Six platinum-platinum 10% rhodium "Ceramo" type thermocouples were used in the boiler test plate. These thermocouples were 1/16 in. O.D., inconel sheathed, magnesium oxide insulated and were specially calibrated at either 1200, 1400, 1600 and 1800°F or 1400, 1600, 1800 and 2000°F by the Thermo Electric Company to an accuracy better than 1°F. Four 1/8 in. O.D., stainless steel sheathed, Chromel-Alumel, "Ceramo" type thermocouples were used in the horizontal thermocouple wells within the sodium pool. A 1/16 in. O.D., stainless steel sheathed, Chromel-Alumel, "Ceramo" type thermocouple was used in the vertical probe. All the Chromel-Alumel thermocouples were accurate to within 3/8 percent, and were not specially calibrated.

The above-mentioned thermocouples were connected through a Leeds and Northrup 16 pole rotary switch to a Leeds and Northrup, type K, precision potentiometer with an external standard cell, battery and galvanometer. The reference junction for these thermocouples was chosen as room temperature, and this reference value was recorded for each data point by means of a 30 gage iron-constantan, glass insulated thermocouple which was read against an ice junction. During several of the runs, the thermocouples located .090 in. from the boiler surface were also recorded continuously on a Minneapolis-Honeywell,

Brown Electronik, single point recorder. All other thermocouples in the apparatus were used to monitor heat losses and to obtain operational information. They were all 30 gage iron-constantan, glass insulated thermocouples and were connected directly to a Minneapolis-Honeywell, Brown Electronik, 20 point recorder which had a range of 0-1000°F.

Pressure in the helium line was accurately measured by an open end manometer and a Marsh compound pressure gage. The pressure in the vapor space of the condenser was recorded by a Taylor high temperature volumetric pressure transducer which had been previously calibrated against the manometer down to a pressure of 40 mm Hg. The condenser air flow rate was measured by observing the pressure drop across a nozzle, which was installed in the air duct. This nozzle was spun out of aluminum, and conformed to ASME specifications.

The main heater voltage drop was recorded by a 0-25 volt DC voltmeter, and the main current was determined by observing the voltage drop across a National Bureau of Standards shunt. This voltage drop across the shunt was recorded by a 0-50 MV millivolt meter. For the shunt, 50 MV equalled 1000 amps. All other heater power supplies were monitored using variacs and ammeters in each circuit.

The pressure in the high vacuum system was determined with two thermocouple gages and one ionization gage. All three gages

were connected to a National Research Corporation, type 710 B, gage control. The vacuum was monitored from 1 mm Hg down to 10^{-6} mm Hg.

A phonograph crystal cartridge was taped directly to the high vacuum line to pick up vibrations in the test section. Because the crystal was limited to temperatures below approximately 140°F, the pickup was positioned about 2 inches from the vacuum chamber wall and was locally cooled by flowing water through copper coils which were soldered to the vacuum line. The noise created during boiling was directly transmitted to this cartridge and the electrical signal was fed to an oscilloscope for observation. During a few runs, a dual channel Sanborn recorder was used. One channel recorded the temperature in the boiler plate while the second channel recorded vibrations in the test system. The coincidence of these two signals was used to study nucleation stability.

4. EXPERIMENTAL PROCEDURE

4.1 Preparation of Test Surfaces

Throughout this research work many types of test surfaces were used, ranging from smooth, high quality mirror finishes to coarse, porous coatings. All but one of these test surfaces were welded directly to sections of boiler pipe whose inside surfaces had either standard pipe finishes or mirror finishes. (See Fig. 10.) The one test section was fabricated by machining a 3 in. diameter solid nickel "A" rod into the shape of a cup having an overall height of 4 1/2 in. The details and dimensions of this cup were identical to those given in Fig. 10, but this test section had no joints nor welds beneath the liquid sodium level.

No theoretical nor experimental method exists today which can predict the number of active sites of a given size on a test surface which has undergone a prescribed polishing procedure. This is because of the complex dependence of the number of active sites on the fluid properties, surface properties, past history of the boiler, etc.

Instead, it is hoped that the micro-structure of a given test surface may be adequately defined if an accurate description is given of the polishing and cleaning procedure which was

used on this test surface. The ultimate objective of this approach is that by following a prescribed experimental polishing procedure, nucleate boiling results for a given surface may be reproduced.

Mirror Finish

In order to obtain a high quality mirror finish, great care had to be exercised at all times. Rough polishing was done on a Buehler Handimet manual grinder. This grinder contained strips of 240, 320, 400 and 600 grit emery paper which were attached by adhesive backing to rectangular glass plates. Water continually flowed over the emery paper keeping it clean and serving as a lubricant. The test surface was placed face down on the 240 emery paper and was stroked over the paper in one direction only, until all the original scratches were removed. This generally took 25 to 50 strokes. The test plate was then rotated 90 degrees and was carefully stroked in this direction over the 320 emery paper until all the scratches left from the 240 grit emery were removed. Once again stroking was in one direction only to obtain a flat surface and a uniform polish. This same procedure was repeated for both the 400 and 600 emery paper, although greater care was exercised as the surface polish improved. Upon completion of the rough polishing, the surface had a high gloss finish but there were many visible scratches.

The test surface was then placed in a Syntron vibratory polishing machine to obtain a fine polish. This machine had a 12 in. diameter flat-bottomed steel bowl covered with a nylon polishing cloth which was kept taut by a cloth clamping ring. The bowl was filled to a depth of 1/4 in. with a suspension of fine grade alumina powder in distilled water. An electromagnet and a set of leaf springs were attached to the bottom of the steel bowl and they provided the vibratory motion during polishing. A variable power transformer controlled the amplitude of these vibrations, depending on the quality of finish desired. The surface was kept in the Syntron for about 20 hours. By this time the surface had no visible scratches and presented a clear image when looked at. (See Fig. 13.)

The test plate was then removed and was cleaned with running tap water, a distilled water jet, and a methanol jet. It was then dried in a hot air jet. The finished surface was cleaned for one minute in a Buehler ultrasonic cleaner and was then carefully covered with masking tape until ready for use. Two surfaces had this type of finish. They were designated MIRROR 1 and MIRROR 2.

During some of the runs, mirror finishes were prepared by sending the test surfaces to the L.A. Donovan plating company where the surfaces were buffed using polishing compound.

The resulting finishes were mirrorlike, but they did have some visible scratches. Four surfaces had this type of finish: MIRROR 3, 4, 5, and 6. MIRROR 4 was fabricated from the solid nickel "A" cup mentioned earlier. The entire inside surface of this test section was polished to a mirrorlike finish.

Lapped Finish

Lapping is generally thought of as a smoothing or polishing procedure. However, in our case it was used to roughen test surfaces. The lapping compound contained small pieces of abrasive suspended in oil which, when rubbed on a metallic surface, effectively saturated the surface with cavities.

Lapping took place on a rectangular steel plate which had been coated with Clover brand lapping compound. Two grades of compound were used: grade A (280 grit) and grade F (100 grit), and the resulting finishes were designated LAP A and LAP F respectively. The test surface was placed face down on the coated plate and the surface was then stroked back and forth about 50 times. The lapping compound was then re-spread on the steel plate, the test piece was rotated 90 degrees and the stroking motion was repeated about another 50 times in this new direction. The test plate was rotated 90 degrees and stroked over the lapping plate two more times. After finishing the fourth portion of the lapping sequence, the test surface was

saturated with cavities. It was thoroughly washed with trichloroethylene to remove the grit and to act as a degreaser. The surface was then dried with a compressed air jet.

When a LAP A surface was required, the above procedure was followed using grade F compound first. The lapping plate and test surface were then thoroughly cleaned with trichloroethylene, and the entire procedure was repeated with grade A compound.

Etched Surface

A solution of Aqua Regia was mixed in a glass beaker using one part concentrated nitric acid to three parts concentrated hydrochloric acid. This solution was then poured into a welded boiler unit to a depth of about 7 inches. This boiler unit contained test surface MIRROR 2. It had four horizontal thermocouple wells welded into the pipe wall (as shown in Fig. 9), and had been used many previous times to boil sodium. All traces of sodium had been removed before adding the acid.

The Aqua Regia attacked both the nickel "A" test surface and the stainless steel 316 pipe wall, and this chemical reaction was carried out under a well ventilated hood. After 10 minutes the solution was removed and the boiler was thoroughly flushed with tap water for about 15 minutes.

A photograph of the etched test surface after sodium had boiled off it and after it had been re-cleaned is shown in Fig. 13. The grain structure is readily apparent. The non-uniform discoloration is probably due to preferential corrosion by the sodium due to the presence of the four wells in the sodium pool.

Artificial Porous Welds

One test section was prepared by taking MIRROR 3 and placing seven rows of artificial welds (i.e., welds which served no useful purpose other than to alter the test surface condition) on the surface.

These welds were deliberately made porous to create many nucleating sites. They were fabricated by heliarc welding with argon gas using too small a gas cup, too much current, and too long a tungsten electrode. These conditions allowed argon gas pockets to form in the molten metal causing "blowback." Figure 13 shows this test surface. Note the large number of exposed cavities.

A cross-sectional cut of a sample porous weld disclosed that many of these cavities were re-entrant in nature as shown in Fig. 14.

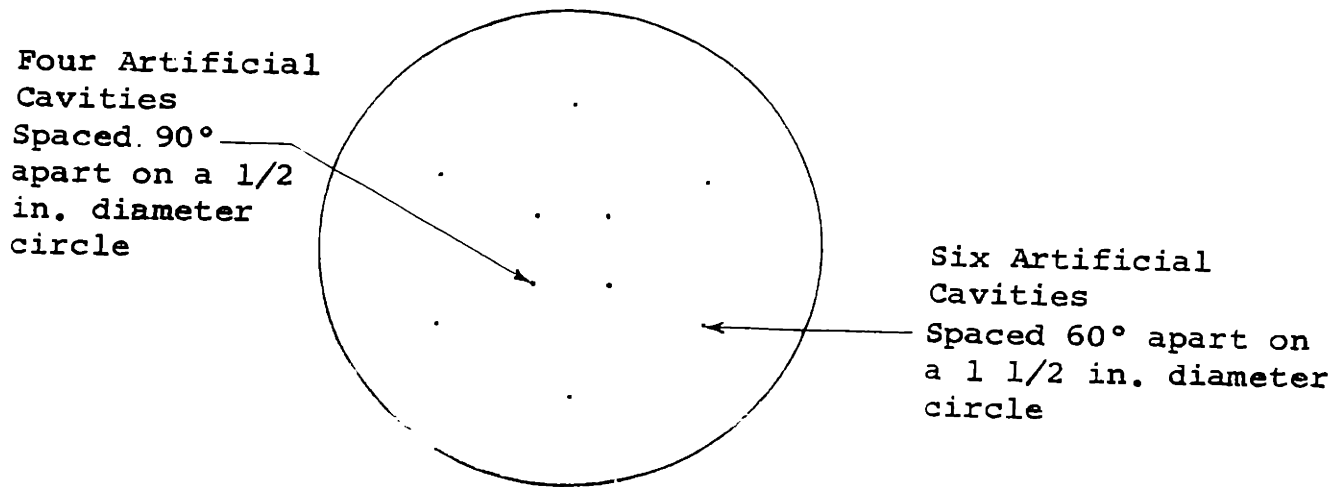
Porous Coating

This surface was fabricated by taking a standard nickel "A" test plate, and lapping the surface to get a smooth, flat finish. After cleaning this surface of oxides and grease, a 2 1/2 in. diameter x 1/32 in. thick disc of porous nickel "A" was then placed on it. This porous plate was manufactured by the Pall Corporation and had a mean pore size of 65 microns. The two pieces were pressed together under a load of about 5 psi and were fired in a wet hydrogen furnace at 1100°C for two hours to create a good metallurgical bond.

A photograph of this test surface is shown in Fig. 13. Note the very rough appearance. The few discolored spots were probably due to surface impurities on the nickel coating which had formed hydrides during the firing procedure. A cross-sectional view of a sample porous coating (with 35 micron pore size) is shown in Fig. 14. This surface seemed to be saturated with re-entrant type cavities.

Artificial Cavities

Ten cylindrical type cavities were placed on the test surface of MIRROR 4. They were .004 in. in diameter and .018 in. deep, and they were formed by an electric discharge drilling machine using a .0039 in. diameter electrode. They were arranged as shown below:

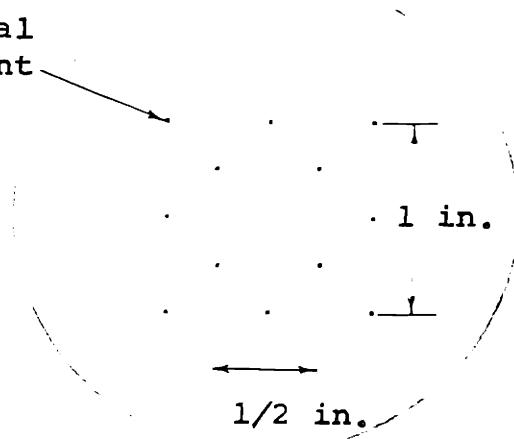
Test Surface

A cross-sectional photograph of a sample cavity is given in Fig. 15. Notice that the cavity is slightly tapered due to the technique used in drilling.

Twelve doubly re-entrant type cavities were placed on MIRROR 6. They were fabricated by drilling a hole .0145 in. diameter x .025 in. deep in the test surface. A plug, .015 in. diameter x .015 in. long, which was tapered on one end with a 45° bevel, was press fitted into the hole in the test surface so that the top of the plug was flush with the top of the surface. This plug had a .004 in. diameter hole drilled along its longitudinal axis to provide a mouth for the cavity. The twelve cavities were arranged as shown below:

Test Surface

Twelve Artificial
Doubly Re-entrant
Type Cavities



A cross-sectional photograph of a sample doubly re-entrant type cavity is shown in Fig. 15.

4.2 Preparation of Equipment

Cleaning Procedures

After the equipment was initially assembled, it was thoroughly cleaned of oxides and grease. The entire apparatus was filled with a 50% dilute solution of hydrochloric acid for twelve hours. The acid was then drained out and the apparatus was flushed several times with distilled water. Trichloroethylene was then added as a degreaser. After soaking for about twelve hours, the trichloroethylene was drained out and the distilled water flushing procedure was repeated. Reagent grade acetone was used as the final rinse.

Before being added to the system, each new boiler section, which consisted of a boiler pipe welded to a test surface, was cleaned separately following the above procedure. Generally the boiler pipe and test surface were individually cleaned before being welded together as a unit. They were re-rinsed with trichloroethylene and acetone after welding. The test surfaces, of course, were never cleaned with acid for fear of altering their prescribed surface finish. Consequently, for the few boiler sections which were welded together before cleaning (MIRROR 1, MIRROR 2, and LAP F), a thin coating of paraffin wax was melted over the test surface before the addition of acid. This coating was then dissolved by trichloroethylene during the de-greasing stage of cleaning.

When each used boiler section was removed from the system, it contained solidified sodium. Therefore, the boiler was immediately immersed in n-butyl alcohol, as described in Appendix E, to react all the sodium. The boiler was then flushed with methyl alcohol and was swabbed clean using a solution of hot soapy water. It was then thoroughly rinsed with distilled water.

Changing Boiler Sections

All water and electrical lines were first disconnected from the vacuum chamber. The two hydraulic jacks with the

steel support ring were positioned under the vacuum chamber and were raised until they began to support the load. The top and side flanges of the vacuum chamber were then opened and the vacuum chamber was lowered to the floor by slowly releasing the pressure within the jacks. The entire vacuum chamber unit was then slid to one side of the enclosure. All thermocouples were removed from the test plate and were bent away from the boiler flange. A portable grinder with a 3 in. diameter x 1/4 in. thick abrasive wheel was then used to grind off the weld on the boiler flange. This generally took about 30 minutes. A helium pressure of 3 psi was maintained inside the boiler during this time. When the crack between the two flange faces was visible around the entire circumference of the flange, the weld was broken open by shocking it with a hammer and chisel. The boiler section was then removed and reacted with alcohol as previously mentioned. All burrs on the edges of the top flange and all traces of sodium were removed. This usually took about 2 minutes during which helium was purged through the system in an effort to prevent oxidation of the sodium inside the apparatus. A new boiler was then clamped in place, taking great care that the thermocouple wells in the test plate were orientated in the same direction as for the previous boiler. The boiler was then welded to the top flange. It took about 15 minutes

to complete this weld and the system was immediately pumped down to less than 1 mm Hg. and re-pressurized with 5 psi of helium. The boiler flange was then leak tested. When this joint was tight the thermocouples were placed in the test plate, the vacuum chamber with a new metallic "O" ring was raised, and the top and side vacuum flanges were tightened until a vacuum of at least 10^{-5} mm Hg. could be obtained.

Leak Testing

Whenever the equipment had been dismantled and re-assembled, leak testing would take place. The entire system was pressurized to 10 psi with helium and all previously opened joints were checked with a soap solution. The system was considered tight if a pressure of 10 psi was held overnight without any change occurring in the open end manometer.

The main vacuum system was leak tested after assembly until a vacuum of between 10^{-5} mm Hg and 10^{-6} mm Hg existed. Leaks were checked by spraying all joints with acetone and watching the response of the thermocouple gages for a vacuum between 10^{-2} and 10^{-3} mm Hg, and of the ionization gage for a vacuum below 10^{-3} mm Hg.

4.3 Operational Details

Transfer of Sodium

Commercial grade sodium was used. It was purchased from the Ethyl Corporation in 1 lb. bricks which were contained in hermetically sealed tin cans. A typical chemical analysis of the "Ethyl" sodium, and a discussion of the sodium purity is given in Appendix E.

In order to load the sodium, the fill tank was first disconnected from the system, and was opened by unbolting the cover. A 1/2 lb. brick of sodium, which had been scraped of all surface oxides, was then placed in the fill tank. A new Viton "O" ring was added and the cover was bolted in place. The fill tank was then re-connected to the system and the entire apparatus was immediately evacuated to 1 mm Hg and pressurized to 10 psi with helium to check for leaks. Insulation was then packed around the fill tank. The air heater was then turned on to approximately 1 KW. This generally heated the condenser air inlet temperature to 240°F using the slight flow of air provided by the M.I.T. exhaust system. The heaters for the fill tank, fill line and main boiler were all turned on and the system was evacuated. Thermocouples attached to the fill tank, fill line, condenser inlet and outlet, and boiler test plate were recorded to monitor the temperatures within

the system. All the heaters were kept on for about 2 hours or until the fill tank was at 450°F, all lines were near 400°F, and the boiler test plate was at 400°F.

At this time the boiler section was evacuated to 28 in. Hg., and the fill tank was pressurized to 5 psi. The sodium fill line valves were opened and sodium flowed into the boiler. During this transfer operation the change of the gross weight of the fill tank was observed in order to get an approximate idea of the amount of sodium transferred. A more exact value of the sodium level in the boiler was determined by lowering the vertical thermocouple probe in the condenser space until the Low Sodium control light went out. The height of the probe above the boiler surface was then recorded. The probe was lowered another 1/2 inch and the Conax electrode gland sealing this probe was re-tightened. The fill valves were then closed; the boiler was pressurized to 5 psi and the fill tank was evacuated to 28 in. Hg. The fill line valves were opened again to blow any excess sodium back into the fill tank and to clear the fill line and filter of any trapped sodium.

On a few occasions the sodium filter blocked up with oxides and dirt, and the sodium fill line became plugged. The fill line was then dismantled and cleaned of all sodium, and the stainless steel wool filter element was replaced.

Nucleate Boiling Run

After the sodium had been transferred into the boiler, and the fill line had been cleared, then the helium pressure over the boiler was adjusted to the desired operating value, and the main heater was gradually increased until boiling commenced. This usually took about 1 1/2 hours. For some of the runs, when the sodium had been solidified in the boiler from a previous run, then this heat up time was about 3 hours. During this interval, all the thermocouples in the boiler plate were periodically recorded and the oscilloscope was observed for any vibration changes.

Shortly after nucleate boiling began, the condenser air blower was turned on, dropping the condenser air inlet temperature to approximately 125°F. During normal operation, all the control lights were out and all the auxiliary heaters were kept on to maintain the auxiliary lines near 400°F.

For any given heat flux level, after equilibrium had been reached, the barometric pressure was recorded, the Taylor gage and open end manometer were recorded as well as the power input to the main heater. All the thermocouples in the test section were then recorded in rapid succession from No. 1 through No. 11. The reference temperature was then determined, and all thermocouples were again recorded from No. 11 through No. 1. Remarks were then noted regarding the type of boiling that was occurring.

The entire data taking procedure for any one heat flux level took about 10 minutes. Great care had to be taken to insure that the pressure or the power level did not wander during this period. The pressure was controlled well by constantly bleeding the system with the mechanical vacuum pump. As the heat flux was increased, the valve to the vacuum pump was cracked open slightly more to insure a constant pressure inside the vapor space. It took about 15 minutes for equilibrium to be reached after the input power level was changed. Data for both increasing and decreasing heat flux were observed.

The system was shut down by turning off all the electrical heaters, by pressurizing the boiler to 5 psi with helium, and by shutting off the main vacuum pumps. The entire system cooled down overnight and the sodium was left to solidify within the boiler.

4.4 Treatment of Data

At any given power level, the reduced and corrected temperature values of thermocouples No. 1, 2, 3, and 4 in the boiler plate were plotted versus boiler plate axial position to obtain a temperature distribution. A straight line always resulted. The heat flux was then calculated directly, knowing the thermal conductivity and thermocouple locations accurately, by using the Fourier heat conduction equation

$$\frac{Q}{A} = R \frac{\Delta T}{\Delta X} \quad (22)$$

The wall temperature was determined by extrapolating the straight line temperature distribution to the boiler surface.

During a few unsteady boiling runs the temperatures in the boiler plate fluctuated as much as 125°F. Since it was impossible to obtain an accurate thermocouple reading during this temperature fluctuation, then for each data point both the approximate maximum and minimum thermocouple values were recorded. The maximum temperatures of thermocouples 1, 2, 3 and 4 were plotted and used to obtain the heat flux and wall surface temperature data "Before Bump" took place, whereas the minimum temperatures of thermocouples 1, 2, 3 and 4 were used to obtain the data "After Bump" occurred.

The wall surface temperature was determined by extrapolating the linear temperature distribution to the boiler surface. The saturation temperature was found by calculating the temperature corresponding to the measured average pressure in the vapor space using the vapor pressure-temperature relationship recommended by Bonilla, Sawhney and Makansi (35)

$$-\log_{10} p = 4.52172 - \frac{5220.42}{T} \quad (23)$$

where p is in atmospheres and T is in degrees Kelvin.

A sample calculation of the data with an error analysis is given in Appendix D.

5. RESULTS AND DISCUSSION

Thirty experimental runs have been completed. Boiling has taken place at pressures of 65 mm, 200 mm and 400 mm Hg absolute, with sodium temperatures ranging from 1200°F to 1500°F. Heat fluxes as high as 236,000 BTU/hr.ft.² have been attained. Most of the data has been taken with nickel "A" boiler surfaces, with sodium pool depths near 3 inches, and with pressures near 65 mm Hg. Tables C-1 through C-15 in Appendix C present all the reduced and corrected data, giving the surface material, roughness, cleanliness and past history, as well as the sodium pool depth for each run. Tabulated results at a given average operating pressure, p , include the saturation temperature, T_{sat} , calculated from this average pressure, the heat flux, Q/A , the wall surface temperature, T_w , and the temperature difference, $(T_w - T_{sat})$. In addition, T_L , the temperature of the sodium measured 1/2 inch beneath the free surface of the liquid, is given. Remarks are also included for each data point describing the "observed" behavior of the test section while the data was being recorded.

During nucleation large boiler wall temperature fluctuations occurred which in some cases were as high as 125°F. These fluctuations were always accompanied by large variations

in the test section noise level as determined from the phonograph cartridge described in Chapter 3. The coincidence between the noise level and the wall temperature of the boiler gave a clear "picture" of when nucleation was occurring. Figures 16, 17 and 18 are illustrated portions of the Sanborn dual channel recorder chart used during Run 28. Figures 16 and 17 show the coincidence between thermocouple No. 4 in the test plate and the test section noise level at heat fluxes of 61,700 and 87,000 BTU/hr.ft.² respectively. Note that each drop in temperature is accompanied by a sudden increase in noise level. Note also that when the noise stops, the temperature rises gradually to its maximum value. The amplitude and frequency of these "bumps" seem to increase with heat flux. Figure 18 shows the temperature-noise level coincidence at the onset of stable nucleate boiling for a heat flux of 135,000 BTU/hr.ft.². The frequency during stable boiling, estimated by counting the number of discernible noise marks, is approximately 1.3 cps. Figure 19 is an enlarged section of Fig. 16. Each "bump" is sharply defined with arrows, showing the direct correspondence between the change in noise level and the change in wall temperature.

These observed temperature fluctuations and "bumping" cycles varied markedly in character, amplitude and frequency

depending on the surface roughness, surface material and surface past history.

5.1 Characteristics of Sodium Nucleate Boiling

Figure 20 presents some typical experimental data with estimated error limits for a nickel "A" surface having a mirror finish. The data of Noyes (6) from a horizontal molybdenum tube at 52 mm Hg is plotted for comparison. It is evident first of all, that the experimental accuracy during nucleate boiling is much better than for non-boiling. The large temperature fluctuations which occurred during "bumping" undoubtedly caused this. In addition, it appears that for this data the slope of the natural convection line is less than one. This is probably because at these low heat flux values, which were generally recorded in the beginning of an experimental run, the measured pressure may have been in error by an amount equal to the partial pressure of the helium cover gas. This greater pressure would increase the calculated saturation temperature and consequently lower the calculated wall superheat. This error would shift the low heat flux points to the left in Fig. 20, and thereby lower the slope of the data. Some degassed natural convection data (i.e., data obtained after the system had been boiling for some time) was taken during Run 13, and the slope of the natural convection line was about one for this case.

Incipience of Nucleate Boiling

Figure 20 also shows that the incipience, or onset, of nucleate boiling does not occur until a superheat of 135°F is reached even though the stable nucleate boiling data has a superheat of only 33°F. This large "overshoot" of superheat with increasing heat flux is characteristic of all the sodium data, although the exact superheat value did vary depending on the surface condition. A short table of results showing this variation is given below:

<u>Surface Condition</u>	<u>Q/A (BTU/hr.ft.²)</u>	<u>ΔT_{sat} at Incipient Boiling (°F)</u>	<u>ΔT_{sat} for Stable Nucleate Boiling (°F)</u>
MIRROR 1	63,700	135	33
LAP F	62,800	84	17
Porous Welds	58,200	79	22
Doubly Re-entrant Cavities	59,200	59	12
Porous Coating	30,600	17	11

In order to understand why this excess superheat exists for sodium, and why it varies with surface condition, we present the analysis of Bergles and Rohsenow (36) which is similar to Hsu's (37) investigation for the criterion of incipient boiling.

Bergles and Rohsenow consider a spherical bubble of radius r in a liquid, and state that at equilibrium,

$$p_V - p_L = \frac{2\sigma}{r} \quad (24)$$

where σ is the surface tension. Using the Clapeyron equation which relates T and p along the saturation line, they give

$$\frac{dp}{dT} \approx \frac{\rho_V h_{fg}}{T_V} \quad (25)$$

Assuming

$$p_V - p_L \approx (T_V - T_{SAT}) \frac{dp}{dT} \quad (26)$$

and substituting Eqs. (25) and (26) into Eq. (24) gives the result

$$T_V = \frac{T_{SAT}}{1 - \frac{2\sigma}{\rho_V h_{fg} r}} \quad (27)$$

which is the critical vapor temperature. They apply this equation to a hemispherical bubble forming at a cavity with a mouth radius r . They postulate that this hemispherical bubble with radius r will grow only if the liquid temperature at a distance $y=r$ from the wall is greater than the critical vapor temperature defined by Eq. (27). They also assume a linear temperature profile within the liquid laminar sublayer given by

$$T_L = T_w - \frac{Q}{A} \frac{y}{k} \quad (28)$$

where y is the distance measured from the wall. Equations (27) and (28) together with the assumed relationship

$$T_L = T_V \quad \text{at} \quad y = r \quad (29)$$

represent the criterion for incipient boiling.

Figure 21 shows the critical vapor temperature equation, Eq. (27), plotted schematically with distance from the wall for water and for sodium at the same operating pressure. In addition, the linear temperature profile, Eq. (28), for each liquid has been superimposed to show incipience graphically for each fluid. Note that at the same distance from the wall, $T_V - T_{\text{sat}}$, is greater for sodium than for water and also note that the slope of the liquid temperature, defined by Eq. (28), is much lower for sodium at the same heat flux level because of the high thermal conductivity of sodium. Consequently, the incipient point for sodium occurs at larger distances from the wall, as seen in Fig. 21. In fact, y_A^* for water at moderate heat fluxes is near 10^{-5} inches whereas y_B^* for sodium is near 10^{-2} inches.

It is postulated that at the tangency point (points A and B in Fig. 21) which determines the minimum amount of superheat necessary to nucleate a surface, if a cavity of radius equal to y^* is available for nucleation (i.e., if it has vapor trapped within it), then nucleate boiling will commence. If, on the other hand, there are no cavities of this size containing trapped vapor or gas, then all the temperatures

will increase until the liquid temperature equals the critical vapor temperature for some smaller, active cavity as shown by points C and D for sodium in Fig. 21.

As pointed out by Bergles and Rohsenow, since γ^* is so small for water, then incipient boiling depends in most cases on the second-order roughnesses of a surface, and these should be independent of surface finish. Assuming relatively poor wetting properties for water, then cavities of this small size should always be available to nucleate. Consequently, incipient boiling in most cases for water occurs at the minimum required superheat, and no "overshoot" exists.

For sodium, however, since γ^* is so large and since sodium wets cavities so well, then very high wall superheats are necessary in order to reach a critical radius which can trap vapor or gases. Therefore "overshoot" occurs. In fact, in order to nucleate from a cavity with a radius near 10^{-5} inches, a superheat of approximately 250°F is necessary for sodium at 1 atm, as pointed out by Hoffman and Krakoviak (38).

In addition, surface conditions should directly affect incipience because the largest cavity which can trap vapor will determine the minimum wall superheat necessary to nucleate. Thus, suppose at the incipient point, point B as shown in Fig. 21, that no active sites exist. Now if the surface

condition is such that an active site exists at point C, then all the temperatures will rise until the liquid temperature equals the critical vapor temperature at point C, and this point will determine the wall superheat for nucleation. If no active cavity exists until point D, then the superheat increases further. This argument also partially explains why the data of Noyes (6) lie at lower superheats in Fig. 20 than the data for this investigation. His tube surface was undoubtedly much rougher and contained larger cavities than the high quality mirror finish used in Run 1 and Run 2, so his data should have lower superheats as explained above.

Quantitatively, at a pressure of 60 mm Hg, with an assumed active cavity radius of .002 in., then Eqs. (27), (28) and (29) predict for the minimum wall superheat at incipient boiling, $\Delta T_{\text{sat}} = 64^\circ\text{F}$. The experimental data for the doubly re-entrant cavities which have a mouth radius of .002 in. shows $\Delta T_{\text{sat}} = 59^\circ\text{F}$. This value agrees quite well with the above predicted value. However, no explanation can be given why the experimentally measured superheat is lowered to 12°F for these doubly re-entrant cavities during stable nucleation. At this low superheat, unreasonably large cavity sizes near .010 in. would have to be active.

However, the following plausible argument is given which can explain this phenomenon. From the Bergles and Rohsenow criterion, a cavity with a radius of .002 in. requires a superheat of 64°F at incipient boiling. When these cavities do nucleate (since the bubble frequency is so low, as noted earlier), then the bubbles which form are large and can cover a large portion of the surrounding surface area. Since this vapor blanket is essentially at the saturation temperature, then the wall superheat for this blanketed region is reduced to zero until the vapor blanket leaves the surface. It is postulated that the thermocouples in the test plate may have been reading the average surface temperature at any particular time, even though locally at each cavity, the surface superheat still had to be 64°F for nucleation. The surface area covered by vapor had no superheat, and this reduced the average surface temperature to the measured value of 12°F. Roughly, 20% of the surface area would have to be covered with vapor to produce an average temperature of 12°F.

Effect of Pressure

Figure 22 shows the well-known effect of pressure on nucleate pool boiling of sodium from a nickel "A" MIRROR 2 surface. It is readily seen that the heat transfer coefficient increases as the pressure increases. This is an

expected result because as the pressure increases then the critical vapor temperature decreases for the same cavity size. Thus, point B in Fig. 21 shifts downward, and incipient boiling occurs at lower wall superheats, thereby raising the heat transfer coefficient.

Instabilities during Nucleation

For sodium then, large superheats are necessary to cause nucleation. A plausible mechanism for the observed instabilities is now given which follows closely the mechanism of Hoffman and Krakoviak (37).

Consider a boiling sodium system with a liquid temperature passing through point D in Fig. 21, and suppose an active site exists at this small radius. Since so much energy is stored within the liquid at this high wall superheat, then when the bubble does form, a large "explosion" of vapor occurs, controlled by the difference between the superheated liquid temperature and the saturated vapor temperature. This vapor blankets the surrounding area next to the cavity, lowering all the temperatures and causing a "bump" to occur. The spreading out of vapor may cover a very large area of the nearby surface and may activate larger nucleating sites. If these larger sites can trap vapor (i.e., if η^* as given by Eq. (21) in Chapter 2 is less than 1), then nucleation will continue at

some lower wall superheat as shown by point C compared to point D in Fig. 21. If these larger cavities, however, cannot trap vapor (i.e., if $n^* > 1$) then boiling will stop and all the temperatures will rise again until the superheat is reached which initially caused nucleation of the smaller cavity at point D. Consequently, a thermal cycling occurs within the boiler and the amplitude of the temperature fluctuations depends on the cavity size distribution (i.e., on surface conditions).

5.2 Reproducibility of Results

By following the cleaning procedure given in Chapter 4, it was possible to reproduce nucleate boiling results for several of the boiler test surfaces.

Figure 23 compares the data of Run 3, Run 4, and Run 11. These runs all were taken for the nickel "A", MIRROR 2 surface, with an approximately constant depth and pressure. The only change between Run 3 and Run 4 was that the sodium was left to solidify in the boiler between these two runs. The boiler was removed after Run 4 and cleaned following the procedure described in Chapter 4. Two months later the boiler unit was welded back into the system and Run 11 was made, using newly calibrated thermocouples in the test plate. The results are quite similar, and are within the estimated experimental error.

Figure 24 compares the data of Run 8 and Run 10 which were for a nickel "A", LAP F surface. The difference between these two runs was that all the plate thermocouples were replaced, and the sodium was left to solidify after Run 8. Again, reproducibility is quite good.

Finally, Fig. 25 compares the results of Run 13 and Run 23 for a nickel "A", MIRROR 3 surface containing artificial porous welds. These runs were made two months apart. After Run 13, which was degassed data taken after boiling for 20 continuous hours, the boiler was removed and re-cleaned, and the test plate, which had become oxidized, was ground off the boiler pipe and re-welded to a new boiler unit. The discrepancy in the results between Run 13 and Run 23 is at the low heat flux levels suggesting that during Run 23, the sodium may have contained helium which would have lowered the required superheat as shown in Section 5.4. Another possible reason for the discrepancy may be because when the test plate was re-welded to the new boiler unit prior to Run 23 some "rogue" nucleation sites may have been present within the new weld.

5.3 Effect of Roughness

Roughness played a significant role in nucleate boiling of sodium, affecting not only the incipient boiling point but also the wall superheat during stable nucleation and the shape of the boiling curve.

Figure 26 compares the data for MIRROR 4, LAP A and MIRROR 6 with 12 artificial doubly re-entrant type cavities. It is clear that roughening the surface lowers the wall superheat and generally increases the slope of the data. The large scatter for MIRROR 4 is because this data was taken after a "bump", during unstable boiling.

Figure 27 shows a similar effect of roughness, comparing the data for MIRROR 2, MIRROR 3 with porous welds, and LAP F. The porous welds definitely improve the boiling heat transfer results. This fact, coupled with the previous results that re-welding may have caused the discrepancy between Run 13 and Run 23, leads to the conclusion that any welds inside a test section may contain "rogue" nucleation sites which can alter sodium nucleate boiling results.

It is interesting to note that both the LAP A and LAP F data show a constantly decreasing slope as given in Figs. 26 and 27. This shape of the boiling curve may be caused by the particular cavity size distribution obtained with lapping, or it may be caused by improved sodium wetting with time, thus forcing smaller cavities to nucleate, and raising the required wall superheat.

5.4 Boiling Hysteresis and Aging Effects

A considerable amount of hysteresis was observed during nucleate boiling of sodium. Figures 28, 29 and 30 show this. It appears that non-condensable gases were initially present in many of the runs, lowering the wall superheat. This reduction in the wall superheat would occur because if non-condensibles were present inside a bubble, then at equilibrium, we would have

$$p_v - p_L = \frac{2\sigma}{R} - p_g \quad (30)$$

where p_g is the partial pressure of non-condensable gases present. If this equation is used in place of Eq. (24) in the analysis of Bergles and Rohsenow, then the critical vapor temperature becomes

$$T_v = \frac{T_{SAT}}{\left(1 + \frac{p_g}{\rho_v h_{fg}}\right) - \frac{2\sigma}{\rho_v h_{fg} r}} \quad (31)$$

For any given radius r , Eq. (31) predicts lower critical temperatures (and consequently lower wall superheats) than Eq. (27).

In general both the incipient boiling point and the stable nucleate boiling wall superheat were lower during the initial phases of a run than after boiling had taken place for some time. Figure 28 shows that the data of Run 13 (degassed 20 hours) coincide with the degassed data of Run 12,

suggesting that only a few hours degassing time is necessary to remove non-condensibles.

As mentioned earlier, this general aging trend of higher wall superheats may also be because with time the sodium deactivates the larger cavities.

5.5 Stability during Nucleation

As mentioned earlier, there were many runs during which the wall temperature fluctuated quite markedly. These fluctuations depended on the surface conditions. Figures 31, 32, 33 and 34 show reproduced temperature-time traces of thermocouples in the boiler plate. These thermocouples were .090 in. from the boiler surface suggesting that the actual surface gradients must have been very severe. The behavior during stable boiling is sharply contrasted with unstable boiling by comparing Fig. 32 (which is a temperature-time trace for MIRROR 3 with porous welds) with the other temperature traces. Note that for the stainless steel 316 test surface, with a LAP A finish, even at heat fluxes as high as $196,000 \text{ BTU/hr.ft.}^2$, boiling stopped for as long as 1 1/2 minutes and the temperature rose during this time interval almost 150°F . We also see that MIRROR 4 with no internal welds was unstable at all heat flux levels, and the addition of ten artificial cylindrical cavities, .004 in. dia. x .018 in. deep, did not improve stability at all.

It is worthwhile to note that even with MIRROR 4--a mirror finish with no internal welds--no superheats were observed which were as high as reported by Balzhiser (39) (400°F superheat with potassium) or Hoffman and Krakoviak (38) (700°F superheat with potassium). This may be because of the commercial grade sodium used in this investigation. Particles of graphite or dirt, contained within the commercial grade sodium or picked up by it during transfer, may have nucleated within the sodium at the superheats observed during this investigation. These particles would have to be about .001 in. in diameter to contain an active site which would nucleate at liquid superheats near 150°F.

Effect of Material

Figure 35 shows the effect of material on nucleation stability of sodium. The data of stainless steel 316 and nickel "A" surfaces are compared. Both surfaces were prepared in an identical way, with a LAP A finish. Note that the stainless steel surface was unstable whereas the nickel surface was stable. This result confirms the earlier prediction in Chapter 2 of the proposed stability model that stability improves as the product $\alpha_w^{-a} \sqrt{R_w \rho_w c_w}$ increases. However, as pointed out by Berenson (10), even though the two surfaces were lapped in an identical manner, a different

microscopic surface finish or cavity size distribution may have resulted because of the difference in hardness between these metals. This alteration of the cavity size distribution may also have caused the observed difference in stability.

Noyes (6) mentions that in his experiments a molybdenum test surface acted erratically whereas a stainless steel surface acted normally. This directly contradicts the prediction of Chapter 2 and the observed results of this investigation, shown in Fig. 35.

However, since no mention was made of surface conditions throughout Noyes' work, it is difficult to formulate any conclusive ideas regarding this discrepancy. Noyes does mention though that one of his surface thermocouples was found to protrude from the stainless steel test section. This may have created an artificial nucleation site on this stainless steel surface which would improve stability and would lower the observed superheats.

Effect of Chemical Treatment

Figure 36 shows what effect chemical etching has on the stability of a surface. Data is compared for Run 11 with MIRROR 2 and for Run 14 after etching MIRROR 2 for ten minutes with Aqua Regia, and after making no other alterations.

Results clearly show that etching has reduced stability. This can be explained if we examine what happens during chemical "polishing" of a surface.

We present the views of Tegar (40) and postulate what happens when an acid is placed over a metal surface. We assume that the metal surface contains many valleys and pits on a microscopic level. When an acid is placed over this surface, and a chemical reaction takes place, it is assumed that a viscous layer of complex ions form and remain near the metal surface. These ions will remain in the cavities and pits, and will prevent any further acid from attacking the inside of the cavities. However, the peaks of the surface will constantly be washed clean of these complex ions due to the turbulent bubble motion of evolved gases. Consequently, all the peaks will tend to be reduced, and the surface will be smoothed out, or "polished". In effect then, for our boiler, the depth of any existing cavities was reduced and at the same time, the effective cavity mouth size was increased. If the cavity depth, L , is decreased, then as shown in Chapter 2, n^* is increased, suggesting that instability should become worse. In addition, if the effective cavity radius is increased, then when nucleation does occur the wall superheat should be lowered. This argument explains the observed results in Fig. 36.

Effect of Artificial Cavities

From Fig. 37 and from the temperature-time trace of Fig. 34, it is clear that cylindrical type artificial cavities are not effective in producing stable boiling, although they do lower the observed superheats during both boiling and non-boiling operation. On the other hand, as verified by the results of Fig. 26 and Fig. 27, the artificial doubly re-entrant cavities and porous welds are very stable, confirming once again the predictions of the proposed stability model of Chapter 2.

It is interesting to note that Hoffman (22) reports that a "hot finger" improved stability during operation of a potassium boiling loop at Oak Ridge. This "hot finger" was a .050 in. dia. x .250 in. deep hole drilled in the boiler wall, and it was heated from below. If we consider this "hot finger" as a nucleating cavity, and substitute the "hot finger" dimensions into the stability criterion, Eq. (21) of Chapter 2, then for sodium, keeping all other constants the same as used in Chapter 2, η^* is reduced from 17,500 to 1.93. This is a rather remarkable and surprising result for it says that a large, deep cavity is far more stable than a small, shallow cavity, even though the L/D ratio for the two cavities is the same. This result, coupled with the fact that the "hot finger"

was heated from below, suggests indeed that this type cavity would improve stability.

Effect of Porous Coating

Results of Run 29 and Run 30 show that the porous coating was the most stable boiler surface used in this investigation. Figure 38 shows the data for this surface. In this figure, the wall temperature is actually the interface temperature between the solid nickel boiler and the porous plate. Consequently the large thermal resistance across the porous plate is included in the results and this lowers the slope of the data. Note that the porous coating nucleates for low heat fluxes at a superheat very near the doubly re-entrant cavity data. Since this porous coating data has a slope slightly greater than one, then if we assume a pure conduction resistance across the porous plate which varies linearly with temperature, and subtract this resistance from the observed results, then we would have nucleate boiling data for the porous coating which would be very similar to the doubly re-entrant cavity data. These results indeed show that the porous plate was saturated with re-entrant type cavities as previously observed in Fig.14.

Effect of Heat Flux

All the unstable data show that as the heat flux is increased, then stability improves. This also agrees with the earlier prediction of Chapter 2 regarding the influence of heat flux on stability. The experimental results show that around 200,000 BTU/hr.ft.², stable boiling occurs in most cases.

5.6 Effect of Pool Depth

Figure 39 shows the data taken for Run 17, Run 18 and Run 19. No changes in surface condition occurred during these runs, and the inside walls of the boiler pipe were polished to a mirror finish to a height 9 inches above the test surface. During these runs, the pool depth was varied from 1.4 in. for Run 17, to 2.7 in. for Run 18, to 6.7 in. for Run 19. Results show that the heat transfer coefficient increases from the 1.4 in. depth to the 2.7 in. depth. This is a reasonable result because at a 1.4 in. depth mostly conduction is occurring in the sodium pool, whereas at a depth of 2.7 in. (which gives a depth to diameter ratio of approximately one), then large laminar natural convection currents may improve the heat transfer results. Upon increasing the depth further to 6.7 in., the heat transfer coefficient decreases. This is a surprising result and no plausible explanation can be given

for this behavior. Furthermore, the data all seem to converge at higher heat flux levels.

We may postulate about the odd behavior upon increasing the depth from 2.7 in. to 6.7 in. This change in heat transfer coefficient may be caused by a turbulent natural convection interference effect occurring in this type geometry. This interference effect was observed by Bayley and Lock (41) for a closed thermosyphon. They postulate that in a vertical system where heat is added at the bottom and heat is removed at the top, then hot liquid currents would rise next to the heated walls inside the liquid pool, but cold liquid condensate from above would be flowing down the walls at the same time. When these two streams meet at the free surface, a certain amount of orderly mixing must take place without disturbing the established natural convection pattern within the liquid pool. If turbulent mixing occurs at the free surface then the natural convection pattern in the pool is disturbed and the heat transfer rate is reduced. Increasing the pool depth to large depth to diameter ratios may cause this turbulent mixing.

In any event, the results show that the chosen geometry of a 2 9/16 in. diameter horizontal disc, welded to a vertical pipe was not a one-dimensional system as originally thought. In addition, for this geometry, the pool depth, and consequently natural convection, may play an important role in the low heat flux region of sodium boiling.

6. SUMMARY WITH RECOMMENDATIONS

6.1 Nucleate Boiling of Sodium

Summary

A simplified theoretical model for bubble nucleation stability has been proposed, and an approximate stability criterion has been developed which suggests that nucleation for sodium should be far more unstable than for ordinary liquids. This simplified model predicts that fluid properties, surface material properties, heat flux and cavity geometry should all affect stability.

An experimental system has been designed and constructed. Commercial grade sodium has boiled off a horizontal flat disc 2 9/16 in. in diameter, made either of stainless steel or nickel; the vapors have risen inside a vertical stainless steel pipe and have condensed due to forced convection of air. Boiling has taken place at pressures of 65 mm, 200 mm, and 400 mm Hg absolute with sodium temperatures ranging from 1200°F to 1500°F. Heat fluxes as high as 236,000 BTU/hr.ft.² have been attained.

Nucleate boiling was studied over a wide range of surface conditions. In general, nucleate boiling results were reproducible for a given type surface. As the pressure

increased, the nucleate boiling heat transfer coefficient was shown to increase. Figure 40 is a comprehensive plot showing curves for most of the heat transfer data taken at an average pressure of 65 mm Hg. The results clearly show how surface conditions affect incipience of boiling, nucleate boiling superheats and also the shape of the nucleate boiling curve. The model of Bergles and Rohsenow (36) for the criterion of incipient boiling was used to explain the large "overshoot" of the sodium data.

Large temperature fluctuations were recorded in the boiler wall and temperature-time charts were shown for a few different surfaces. These temperature fluctuations were accompanied by "bumps" which were especially significant during unstable boiling. The coincidence between the wall temperature and the test section noise level was recorded to "observe" the test section behavior. Large nucleate boiling hysteresis effects were also noted which seemed to depend on the non-condensable gas content in the system.

Unstable boiling was "observed" on several occasions and it was experimentally shown that surface material, chemical treatment, heat flux and cavity geometry all influenced the nucleation stability of sodium. These results confirmed the predictions of the proposed stability model.

An effect of pool depth on boiling results was observed. This effect was not entirely explainable.

Conclusions

The above results lead to the following conclusions:

1. Surface roughness and past history can significantly affect the incipient boiling, the nucleate boiling wall superheat, and the slope of the boiling curve of sodium.
2. Surface roughness, surface material, chemical treatment and heat flux all alter nucleation stability of sodium.
3. Any welds inside a test section may contain "rogue" nucleation sites which can affect sodium nucleate boiling results.
4. For sodium, the proposed stability mechanism of interface penetration controlled by condensation seems plausible.
5. Only re-entrant type cavities are effective in maintaining nucleation stability of sodium.
6. Natural convection in this type geometry, particularly at low boiling heat fluxes, may have an appreciable influence on the heat transfer results of sodium.

6.2 Recommendations

It is recommended that:

1. In designing an alkali metal boiler, some type of artificial nucleating site should be used to maintain stability. This device may be in the form of a doubly re-entrant type cavity; a patch of porous plate or porous weld; or a "hot finger."
2. Further work on the mechanism of stability should be performed, investigating the effects of material and pressure experimentally, and investigating the effects of inertia and viscosity theoretically.
3. The bubble growth cycle for the alkali metals should be studied. A doubly re-entrant type cavity should be locally instrumented to measure local wall temperature, noise level and possibly bubble sizes.
4. The effect of sodium purity should be investigated as well as the effect of additives on the nucleate boiling curve.
5. The effect of surface conditions for other alkali metals during boiling should be performed.
6. Finally, a study of natural convection should be made for this type geometry, which if coupled with a study of the bubble growth cycle, may furnish new insight into the mechanism of nucleate boiling at low heat flux levels.

NOMENCLATURE

- a = empirical exponent from ref. (29) which varies with surface roughness
- A = surface area of the liquid-vapor interface
- A_c = cross-sectional area of a cavity
- b = empirical coefficient defined by $\frac{2\Delta q}{Q_0}$ and approximately equal to 20
- c = empirical coefficient from ref. (29) which varies with surface roughness
- C_L = specific heat of the liquid
- C_w = specific heat of the boiler wall
- f = bubble frequency
- h = height of a spherical segment
- h_{fg} = latent heat of vaporization
- J = mechanical equivalent of heat
- k_L = thermal conductivity of the liquid
- k_w = thermal conductivity of the boiler wall
- K = $c \left[Q_0 \sqrt{f/\alpha_w} \right]^{-a} \frac{Q_0}{k_w}$ = empirical coefficient used to determine the minimum wall temperature during bubble nucleation at a cavity
- l = $\left(\frac{\rho_V}{\rho_L} \right) L$ = condensate thickness within a cavity
- L = overall depth of a cavity
- p = pressure
- p_L = pressure in the liquid
- p_V = pressure in the vapor
- p_g = partial pressure of non-condensable gas

- $Q_0 = \frac{Q}{A}$ = heat flux per unit area in the boiler wall
 Δq = step change in heat flux near a cavity during bubble growth
 $Q(t)$ = fictitious volumetric heat source within the liquid during interface penetration into a cavity
 r = radius of hemispherical bubble on a surface
 R = radius of curvature of liquid-vapor interface
 R_c = cavity radius
 t = time during interface penetration into a cavity
 t^* = time for the liquid-vapor interface to reach its maximum penetration into a cavity
 s = Laplace transform variable
 T = temperature
 T_L = temperature of the liquid
 $T_m = T_v$ = temperature of the liquid-vapor interface
 T_0 = initial temperature of both the liquid and the boiler wall during interface penetration into a cavity
 T_{MAX} = local maximum surface temperature of the boiler wall during bubble nucleation at a cavity
 T_{MIN} = local minimum surface temperature of the boiler wall during bubble nucleation at a cavity
 T_{SAT} = saturation temperature at the liquid pressure
 T_w = surface temperature of the boiler wall
 $T_v = T_m$ = saturation temperature at the vapor pressure
 x = axial position in boiler test plate
 $x(t)$ = liquid-vapor interface penetration distance into a cavity during bubble nucleation

- x^* = maximum interface penetration distance into a cavity
- y = distance into the liquid, measured from the boiler surface
- $V(t)$ = $\frac{dx(t)}{dt}$ = velocity of the liquid-vapor interface during penetration into a cavity.
- $\mathcal{V}(t)$ = vapor volume change during interface penetration into a cavity
- α_L = thermal diffusivity of the liquid
- α_w = thermal diffusivity of the boiler wall
- λ = distance into the liquid within a cavity, measured from the liquid-vapor interface
- ε = empirical coefficient, less than one, used to approximate the wall temperature rise during the bubble waiting period
- η^* = $\frac{x^*}{l}$ = dimensionless interface penetration distance
- σ = surface tension
- ρ_L = density of the liquid
- ρ_w = density of the boiler wall
- θ = dynamic contact angle
- τ = bubble growth time during nucleation from a cavity

BIBLIOGRAPHY

1. "Final Summary Safeguards Report for the Hallam Nuclear Power Facility", NAA-SR-5700.
2. Smith, C.R., Tang, Y.S., and Ross, P.T., "Potassium-Mercury Amalgam Heat Transfer and Two-Phase Flow Investigation", Allison Research and Engineering Report, Vol. 1 (1964).
3. Lyon, R.E., Foust, A.S., and Katz, D.L., "Boiling Heat Transfer with Liquid Metals", Chem. Engr. Prog. Symposium Series No. 17, 51 (1955).
4. Madsen, N., and Bonilla, C.F., "Heat Transfer to Boiling Sodium-Potassium Alloy", 3rd. National Heat Transfer Conference, Storrs, Conn. (1959).
5. Noyes, R.C., "An Experimental Study of Sodium Pool Boiling Heat Transfer", NAA-SR-6769 (1962).
6. Noyes, R.C., "Boiling Studies for Sodium Reactor Safety, Part 1", NAA-SR-7909 (1963).
7. Brooks, R.D., "Alkali Metals Boiling and Condensing Investigations, Vol. 1 Experimental Program", Final Report, NASA Contract NAS. 5-681 (1964).
8. Colver, C.P., "A Study of Saturated Pool Boiling Potassium up to Burnout Heat Fluxes", Ph.D. Thesis, University of Michigan (1963).
9. Corty, C., and Foust, A.S., "Surface Variables in Nucleate Boiling", A.I.Ch.E. Heat Transfer Conference, St. Louis, Mo. (1953).
10. Berenson, P.J., "Experiments on Pool Boiling Heat Transfer", Int'l. Jl. of Heat and Mass Transfer, 5, October (1962).
11. Bonilla, C.F., Grady, J.J., and Avery, G.W., "Pool Boiling Heat Transfer from Scored Surfaces", 6th. National Heat Transfer Conference, Boston, Mass. (1963).
12. Stock, B.J., "Observations on Transition Boiling Heat Transfer Phenomena", ANL-6175 (1960).

13. Harrison, W.B., and Levine, Z., "Wetting Effects on Boiling Heat Transfer", ASME-A.I.Ch.E. Heat Transfer Conference, State College, Pa. (1957).
14. Dunskus, T., and Westwater, J.W., "The Effect of Trace Additives on the Heat Transfer to Boiling Isopropanol", ASME-A.I.Ch.E. Heat Transfer Conference, Buffalo, N.Y. (1960).
15. Denney, V.E., "Some Effects of Surface Microgeometry on Natural Convection and Pool Boiling Heat Transfer to Saturated Carbon Tetrachloride", Ph.D. Thesis, University of Minnesota (1961).
16. Averin, E.K., "The Effect of the Material and of the Mechanical Treatment of the Surface on the Heat Exchange in the Boiling of Water", Izv. A. K. Nauk, USSR, Otd. Tekh. Nauk, 3, pp. 116-122 (1954) (AERE-Lib/Trans.-562).
17. Young, R.K., and Hummel, R.L., "Higher Coefficients for Heat Transfer with Nucleate Boiling", 7th. National Heat Transfer Conference, Cleveland, Ohio (1964).
18. Wahl, M.H., MSA Research Corp., Private Correspondence (1962).
19. Addison, C.C., Iberson, E., and Manning, J.A., "The Role of Oxide Films in the Wetting of Iron, Cobalt and Nickel by Liquid Sodium, and by Solutions of Barium and Calcium in Liquid Sodium", Jour. Chem. Soc., pp. 2699-2705, July (1962).
20. Bankoff, S.G., "Ebullition from Solid Surfaces in the Absence of a Pre-existing Gaseous Phase", Heat Transfer and Fluid Mechanics Institute, Stanford, Cal. (1956).
21. Westwater, J.W., Advances in Chemical Engineering, Vol. 1 (1956).
22. Hoffman, E.E., "Metals and Ceramics Div. Annual Progress Report", ORNL-3470, pp. 114-118 (1963).
23. Bankoff, S.G., "Prediction of Surface Temperatures at Incipient Boiling", Chem. Engr. Prog. Symposium Series, Chicago, Ill. (1959).

24. Florschuetz, L.W., and Chao, B.T., "On the Mechanics of Vapor Bubble Collapse", 7th. National Heat Transfer Conference, Cleveland, Ohio (1964), Paper No. 64-HT-23.
25. Fabric, S., "Vapor Nucleation on Surfaces Subjected to Transient Heating", Ph.D. Thesis, University of California (1964).
26. Moore, F.D., and Mesler, R., "The Measurement of Rapid Temperature Fluctuations during Nucleate Boiling of Water", A.I.Ch.E. Jl. (1961).
27. Bonnet, C., Macke, E., and Morin, R., "Visualisation de L'ebullition Nucleee de L'eau a Pression Atmospherique et Mesure Simultanee des Variations de Temperature de Surface", EUR 1622. f Ispra, Italy (1964).
28. Marcus, B.D., "Experiments on the Mechanism of Saturated Nucleate Pool Boiling Heat Transfer", Ph.D. Thesis, Cornell University (1963).
29. Hsu, S.T., and Schmidt, F.W., "Measured Variations in Local Surface Temperatures in Pool Boiling of Water", ASME-A.I.Ch.E. Heat Transfer Conference, Buffalo, New York (1960).
30. McFadden, P.W., and Grassman, P., "The Relation Between Bubble Frequency and Diameter during Nucleate Pool Boiling", Int'l. Jl. of Heat and Mass Transfer, 5, March-April (1962).
31. Lowery, A.J. and Westwater, J.W., "Heat Transfer to Boiling Methanol, Effect of Added Agents", Indust. and Engr. Chemistry, 49, 1445-1448 (1957).
32. Griffith, P., and Wallis, J.D., "The Role of Surface Conditions in Nucleate Boiling", ASME-A.I.Ch.E. Heat Transfer Conference, Storrs, Conn. (1959).
33. Sparrow, E.M., and Lin, S.H., "Absorption of Thermal Radiation in a V-Groove Cavity", Int'l. Jl. of Heat and Mass Transfer, 5, November (1962).
34. National Research Corporation Data Sheet, Stabilized Grain Size Tantalum (1964).

35. Bonilla, C.F., Sawhney, D.L., and Makansi, M.M., "Vapor Pressure of Alkali Metals, III Rubidium, Cesium, and Sodium-Potassium Alloy up to 100 Pounds per Square Inch", Proceedings of 1962 High-Temperature Liquid-Metal Heat Transfer Technology Meeting, BNL 756 (1962).
36. Bergles, A.E., and Rohsenow, W.M., "Forced Convection Surface Boiling Heat Transfer and Burnout in Tubes of Small Diameter", M.I.T. Report No. 8767-21 (1962).
37. Hsu, Y.Y., "On the Size Range of Active Nucleation Cavities on a Heating Surface", Trans. ASME, 84, 207 (1962).
38. Hoffman, H.W., and Krakoviak, A.I., "Convective Boiling with Liquid Potassium", Heat Transfer and Fluid Mechanics Institute, Stanford, Cal. (1964).
39. Balzhiser, R.E., "Investigation of Boiling Liquid Metal Heat Transfer", University of Michigan, Report RTD-TDR-63-4130 (1963).
40. Tegart, W.J., McG., The Electrolytic and Chemical Polishing of Metals, Pergamon Press, New York (1959).
41. Bayley, F.J., and Lock, G.S.H., "Heat Transfer Characteristics of the Closed Thermosyphon", 7th. National Heat Transfer Conference, Paper No. 64-HT-6, Cleveland, Ohio (1964).
42. Hogan, C.L., and Sawyer, R.B., "The Thermal Conductivity of Metals at High Temperature", JI. of Applied Physics, 23, 177 (1952).

APPENDIX A

SOLUTION OF THE APPROXIMATE ENERGY

EQUATION IN THE LIQUID, EQ. (5)

The approximate energy equation (given in Chapter 2) with its initial and boundary conditions is

$$\frac{\partial T_L(\lambda, t)}{\partial t} = \alpha_L \frac{\partial^2 T_L(\lambda, t)}{\partial \lambda^2} + \frac{Q(t)}{\rho_L c_L} \quad (A-1)$$

$$\text{at } t = 0: \quad T_L(\lambda, 0) = T_0, \quad Q(0) = 0 \quad (A-2)$$

$$\text{at } t > 0: \quad A k_L \left. \frac{\partial T_L(\lambda, t)}{\partial \lambda} \right|_{\lambda=0} = \rho_v h_{fg} \frac{dV}{dt} \quad (A-3)$$

$$T_L(0, t) = T_m = T_v = \text{constant} \quad (A-4)$$

$$T_L(\infty, t) = T_w(t) \quad (A-5)$$

Setting $\lambda \rightarrow \infty$ in Eq. (A-1) and applying Eq. (A-5) gives

$$\frac{dT_w(t)}{dt} = \frac{Q(t)}{\rho_L c_L} \quad (A-6)$$

Defining a new variable

$$\Phi(\lambda, t) = T(\lambda, t) - T_0 \quad (A-7)$$

where T_0 is the initial wall temperature, then the preceding equations take the following form.

Equation (A-6) becomes

$$\frac{Q(t)}{\rho_L c_L} = \frac{d\Phi_w(t)}{dt}$$

Equations (A-1) through (A-5) become

$$\frac{\partial^2 \Phi_L(\lambda, t)}{\partial \lambda^2} - \frac{1}{\alpha_L} \frac{\partial \Phi_L(\lambda, t)}{\partial t} = - \frac{1}{\alpha_L} \frac{d\Phi_w(t)}{dt} \quad (\text{A-8})$$

$$\Phi_L(\lambda, 0) = 0, \quad \Phi_w(0) = 0 \quad (\text{A-9})$$

$$\Phi_L(\infty, t) = \Phi_w(t) < \infty \quad (\text{A-10})$$

$$\Phi_L(0, t) = T_m - T_0 = \text{constant} \quad (\text{A-11})$$

and

$$\left. \frac{\partial \Phi_L(\lambda, t)}{\partial \lambda} \right|_{\lambda=0} = F(t) \quad (\text{A-12})$$

where

$$F(t) = \frac{\rho_V h_{fg}}{R_L} \frac{1}{A} \frac{d\mathcal{V}}{dt} \quad (\text{A-13})$$

If we take the Laplace transform of Eq. (A-8) and use Eq. (A-9), we get

$$\frac{d^2 \bar{\Phi}_L(\lambda, s)}{d\lambda^2} - \frac{s}{\alpha_L} \bar{\Phi}_L(\lambda, s) = - \frac{s}{\alpha_L} \bar{\Phi}_w(s) \quad (\text{A-14})$$

which is a linear, second order non homogeneous ordinary differential equation. Equation (A-14) has a well-known solution

$$\bar{\Phi}_L(\lambda, s) = C_1 e^{-\lambda \sqrt{s/\alpha_L}} + C_2 e^{\lambda \sqrt{s/\alpha_L}} + \bar{\Phi}_w(s) \quad (\text{A-15})$$

From Eq. (A-10) we see that $C_2 \equiv 0$, or that

$$\bar{\Phi}_L(\lambda, s) = C_1 e^{-\lambda \sqrt{s/\alpha_L}} + \bar{\Phi}_w(s) \quad . \quad (A-16)$$

Now, Eq. (A-12) in the Laplace domain requires that

$$\left. \frac{d\bar{\Phi}_L(\lambda, s)}{d\lambda} \right|_{\lambda=0} = \bar{F}(s) \quad .$$

Applying this condition to Eq. (A-16) gives

$$C_1 = -\sqrt{\alpha_L/s} \bar{F}(s)$$

so that Eq. (A-16) becomes

$$\bar{\Phi}_L(\lambda, s) = \bar{\Phi}_w(s) - \bar{F}(s) \frac{e^{-\lambda \sqrt{s/\alpha_L}}}{\sqrt{s/\alpha_L}} \quad . \quad (A-17)$$

Inverting Eq. (A-17) into the time domain gives

$$\Phi_L(\lambda, t) = \Phi_w(t) - \sqrt{\frac{\alpha_L}{\pi}} \int_0^t \frac{F(\tau) e^{-\frac{\lambda^2}{4\alpha_L(t-\tau)}}}{\sqrt{t-\tau}} d\tau \quad (A-18)$$

where we have utilized the Convolution Theorem:

$$\mathcal{L}^{-1}\{f_1(s) f_2(s)\} = \int_0^t F_1(\tau) F_2(t-\tau) d\tau \quad .$$

Since we are interested only in the solution at $\lambda = 0$,

we may apply Eq. (A-11) to Eq. (A-18) and arrive at

$$T_m - T_o = T_w(t) - T_o - \sqrt{\frac{\alpha_L}{\pi}} \int_0^t \frac{F(\tau) d\tau}{\sqrt{t-\tau}} \quad (A-19)$$

where $F(\tau)$ is given by Eq. (A-13).

In order to eliminate $F(\bar{\tau})$ from Eq. (A-19) we must now compute the surface area of the meniscus, A , and the vapor volume change, $\frac{dV}{dt}$.

We assume that A is the area of the curved surface of a spherical segment of height h , and of spherical radius R

$$A = 2\pi R h \quad . \quad (A-20)$$

But, as seen below,

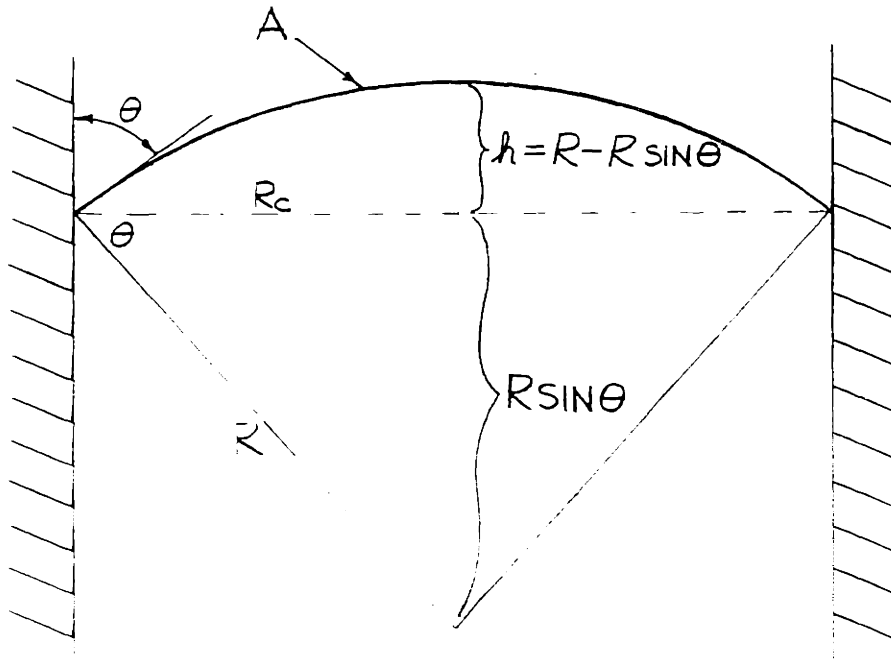
$$h = R(1 - \sin \theta), \text{ and}$$

$$R = R_c / \cos \theta$$

so that

$$A = \frac{2\pi R_c^2}{(1 + \sin \theta)} \quad . \quad (A-21)$$

where R_c is the cavity radius, and θ is the dynamic contact angle.



We define the vapor volume change as

$$\frac{dV}{dt} = \frac{d}{dt} \left\{ \pi R_c^2 (L - X(t)) \right\} \quad (A-22)$$

where L is the overall length of the cavity. Carrying out the differentiation in Eq. (A-22) gives

$$\frac{dV}{dt} = -\pi R_c^2 \frac{dX(t)}{dt} \quad (A-23)$$

Therefore, substituting Eq. (A-21) and Eq. (A-23) in Eq. (A-13) gives

$$F(\tau) = -\frac{\rho_v h_{fg}}{R_L} (1 + \sin \theta) \frac{dX}{d\tau} \quad , \quad (A-24)$$

or upon substituting this result into Eq. (A-19), we arrive at the desired result

$$T_m - T_0 = T_w(t) - T_0 + K_L \int_0^t \frac{dX/d\tau}{\sqrt{t-\tau}} d\tau \quad (A-25)$$

where

$$K_L = \frac{\rho_v h_{fg}}{2\sqrt{\pi R_L R_c}} (1 + \sin \theta) \quad .$$

APPENDIX B
ANALYSIS TO ESTIMATE THE WALL
TEMPERATURE RESPONSE DURING NUCLEATION

It is generally agreed that with nucleate boiling the local surface temperature drops rapidly during the bubble growth time and gradually rises to its original value during the bubble delay time (or, bubble waiting period).

The exact form of this surface temperature response, however, is not well known. Both Moore and Mesler (26) and Bonnet, et al (27) postulate a mathematical model during nucleation. They impose a step change in the rate of surface heat removal, Δq , for a period of time, τ , as shown in Fig. 41, and solve the transient conduction problem in the boiler wall. The solution at the surface of a semi-infinite body initially at a uniform temperature, T_{MAX} , is

$$T_{MAX} - T_w(t') = \frac{2\Delta q}{\sqrt{\pi} R_w \rho_w c_w} \sqrt{t'}, \quad t' \leq \tau \quad (B-1)$$

$$T_{MAX} - T_w(t') = \frac{2\Delta q}{\sqrt{\pi} R_w \rho_w c_w} \left\{ \sqrt{t'} - \sqrt{t' - \tau} \right\}, \quad t' \geq \tau. \quad (B-2)$$

Both Moore and Mesler, and Bonnet, et al show that this step change in heat flux, Δq , is an order of magnitude greater than the average heat flux per unit area in the boiler, Q_0 . In this analysis, we assume that the ratio, $\Delta q/Q_0$, is constant and we define

$$b = \frac{2\Delta q}{Q_0} \approx 20 \quad (B-3)$$

In our stability model we have assumed the wall has already cooled to its minimum value T_0 just as the liquid-vapor interface is at the cavity mouth. Consequently, during interface penetration $t' \geq \tau$ and we are concerned only with Eq. (B-2). If we define $t = t' - \tau$, then Eq. (B-2) becomes

$$T_{MAX} - T_W(t) = \frac{bQ_0}{\sqrt{\pi R_W \rho_W C_W}} \left\{ \sqrt{t + \tau} - \sqrt{t} \right\}, \quad (B-4)$$

where now $t \geq 0$, and where at $t = 0$

$$T_{MAX} - T_W(0) \equiv T_{MAX} - T_{MIN} = \frac{bQ_0}{\sqrt{\pi R_W \rho_W C_W}} \sqrt{\tau} \quad (B-5)$$

In order to simplify Eq. (B-4) we assume that

$$t = \varepsilon \tau, \quad \varepsilon < 1 \quad (B-6)$$

(i.e., we assume that the interface penetration time is less than the assumed bubble growth time, τ), and use this result

to get the approximate relation

$$\sqrt{t + \tau} = \sqrt{\tau}(\sqrt{1 + \epsilon}) \simeq \sqrt{\tau}\left(1 + \frac{\epsilon}{2}\right) \quad . \quad (B-7)$$

This approximation gives a wall temperature colder than that predicted by Eq. (B-2) for $0 < t < \epsilon\tau$. From the form of Eq. (A-25), we see that as the wall temperature decreases, the collapse rate, $dX/d\tau$, of the interface increases since T_m and T_o are constant. Consequently, the assumption Eq. (B-6) imposes a more stringent condition for stability during this time interval $0 < t < \epsilon\tau$.

Substituting Eq. (B-7) into Eq. (B-4) and using Eq. (B-5) gives

$$T_{MAX} - T_w(t) = \left(1 + \frac{\epsilon}{2}\right)(T_{MAX} - T_{MIN}) - \frac{0Q_o}{\sqrt{\pi R_w \rho_w c_w}} \sqrt{t} \quad , \quad (B-8)$$

or upon some algebraic rearranging,

$$T_w(t) = \left\{ T_{MIN} - \frac{\epsilon}{2}(T_{MAX} - T_{MIN}) \right\} + \frac{0Q_o}{\sqrt{\pi R_w \rho_w c_w}} \sqrt{t} \quad (B-9)$$

which is shown as a dotted curve in Fig. 41. We now identify point A of the dotted curve in Fig. 41 as the initial wall temperature, T_o , of the solution in Appendix A. Hence

$$T_o \equiv T_{MIN} - \frac{\epsilon}{2}(T_{MAX} - T_{MIN}) \quad , \quad (B-10)$$

and our final result for Eq. (B-9) becomes

$$T_w(t) - T_o = \frac{bQ_o}{\sqrt{\pi R_w \rho_w c_w}} \sqrt{t} \quad (\text{B-11})$$

which is Eq. (12) of Chapter 2.

We may now rearrange Eq. (B-10) to get

$$T_o - T_{SAT} = T_{MIN} - T_{SAT} - \frac{\epsilon}{2}(T_{MAX} - T_{MIN}) \quad (\text{B-12})$$

or

$$T_o = T_{SAT} + (T_{MAX} - T_{SAT}) - \left(1 + \frac{\epsilon}{2}\right)(T_{MAX} - T_{MIN}). \quad (\text{B-13})$$

It is interesting to note that from Eq. (B-5) the maximum temperature drop during nucleation varies with the average heat flux, surface properties and also bubble frequency (represented by the term $\sqrt{\tau}$). A more useful form for this maximum temperature variation is given by Hsu and Schmidt (29) as

$$T_{MAX} - T_{MIN} = \Delta T_{MAX} = c \left[Q_o \sqrt{f/\alpha_w} \right]^{-a} \frac{Q_o \Delta T_{SAT}}{R_w} \quad (\text{B-14})$$

where $\Delta T_{SAT} = T_{MAX} - T_{SAT}$, and where c is an empirical coefficient which varies with surface roughness,

Q_o is the average heat flux per unit area, f is the bubble frequency in number per hour, α_w is the thermal diffusivity of the surface, k_w is the thermal conductivity of the surface and a is an empirical exponent which varies with roughness.

If we let

$$K = c \left[Q_o \sqrt{f/\alpha_w} \right]^{-a} \frac{Q_o}{k_w} \quad (B-15)$$

then upon substituting Eq. (B-14) into Eq. (B-13) and assuming

$T_{MAX} \simeq T_m$ (the interface temperature which was assumed equal to the saturation temperature of the trapped vapor), we get

$$T_o = T_{SAT} + \left[1 - \left(1 + \frac{\epsilon}{2} \right) K \right] (T_m - T_{SAT}), \quad (B-16)$$

which is Eq. (13) of Chapter 2.

Hsu and Schmidt (29) present the following table of coefficients and exponents for Eq. (B-14).

<u>Surface Description</u>	<u>a</u>	<u>c</u>
Aluminum, 13RMS	0.706	41.2
Stainless Steel, 5.2RMS	1.030	297.6
Stainless Steel, 19RMS	0.630	5.865
Stainless Steel, 21RMS	0.688	16.44
Stainless Steel, 140RMS	0.920	484.6

Note that neither σ nor ρ vary in a systematic fashion. If we use the results for the stainless steel, 140PMS surface, assuming a heat flux of 50,000 BTU/hr.ft.², and using averaged frequency values as indicated below, we obtain the following table for γ .

<u>Liquid</u>	<u>\bar{f} (cps.)</u>	<u>γ</u>
Methyl Alcohol	27 (Ref. 30)	0.274
Water	32 (Ref. 29, 30)	0.246
Nitrogen	95 (Ref. 30)	0.352
Sodium	1.3*	0.830

It is important to see here that γ is less than one in all cases.

* The frequency value for sodium was estimated by counting the boiling noise during nucleation, from the results given in Fig. 18.

APPENDIX C

TABULATION OF RESULTS

Table C-1

Run: 1

Date: 3/25/64

Surface Condition: nickel "A", MIRROR 1; previously run and re-cleaned three times.

Sodium Condition: solidified from previous run; depth 5.6 in.

P (mm)	T _{sat} (°F)	T _L (°F)	Q/A (BTU/hr.ft. ²)	T _w (°F)	T _w -T _{sat} (°F)	Remarks
69	1229	1202	23,900	1239	10	Nat.Conv.
70	1231	1257	41,400	1290	59	Nat.Conv.
69	1229	1282	52,000	1332	103	Before Bump
69	1229	1314	97,200	1362	133	Before Bump
69	1229	1223	73,700	1263	34	Stable Boil.
67	1226	1215	82,400	1265	39	Stable Boil.

Run: 2

Date: 4/3/64

Surface Condition: unchanged from Run 1.

Sodium Condition: solidified from Run 1; depth 5.6 in.

P (mm)	T _{sat} (°F)	T _L (°F)	Q/A (BTU/hr.ft. ²)	T _w (°F)	T _w -T _{sat} (°F)	Remarks
60	1211	1219	32,600	1249	38	Nat.Conv.
61	1213	1249	47,800	1311	98	Before Bump
55	1200	1300	63,700	1334	134	Before Bump
64	1220	1224	114,700	1263	43	Stable Boil.
66	1224	1226	152,500	1284	60	Stable Boil.
66	1224	1224	60,400	1257	33	Stable Boil.

Table C-2

Run: 3

Date: 5/1/64

Surface Condition: nickel "A", MIRROR 2; unoxidized; sprayed with acetone before assembly.

Sodium Condition: transferred from fill tank; depth 3.5 in.

P (mm)	T _{sat} (°F)	T _L (°F)	Q/A (BTU/hr.ft. ²)	T _w (°F)	T _w -T _{sat} (°F)	Remarks
61	1213	1158	31,800	1245	32	Nat.Conv.
63	1218	1208	69,700	1250	32	Stable Boil.
56	1202	1203	104,000	1237	35	Stable Boil.
58	1207	1208	127,500	1245	38	Stable Boil.
60	1211	1213	149,000	1256	45	Stable Boil.
64	1220	1223	175,000	1267	47	Stable Boil.
65	1222	1223	208,000	1273	51	Stable Boil.
65	1222	1222	232,000	1277	55	Stable Boil.
62	1215	1179	23,000	1253	38	Nat.Conv.
64	1220	1218	78,200	1253	33	Stable Boil.
64	1220	1218	126,000	1253	33	Stable Boil.
61	1213	1193	14,700	1247	34	Nat.Conv.

Run: 4

Date: 5/6/64

Surface Condition: unchanged from Run 3.

Sodium Condition: solidified from Run 3; depth 3.5 in.

P (mm)	T _{sat} (°F)	T _L (°F)	Q/A (BTU/hr.ft. ²)	T _w (°F)	T _w -T _{sat} (°F)	Remarks
60	1211	1085	11,300	1218	7	Nat.Conv.
60	1211	1145	29,000	1245	34	Nat.Conv.
62.5	1216	1154	43,600	1250	34	Before Bump
64.5	1221	1211	57,000	1248	27	Stable Boil.
63.5	1218	1214	73,000	1251	33	Stable Boil.
65	1222	1218	111,000	1254	32	Stable Boil.
62	1215	1209	164,000	1257	42	Stable Boil.
200	1382	1368	74,200	1393	11	Stable Boil.
199	1381	1368	124,200	1394	13	Stable Boil.
199	1381	1369	171,000	1399	18	Stable Boil.
403	1500	1486	78,300	1507	7	Stable Boil.
401.5	1499	1486	137,000	1508	9	Stable Boil.
403	1500	1486	193,000	1513	13	Stable Boil.

Table C-3

Run: 5

Date: 5/12/64

Surface Condition: unchanged from Run 4.

Sodium Condition: solidified from Run 4; depth 3.5 in.

P (mm)	T _{sat} (°F)	T _L (°F)	Q/A (BTU/hr.ft. ²)	T _w (°F)	T _w -T _{sat} (°F)	Remarks
398	1497	1434	63,500	1503	6	Stable Boil.
402	1499	1481	76,200	1506	7	Stable Boil.
408	1501	1487	103,000	1508	7	Stable Boil.
400	1498	1488	122,000	1508	10	Stable Boil.

Run: 6

Date: 5/22/64

Surface Condition: unchanged from Run 5.

Sodium Condition: solidified from Run 5; depth 3.5 in.

P (mm)	T _{sat} (°F)	T _L (°F)	Q/A (BTU/hr.ft. ²)	T _w (°F)	T _w -T _{sat} (°F)	Remarks
398.5	1497	1289	38,500	1525	28	Nat.Conv.
397	1497	1441	58,200	1505	8	Unsta.Boil.
392	1494	1479	79,500	1501	7	Stable Boil.
397	1497	1487	101,500	1505	8	Stable Boil.
192	1376	1336	35,200	1428	52	Nat.Conv.
191.5	1376	1348	52,300	1385	9	Unsta.Boil.
192	1376	1364	77,200	1387	11	Stable Boil.
196	1379	1370	94,500	1393	14	Stable Boil.
201	1383	1375	119,000	1399	16	Stable Boil.
200	1382	1372	113,000	1397	15	Stable Boil.
197.5	1380	1371	148,000	1396	16	Stable Boil.
197.5	1380	1371	65,500	1391	11	Stable Boil.

Run: 7

Date: 5/25/64

Surface Condition: unchanged from Run 6.

Sodium Condition: solidified from Run 6; depth 3.5 in.

P (mm)	T _{sat} (°F)	T _L (°F)	Q/A (BTU/hr.ft. ²)	T _w (°F)	T _w -T _{sat} (°F)	Remarks
56	1202	-	38,600	1234	32	Nat.Conv.
56	1202	-	43,500	1242	40	Before Bump
55.5	1201	-	54,700	1271	70	Before Bump
55.5	1201	-	52,400	1234	33	After Bump
55.5	1201	-	65,700	1225	24	Unsta.Boil.

Table C-4

Run: 8

Date: 5/29/64

Surface Condition: nickel "A", LAF F; unoxidized; sprayed
with acetone before assembly.
Sodium Condition: transferred from fill tank; depth 2.5 in.

P (mm)	T _{sat} (°F)	T _L (°F)	Q/A (BUT/hr.ft. ²)	T _w (°F)	T _w -T _{sat} (°F)	Remarks
60	1211	-	35,900	1227	16	Nat.Conv.
60	1211	-	46,200	1260	49	Before Bump
60	1211	-	57,100	1228	17	After Bump
60	1211	-	76,900	1229	18	Mixed Boil.
61.5	1214	-	100,500	1233	19	Stable Boil.
62	1215	-	126,500	1236	21	Stable Boil.
62	1215	-	153,000	1239	24	Stable Boil.
63	1218	-	190,000	1246	28	Stable Boil.
64	1220	-	218,000	1251	31	Stable Boil.
64	1220	-	236,000	1260	40	Stable Boil.
65	1222	-	198,000	1252	30	Stable Boil.
66	1224	-	143,000	1246	22	Mixed Boil.

Run: 9

Date: 6/20/64

Surface Condition: unchanged from Run 8.
Sodium Condition: solidified from Run 8; depth 2.5 in.

P (mm)	T _{sat} (°F)	T _L (°F)	Q/A (BTU/hr.ft. ²)	T _w (°F)	T _w -T _{sat} (°F)	Remarks
54	1198	-	39,200	1252	54	Nat.Conv.
59	1209	-	50,500	1297	88	Before Bump
59	1209	-	60,000	1231	22	After Bump
56	1202	-	79,000	1226	24	Stable Boil.
56	1202	-	92,000	1236	34	Stable Boil.
56	1202	-	121,000	1244	42	Stable Boil.
60	1211	-	151,000	1260	49	Stable Boil.
63	1218	-	188,000	1273	55	Stable Boil.
63	1218	-	157,000	1267	49	Stable Boil.
59	1209	-	133,000	1250	41	Stable Boil.
63	1218	-	64,000	1247	29	Stable Boil.
62	1215	-	126,000	1257	42	Stable Boil.

Table C-5

Run: 10

Date: 6/26/64

Surface Condition: unchanged from Run 9.

Sodium Condition: solidified from Run 9; depth 2.5 in.

P (mm)	T _{sat} (°F)	T _L (°F)	Q/A (BTU/hr.ft. ²)	T _w (°F)	T _w -T _{sat} (°F)	Remarks
60	1211	-	35,500	1246	35	Nat.Conv.
62	1215	-	46,800	1263	48	Before Bump
62	1215	-	75,200	1227	12	After Bump
57	1205	-	109,000	1226	21	Stable Boil.
55	1200	-	142,000	1228	28	Stable Boil.
59	1210	-	172,000	1239	29	Stable Boil.
58	1207	-	144,000	1234	27	Stable Boil.
56.5	1203	-	104,000	1221	18	Stable Boil.
56	1202	-	62,800	1287	85	Before Bump
58	1207	-	74,200	1233	26	After Bump
60	1211	-	39,600	1277	66	Before Bump
61	1213	-	134,300	1235	22	Stable Boil.
57	1205	-	209,000	1234	29	Stable Boil.

Run: 11

Date: 7/2/64

Surface Condition: nickel "A", MIRROR 2; oxidized; re-cleaned from Run 7.

Sodium Condition: transferred from fill tank; depth 3.0 in.

P (mm)	T _{sat} (°F)	T _L (°F)	Q/A (BTU/hr.ft. ²)	T _w (°F)	T _w -T _{sat} (°F)	Remarks
59	1209	1180	34,400	1242	33	Nat.Conv.
56	1202	1195	63,500	1237	35	After Bump
56	1202	-	58,200	1263	61	Before Bump
60.5	1212	1211	91,700	1250	38	Stable Boil.
54	1198	1196	132,000	1243	45	Stable Boil.
63.5	1219	1217	160,000	1270	51	Stable Boil.
65	1222	1220	183,000	1280	58	Stable Boil.
65.5	1223	1221	147,800	1270	47	Stable Boil.
58	1206	1204	119,000	1245	39	Stable Boil.
54	1198	1195	78,500	1231	33	Stable Boil.
57	1204	1192	56,500	1232	28	After Bump
57	1204	1204	49,800	1276	72	Before Bump
60	1211	1211	112,500	1252	41	Stable Boil.

Table C-6

Run: 12

Date: 7/9/64

Surface Condition: nickel "A", MIRROR 3 with porous welds; unoxidized; sprayed with acetone before assembly.

Sodium Condition: transferred from fill tank; depth 2.5 in.

P (mm)	T _{sat} (°F)	T _L (°F)	Q/A (BTU/hr.ft. ²)	T _w (°F)	T _w -T _{sat} (°F)	Remarks
62	1215	1215	26,000	1233	18	Nat.Conv.
58.5	1208	1208	37,600	1245	37	Before Bump
58.5	1208	1193	45,400	1225	17	After Bump
58.5	1208	1201	68,700	1225	17	Mixed Boil.
59	1209	1202	106,000	1230	21	Stable Boil.
60	1211	1206	130,500	1235	24	Stable Boil.
61	1213	1209	180,000	1242	29	Stable Boil.
61.5	1214	1211	208,000	1246	32	Stable Boil.
62	1215	1213	140,000	1245	30	Stable Boil.
62	1215	1211	117,500	1243	28	Stable Boil.
62	1215	1208	84,000	1239	24	Stable Boil.
62	1215	1208	66,900	1237	22	Stable Boil.
62	1215	1210	113,500	1241	26	Stable Boil.
62	1215	1211	137,500	1244	29	Stable Boil.

Run: 13

Date: 7/10/64

Surface Condition: unchanged from Run 12; aged for 20 hours with boiling sodium.

Sodium Condition: boiled continuously from Run 12; depth 2.5 in.

P (mm)	T _{sat} (°F)	T _L (°F)	Q/A (BTU/hr.ft. ²)	T _w (°F)	T _w -T _{sat} (°F)	Remarks
61	1213	1213	67,000	1256	43	Mixed Boil.
50	1190	1182	22,700	1205	15	Nat.Conv.
50	1189	1183	36,800	1213	24	Nat.Conv.
54	1197	1192	53,900	1235	38	Nat.Conv.
60	1212	1206	67,800	1245	33	Mixed Boil.
69	1229	1223	94,300	1255	26	Stable Boil.
77	1244	1238	109,000	1270	26	Stable Boil.
80	1250	1250	138,000	1278	28	Stable Boil.
83	1261	1261	152,000	1290	29	Stable Boil.
80	1249	1245	113,700	1275	26	Stable Boil.
74	1239	1234	82,000	1263	24	Stable Boil.
60	1211	1211	58,200	1290	79	Before Bump

Table C-7

Run: 14

Date: 7/27/64

Surface Condition: nickel "A", MIRROR 2; re-cleaned after Run 11 and etched in Aqua Regia for ten minutes.

Sodium Condition: transferred from fill tank; depth 3.5 in.

P (mm)	T _{sat} (°F)	T _L (°F)	Q/A (BTU/hr.ft. ²)	T _w (°F)	T _w -T _{sat} (°F)	Remarks
61.5	1214	1167	26,600	1253	39	Nat.Conv.
64	1219	1204	47,700	1282	63	Before Bump
64	1219	1188	56,700	1243	24	After Bump
56.5	1203	-	65,200	1296	93	Before Bump
56.5	1203	-	64,300	1225	22	After Bump
56	1203	-	92,200	1322	119	Before Bump
56	1203	-	101,500	1235	32	After Bump
59	1209	-	114,600	1333	124	Before Bump
59	1209	-	114,500	1248	39	After Bump
60.5	1212	-	135,000	1339	127	Before Bump
63	1218	-	154,000	1261	43	After Bump
69	1229	1221	185,000	1280	51	Stable Boil.

Run: 15

Date: 8/1/64

Surface Condition: nickel "A", MIRROR 4; unoxidized; containing no internal welds.

Sodium Condition: transferred from fill tank; depth 2.5 in.

P (mm)	T _{sat} (°F)	T _L (°F)	Q/A (BTU/hr.ft. ²)	T _w (°F)	T _w -T _{sat} (°F)	Remarks
55	1200	1201	28,100	1238	38	Before Bump
55	1200	1186	29,500	1219	19	After Bump
58	1207	1207	39,000	1271	64	Before Bump
58	1207	1198	50,600	1230	23	After Bump
54.5	1199	-	65,500	1281	82	Before Bump
54.5	1199	-	73,600	1230	31	After Bump
53.5	1197	-	90,600	1281	84	Before Bump
53.5	1197	1191	84,700	1233	36	After Bump
51.5	1193	-	111,500	1292	99	Before Bump
51.5	1193	1197	118,500	1238	45	After Bump
52	1194	-	155,000	1293	99	Before Bump
52	1194	1199	155,000	1260	66	After Bump

Table C-8

Run: 16

Date: 8/3/64

Surface Condition: unchanged from Run 15.

Sodium Condition: solidified from Run 15; depth 2.5 in.

P (mm)	T _{sat} (°F)	T _L (°F)	Q/A (BTU/hr.ft. ²)	T _w (°F)	T _w -T _{sat} (°F)	Remarks
61	1213	-	31,900	1253	40	Nat.Conv.
55	1200	-	57,200	1261	61	Before Bump
54	1198	-	76,500	1280	82	Before Bump
55	1200	-	105,600	1300	100	Before Bump
56.5	1203	-	108,600	1227	24	After Bump
58.5	1208	-	121,000	1304	96	Before Bump
61.5	1212	-	128,500	1250	38	After Bump
65	1222	-	164,000	1270	48	Mixed Boil.
66	1224	-	93,000	1250	26	After Bump
68.5	1228	-	216,000	1281	53	Mixed Boil.

Run: 17

Date: 8/6/64

Surface Condition: nickel "A", machined surface; unoxidized;
welded to polished S.S. 316 pipe.

Sodium Condition: transferred from fill tank; depth 1.4 in.

P (mm)	T _{sat} (°F)	T _L (°F)	Q/A (BTU/hr.ft. ²)	T _w (°F)	T _w -T _{sat} (°F)	Remarks
54.5	1199	1177	32,500	1206	7	Mixed Boil.
55	1200	1196	45,400	1214	14	Stable Boil.
55	1200	1196	59,600	1219	19	Stable Boil.
57	1205	1194	38,000	1221	16	Stable Boil.
57	1205	1202	56,900	1223	18	Stable Boil.
58	1206	1202	86,700	1229	23	Stable Boil.
59	1209	1205	106,600	1236	27	Stable Boil.
58	1207	1200	127,000	1238	31	Stable Boil.
57.5	1206	1204	176,000	1237	31	Stable Boil.
54.5	1197	1195	190,000	1225	28	Stable Boil.
62.5	1216	1212	162,000	1243	27	Stable Boil.

Table C-9

Run: 18

Date: 8/11/64

Surface Condition: unchanged from Run 17.

Sodium Condition: 1.4 in. solidified from Run 17; remaining sodium transferred from fill tank; depth 2.7 in.

P (mm)	T _{sat} (°F)	T _L (°F)	Q/A (BTU/hr.ft. ²)	T _w (°F)	T _w -T _{sat} (°F)	Remarks
57	1204	1195	54,700	1213	9	Stable Boil.
57	1204	1202	77,200	1216	12	Stable Boil.
57	1204	1200	96,500	1218	14	Stable Boil.
63	1218	1209	56,500	1232	14	Stable Boil.
56	1202	1205	76,000	1214	12	Stable Boil.
58	1207	1205	89,200	1221	14	Stable Boil.
59.5	1210	1209	107,000	1233	23	Stable Boil.
59.5	1210	1209	127,000	1232	22	Stable Boil.
60	1211	1210	140,000	1240	29	Stable Boil.
60	1211	1208	160,000	1242	31	Stable Boil.
60	1211	1208	176,000	1243	32	Stable Boil.
60	1210	1210	216,000	1243	33	Stable Boil.

Run: 19

Date: 8/17/64

Surface Condition: unchanged from Run 18.

Sodium Condition: 2.7 in. solidified from Run 18; remaining sodium transferred from fill tank; depth 6.7 in.

P (mm)	T _{sat} (°F)	T _L (°F)	Q/A (BTU/hr.ft. ²)	T _w (°F)	T _w -T _{sat} (°F)	Remarks
53	1196	1154	51,8000	1221	25	Stable Boil.
57	1204	1183	70,000	1235	31	Stable Boil.
58.5	1208	1204	92,800	1241	33	Stable Boil.
58.5	1207	1203	109,000	1241	34	Stable Boil.
58.5	1208	1204	132,500	1238	30	Stable Boil.
58.5	1207	1203	142,500	1238	31	Stable Boil.
58.5	1209	1205	171,500	1243	34	Stable Boil.
60.	1211	1211	202,000	1249	38	Stable Boil.
63	1217	1215	121,600	1247	30	Stable Boil.
62.5	1214	1209	83,400	1242	28	Mixed Boil.

Table C-10

Run: 20

Date: 8/22/64

Surface Condition: nickel "A", LAP A; unoxidized; sprayed with acetone.

Sodium Condition: transferred from fill tank; depth 3.4 in.

P (mm)	T _{sat} (°F)	T _L (°F)	Q/A (BTU/hr.ft. ²)	T _w (°F)	T _w -T _{sat} (°F)	Remarks
58.5	1208	1152	36,900	1226	18	Nat.Conv.
61.5	1214	1160	51,700	1229	15	After Bump
62	1215	1188	60,400	1232	17	Mixed Boil.
61	1213	1206	72,000	1230	17	Mixed Boil.
61	1213	1209	96,000	1232	19	Mixed Boil.
61	1213	1209	127,000	1235	22	Mixed Boil.
61	1213	1214	149,000	1240	27	Stable Boil.
62	1215	1217	176,000	1247	32	Stable Boil.
62.5	1216	1217	192,000	1251	35	Stable Boil.
60.5	1212	1206	143,000	1238	26	Stable Boil.
59.5	1210	1207	112,000	1234	24	Mixed Boil.

Run: 21

Date: 9/2/64

Surface Condition: nickel "A", MIRROR 5; unoxidized; sprayed with acetone.

Sodium Condition: transferred from fill tank; depth 2.4 in.

P (mm)	T _{sat} (°F)	T _L (°F)	Q/A (BTU/hr.ft. ²)	T _w (°F)	T _w -T _{sat} (°F)	Remarks
57	1205	1211	24,500	1228	23	Nat.Conv.
60.5	1212	1225	36,500	1242	30	Before Bump
60.5	1212	1207	42,800	1224	12	After Bump
57	1205	1199	54,700	1220	15	After Bump
57	1205	1203	83,500	1224	19	After Bump
59	1209	1209	118,100	1235	26	After Bump
60	1211	1211	164,000	1237	25	Mixed Boil.
58	1207	1207	216,000	1234	27	Stable Boil.
57.5	1205	-	47,500	1268	63	Before Bump
57.5	1205	1204	60,600	1237	32	After Bump
60	1211	1210	98,800	1245	34	After Bump
62	1215	1215	123,000	1247	32	After Bump

Table C-11

Run: 22

Date: 9/5/64

Surface Condition: nickel "A", MIRROR 3 with porous welds; re-cleaned and re-welded to polished nickel pipe after Run 13; oxidized.

Sodium Condition: transferred from fill tank; depth 2.5 in.

P (mm)	T _{sat} (°F)	T _L (°F)	Q/A (BTU/hr.ft. ²)	T _w (°F)	T _w -T _{sat} (°F)	Remarks
53.5	1197	1191	46,200	1207	10	Nat.Conv.
52	1194	1190	56,700	1208	14	Mixed Boil.
52	1194	1191	99,600	1207	13	Stable Boil.
53	1196	1194	123,500	1210	14	Stable Boil.
54	1198	1200	146,500	1218	20	Stable Boil.
52	1194	1191	160,000	1217	23	Stable Boil.

Run: 23

Date: 9/10/64

Surface Condition: unchanged from Run 22.

Sodium Condition: solidified from Run 22; depth 2.5 in.

P (mm)	T _{sat} (°F)	T _L (°F)	Q/A (BTU/hr.ft. ²)	T _w (°F)	T _w -T _{sat} (°F)	Remarks
55	1200	1200	44,300	1230	30	Nat.Conv.
56.5	1203	1217	62,800	1257	54	Before Bump
57.5	1205	-	77,300	1280	75	Before Bump
57.5	1205	1197	77,600	1220	15	After Bump
56.5	1203	1198	88,500	1224	21	Stable Boil.
56.5	1204	1203	116,200	1227	23	Stable Boil.
59	1209	1208	157,500	1235	26	Stable Boil.
60.5	1212	1212	184,000	1240	28	Stable Boil.
60	1211	1210	140,000	1240	29	Stable Boil.
61	1213	1213	107,000	1235	22	Mixed Boil.
62	1215	1213	89,200	1233	18	Mixed Boil.
62	1215	1214	67,800	1228	13	Mixed Boil.
62	1215	1229	51,700	1267	52	Before Bump
61.5	1214	1212	143,400	1238	24	Stable Boil.
58.5	1208	1207	218,000	1237	29	Stable Boil.

Table C-12

Run: 24

Date: 9/14/64

Surface Condition: nickel "A", MIRROR 4 with no internal welds.
plus ten cylindrical cavities, .004 in. dia.;
re-cleaned and re-polished from Run 16.

Sodium Condition: transferred from fill tank; depth 2.7 in.

P (mm)	T _{sat} (°F)	T _L (°F)	Q/A (BTU/hr.ft. ²)	T _w (°F)	T _w -T _{sat} (°F)	Remarks
54.5	1199	1201	31,500	1213	14	Nat.Conv.
60	1211	1210	59,000	1221	10	After Bump
60	1211	1236	56,500	1250	39	Before Bump
56	1202	1225	92,500	1265	63	Before Bump
56	1202	1253	134,200	1292	90	Before Bump
56	1202	-	133,000	1240	38	After Bump
58.5	1208	-	166,000	1311	103	Before Bump
59	1209	-	168,000	1252	43	After Bump

Run: 25

Date: 9/22/64

Surface Condition: stainless steel 316, LAP A; unoxidized;
sprayed with acetone before assembly.

Sodium Condition: transferred from fill tank; depth 2.6 in.

P (mm)	T _{sat} (°F)	T _L (°F)	Q/A (BTU/hr.ft. ²)	T _w (°F)	T _w -T _{sat} (°F)	Remarks
59	1209	1206	26,700	1217	8	Nat.Conv.
60	1211	1224	39,100	1241	30	Before Bump
60	1211	1249	86,500	1279	68	Before Bump
61	1213	1212	77,500	1230	17	After Bump
60.5	1212	1211	113,500	1236	24	After Bump
56	1202	1247	155,000	1295	93	Before Bump
54	1198	1201	190,000	1236	38	After Bump
54	1198	1262	132,000	1311	113	Before Bump
53	1200	1248	88,400	1303	103	Before Bump

Table C-13

Run: 26

Date: 9/23/64

Surface Condition: unchanged from Run 25.

Sodium Condition: solidified from Run 25; depth 2.6 in.

P (mm)	T _{sat} (°F)	T _L (°F)	Q/A (BTU/hr.ft. ²)	T _w (°F)	T _w -T _{sat} (°F)	Remarks
59	1210	1216	49,500	1222	12	Nat.Conv.
57	1205	1233	73,300	1245	40	Nat.Conv.
55	1200	1201	93,400	1215	15	Stable Boil.
55	1200	1207	125,000	1222	22	Stable Boil.
56	1202	1211	158,000	1232	30	Stable Boil.
57.5	1205	1212	196,000	1244	39	Stable Boil.
58.5	1207	1214	113,200	1232	25	After Bump
59.5	1210	1217	96,800	1228	18	Stable Boil.
60	1211	1214	57,400	1222	11	After Bump
60.5	1212	1219	64,800	1226	14	After Bump
62	1215	1221	135,000	1241	26	Stable Boil.

Run: 27

Date: 10/9/64

Surface Condition: nickel "A", MIRROR 6 with twelve doubly re-entrant cavities, .004 in. mouth dia.; unoxidized.

Sodium Condition: transferred from fill tank; depth 3.7 in.

P (mm)	T _{sat} (°F)	T _L (°F)	Q/A (BTU/hr.ft. ²)	T _w (°F)	T _w -T _{sat} (°F)	Remarks
56.5	1203	1213	41,200	1229	26	Nat.Conv.
59	1209	1211	59,300	1229	20	After Bump
61	1213	1217	98,200	1228	15	After Bump
59.5	1210	1211	126,500	1223	13	Stable Boil.
59.5	1210	1214	166,000	1224	14	Stable Boil.
59.5	1210	1214	192,500	1225	15	Stable Boil.
59.5	1210	1214	182,000	1224	14	Stable Boil.
59.5	1210	1213	142,000	1226	16	Stable Boil.
59.5	1210	1212	92,800	1223	13	Mixed Boil.
59	1209	1227	37,200	1252	43	Nat.Conv.
59	1209	1204	67,100	1222	13	After Bump
60	1211	1214	94,500	1223	12	Stable Boil.
61.5	1214	1216	152,000	1227	13	Stable Boil.

Table C-14

Run: 28

Date: 10/12/64

Surface Condition: unchanged from Run 27.

Sodium Condition: solidified from Run 27; depth 3.7 in.

P (mm)	T _{sat} (°F)	T _L (°F)	Q/A (BTU/hr.ft. ²)	T _w (°F)	T _w -T _{sat} (°F)	Remarks
56.5	1203	1203	42,800	1233	30	Nat.Conv.
56.5	1203	1188	64,200	1215	12	After Bump
55.5	1201	1216	59,200	1260	59	Before Bump
55.5	1201	1197	87,600	1213	12	After Bump
55	1200	1200	116,500	1213	13	Stable Boil.
57	1204	1204	157,000	1218	14	Stable Boil.
55	1200	1199	178,500	1215	15	Stable Boil.
51.5	1194	1193	206,000	1209	15	Stable Boil.
51	1192	1189	101,500	1205	13	Mixed Boil.

Run: 29

Date: 10/31/64

Surface Condition: nickel "A", hand-lapped and coated with 1/32 in. porous nickel plate, 65 μ pore size; hydrogen fired.

Sodium Condition: transferred from fill tank; depth 0.9 in.

P (mm)	T _{sat} (°F)	T _L (°F)	Q/A (BTU/hr.ft. ²)	T _{wi} (°F)	T _{wi} -T _{sat} (°F)	Remarks
51.5	1193	1185	38,800	1206	13	Mixed Boil.
52	1194	1191	53,600	1213	19	Mixed Boil.
52	1194	1191	79,200	1219	25	Stable Boil.
52	1194	1192	108,000	1226	32	Stable Boil.
53	1196	1195	139,300	1238	42	Stable Boil.
54	1198	1198	179,000	1248	50	Stable Boil.
60	1211	1208	133,000	1250	39	Stable Boil.
61	1213	1210	30,600	1230	17	Stable Boil.
61	1213	1210	23,900	1229	16	Stable Boil.
62	1215	1213	65,200	1236	21	Stable Boil.
58.5	1208	1205	128,500	1249	41	Stable Boil.
60	1211	1209	216,000	1263	52	Stable Boil.

Table C-15

Run: 30

Date: 11/3/64

Surface Condition: unchanged from Run 29.

Sodium Condition: 0.9 in. solidified from Run 29; remaining sodium transferred from fill tank; depth 2.5 in.

P (mm)	T _{sat} (°F)	T _L (°F)	Q/A (BTU/hr.ft. ²)	T _{wi} (°F)	T _{wi} - T _{sat} (°F)	Remarks
54	1198	1189	40,300	1208	10	Mixed Boil.
54	1199	1200	59,000	1214	15	Stable Boil.
55.5	1201	1202	78,600	1225	24	Stable Boil.
53	1196	1192	100,500	1225	29	Stable Boil.
56	1202	1200	137,000	1240	38	Stable Boil.
57	1204	1203	170,000	1252	48	Stable Boil.
58	1207	1205	224,000	1264	57	Stable Boil.
56	1202	1188	28,400	1215	13	Mixed Boil.
58.5	1208	1206	77,600	1230	22	Stable Boil.
59	1209	1206	135,000	1245	36	Stable Boil.

APPENDIX D

SAMPLE CALCULATION WITH ERROR ANALYSIS

We arbitrarily utilize the data of point 4 for Run 2, which was obtained during stable nucleate boiling from a nickel "A" surface with a mirror finish.

We assume that each thermocouple position is known to $\pm .010$ inches. The thermal conductivity of nickel is calculated using the experimental results of Hogan and Sawyer (42). They give an accuracy of $\pm 5\%$.

The pressure data recorded for the above point is given below as:

$$p(\text{manometer}) = 65 \pm 0.3 \text{ mm Hg}$$

$$p(\text{Taylor gage}) = 63 \pm 2.5 \text{ mm Hg}$$

Therefore, the average pressure is

$$\bar{p} = 64 \pm 2.5 \text{ mm Hg} \quad (D-1)$$

Calculation of Q/A

The reduced and corrected temperatures for this point are given in Table D-1.

Table D-1

<u>T.C. No.</u>	<u>Distance from Boiler Surface (in.)</u>	<u>Temperature (°F)</u>
1	.660 ± .010	1449 ± 11
2	.470 ± .010	1401 ± 8
3	.280 ± .010	1352 ± 6
4	.090 ± .010	1288 ± 4
5	.090 ± .010	1293 ± 1
6	.090 ± .010	1302 ± 3
11	1/2 in. beneath sodium free surface	1224 ± 5

It should be mentioned here that in every experimental run, T.C. 5 and 6 read higher than T.C. 4. This is evident in the above table and suggests that either a non-uniformity existed in the boiler test plate due to the geometry of the filaments, or some radiation error was distorting the reading of T.C. 4, 5 and 6.

Since T.C. 4 responded to nucleation "bumps" more vigorously than T.C. 5 and 6 (indicating it was reading a more correct wall temperature) and since only T.C. 4 had a value which agreed with a straight line drawn through T.C. 1, 2 and 3, then only T.C. 4 was used to obtain quantitative data, and the effect of T.C. 5 and 6 was neglected.

If T.C. 1, 2, 3 and 4 are plotted versus position from the boiler surface with prescribed error limits included, then connecting the extremes of the data gives the maximum and minimum sloped lines for these points. If we utilize the standard Fourier conduction equation

$$\frac{Q}{A} = k \frac{\Delta T}{\Delta X} \quad (D-2)$$

with the thermal conductivity given by

$$k = 20.3 + .00965 T \quad (D-3)$$

which equation fits the data of Hogan and Sawyer (42), then the maximum and minimum heat flux values are obtained:

$$\begin{aligned} \frac{Q}{A}_{MAX} &= 121,000 \text{ BTU/hr.ft.}^2 \\ \frac{Q}{A}_{MIN} &= 108,500 \text{ BTU/hr.ft.}^2 \end{aligned}$$

where k is evaluated at the average plate temperature T in °F. Averaging these heat flux values gives the final result

$$\frac{Q}{A} = 114,700 \pm 6,200 \text{ BTU/hr.ft.}^2 \quad (D-4)$$

Calculation of T_w

We use Eq. (D-2) between T.C. 4 and the boiler surface to get

$$T_w = T_4 - \frac{Q/A \times X_4}{k} \quad (D-5)$$

Substituting in for T_4 , Q/A , X_4 and k gives

$(T_4 - T_w) = 25^\circ\text{F}$, or $T_w = 1263^\circ\text{F}$. The most probable error for the wall temperature is given by

$$\delta T_w = \sqrt{\delta T_4^2 + (T_4 - T_w)^2 \left[\left(\frac{\delta Q/A}{Q/A} \right)^2 + \left(\frac{\delta R}{R} \right)^2 + \left(\frac{\delta X_4}{X_4} \right)^2 \right]} \quad (\text{D-6})$$

where

$$\frac{\delta Q/A}{Q/A} = \text{fractional error in heat flux} = .054$$

$$\frac{\delta R}{R} = \text{fractional error in thermal conductivity} = .050$$

$$\frac{\delta X_4}{X_4} = \text{fractional error in T.C. 4 position} = .110$$

Since δT_4 is $\pm 4^\circ\text{F}$ from Table D-1 and since $(T_4 - T_w)$ is 25°F , then

$$\delta T_w = 5.2^\circ\text{F}$$

and we have for the wall temperature

$$T_w = 1263 \pm 5.2^\circ\text{F} \quad (\text{D-7})$$

Calculation of $(T_w - T_{\text{sat}})$

The saturation temperature is calculated using Eq. (23) of Chapter 4:

$$\text{LOG}_{10} p = 4.52172 - \frac{5220.42}{T} \quad (\text{D-8})$$

where p is in atmospheres and T is in degrees Kelvin.

Using \bar{p} from Eq. (D-1) in Eq. (D-8), we get:

$$T_{SAT} = 1220 \pm 5^{\circ}F \quad (D-9)$$

Note that T_{II} in Table D-1 agrees quite well with this calculated value.

If we subtract Eq. (D-9) from Eq. (D-7), we get the wall superheat for this data point

$$T_W - T_{SAT} = 43 \pm 7^{\circ}F \quad (D-10)$$

APPENDIX E
SODIUM TECHNOLOGY

Commercial grade sodium was used. A typical chemical analysis of this sodium, as furnished by the Ethyl Corporation, is shown in Table E-1. A qualitative analysis of two sodium samples, obtained from two separate shipments, was performed by the Jarrell-Ash Company in Waltham, Mass. Their results are given in Table E-2, showing that at least qualitatively, the purity of "Ethyl" sodium remained constant.

Sodium was filtered two times before entering the boiler. First of all, oxides and "slag" from the solid sodium brick floated on the top of the liquid sodium within the fill tank, and since the sodium was drawn from the very bottom of the pool, then the impurities were left behind. Large deposits of these impurities were noticed each time the fill tank was re-opened. In addition, all the sodium passed through a firmly packed, fine grade, stainless steel wool filter, before entering the boiler.

No other systematic effort was made to continually monitor the oxygen content or any other impurities within the sodium during a boiling run.

Sodium was cleaned from all the equipment by reacting it with n-butyl alcohol. This was generally done by immersing each piece of equipment into a 55 gallon drum of the alcohol. The drum was covered with a Flame Tamer self-extinguishing head manufactured by CAH Industries, Franklin Park, Illinois, and the reaction took place out of doors. The reaction was always very moderate. No fires ever resulted, and the alcohol remained sufficiently cool even when reacting the sodium from the large vacuum chamber. After approximately 5 pounds of sodium had been reacted with the alcohol, the contaminated alcohol and residue was discarded through the M.I.T. safety office.

As mentioned in Chapter 3, sodium leaked through the bolted flange of the boiler pipe during the initial operation of the system. When this occurred, the sodium vapors entered the high vacuum system indicating a sudden increase in pressure in the vacuum chamber. At the same time, the resistance of the main heater filaments suddenly dropped. All the heaters were immediately shut off, and the vacuum pumps were kept operating. The vacuum was reduced from 10^{-3} mm Hg to 6×10^{-6} mm Hg in about 2 hours. Figure 42 shows two photographs exhibiting the sodium deposits near the boiler flange and within the vacuum chamber.

Corrosion of the test surfaces was never appreciable in any of the boilers, probably because each boiler surface was operated only for about 20 hours. Considerable graphite precipitation was noticed on the inside surface of the stainless steel pipe, particularly in the higher temperature areas.

Table E-1

TYPICAL ANALYSIS AND IMPURITY SPECIFICATIONS

FOR "ETHYL" SODIUM

(Data expressed as ppm by weight)

Commercial Grade

<u>Component</u>	<u>Typical Analysis</u>	<u>Specification</u>
Oxygen	26	-
Calcium	400	500
Nitride	< 10	10
Chloride	17	40
Sulfate	< 30	30
Potassium	600	-
Iron	< 20	40
Copper	< 10	20
Aluminum	< 10	30
Magnesium	20	30
Bismuth	< 10	30
Lithium	< 10	50
Silicon	< 30	30
Tin	< 20	20
Lead	< 10	30
Nickel	< 10	20
Manganese	< 10	20
Strontium	30	50
Barium	10	20

Minimum Purity

(Data expressed as Wt %)

Sodium	-	99.6*
--------	---	-------

* Includes potassium expressed as equivalent sodium.

Table E-2
QUALITATIVE ANALYSIS OF TWO
METALLIC SODIUM SAMPLES
(Data expressed as weight %)

<u>Component</u>	<u>Analysis</u>	
	<u>Sample 1</u>	<u>Sample 2</u>
Magnesium	.001 - .01	.01
Aluminum	.0001	.0001 - .001
Silicon	.0001	.001
Copper	.0001	.0001
Potassium	.001 - .01	.001 - .01
Calcium	0.1	0.1 - 1.0
Sodium	Balance	Balance

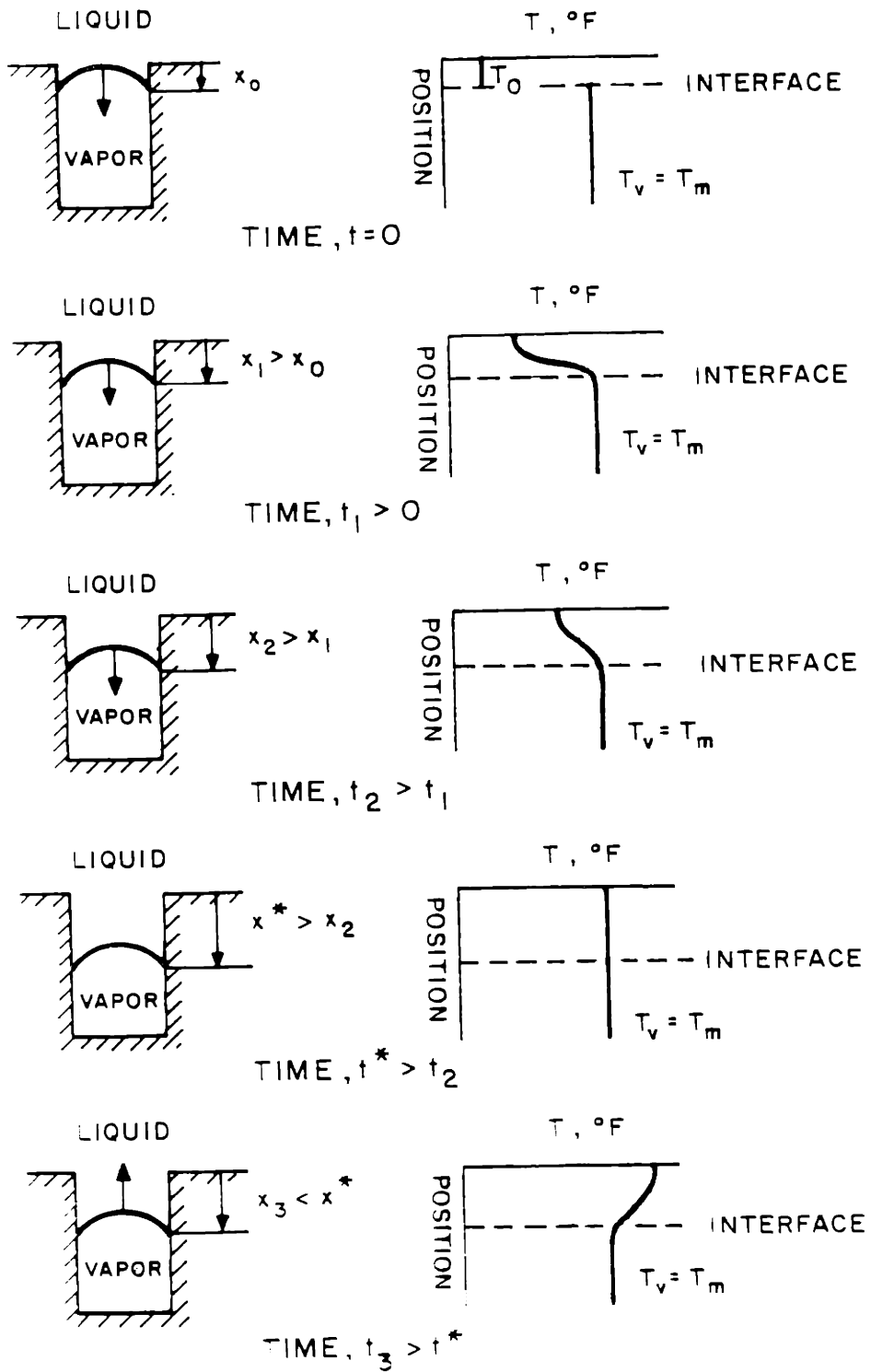


FIG. 1 DIAGRAM OF PROPOSED NUCLEATION CYCLE SHOWING INTERFACE POSITION AND LIQUID TEMPERATURE DISTRIBUTION.

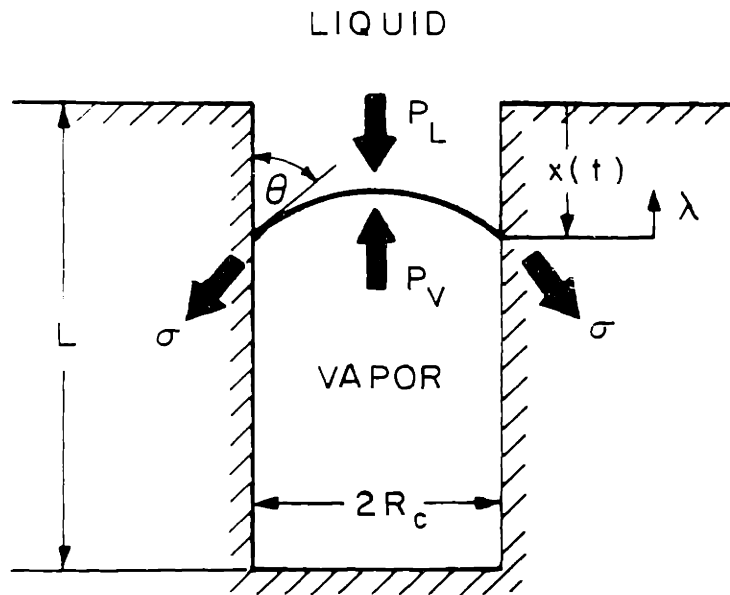


FIG. 2 IDEALIZED CAVITY SHOWING INTERFACE FORCE BALANCE.

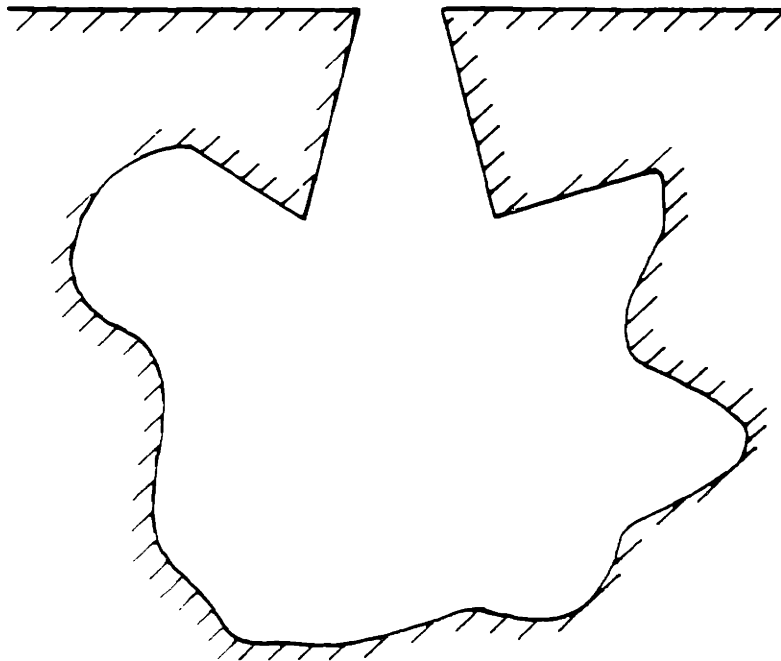


FIG. 3 DOUBLY RE-ENTRANT TYPE CAVITY.

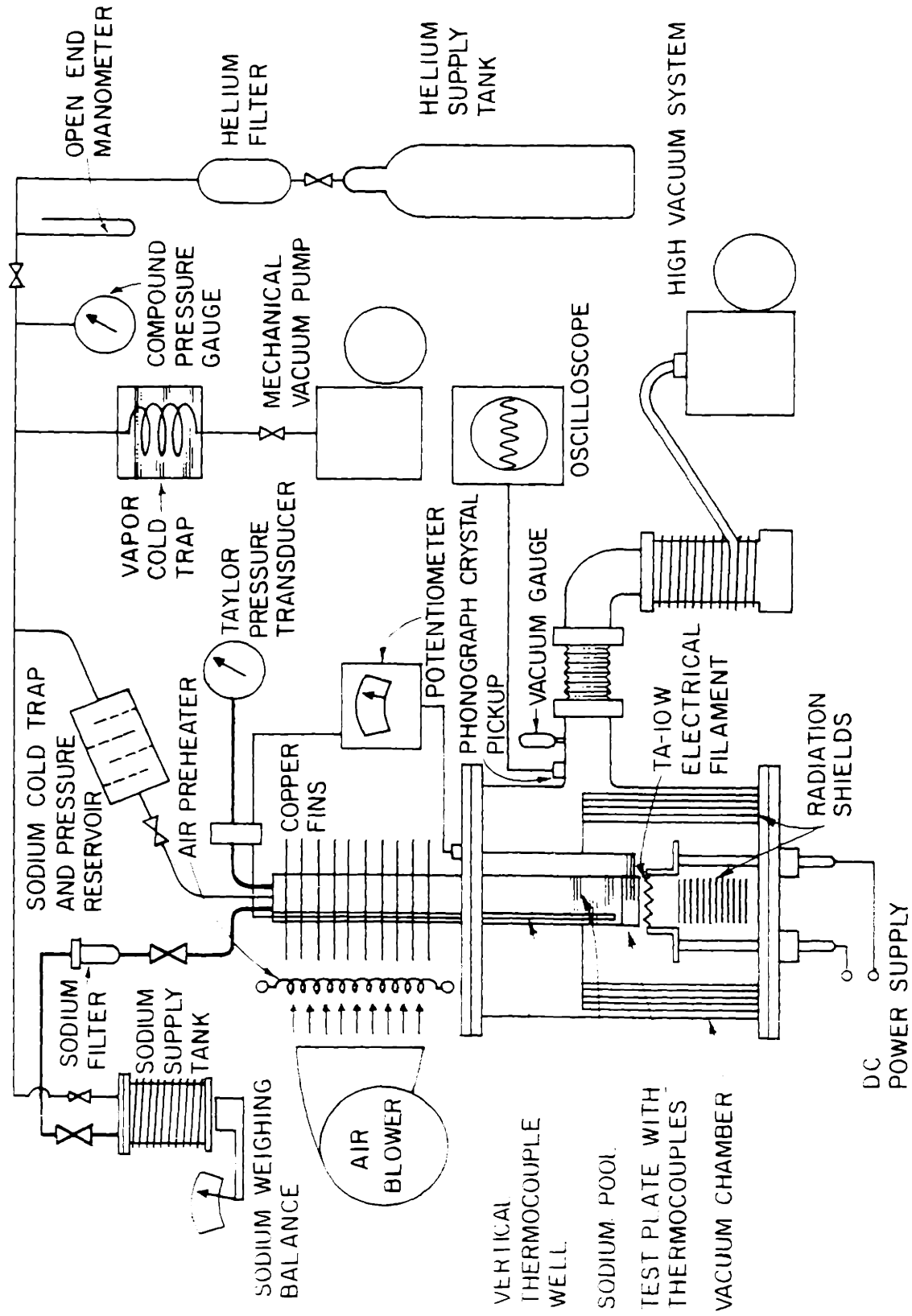


FIG 4 SCHEMATIC DIAGRAM OF APPARATUS

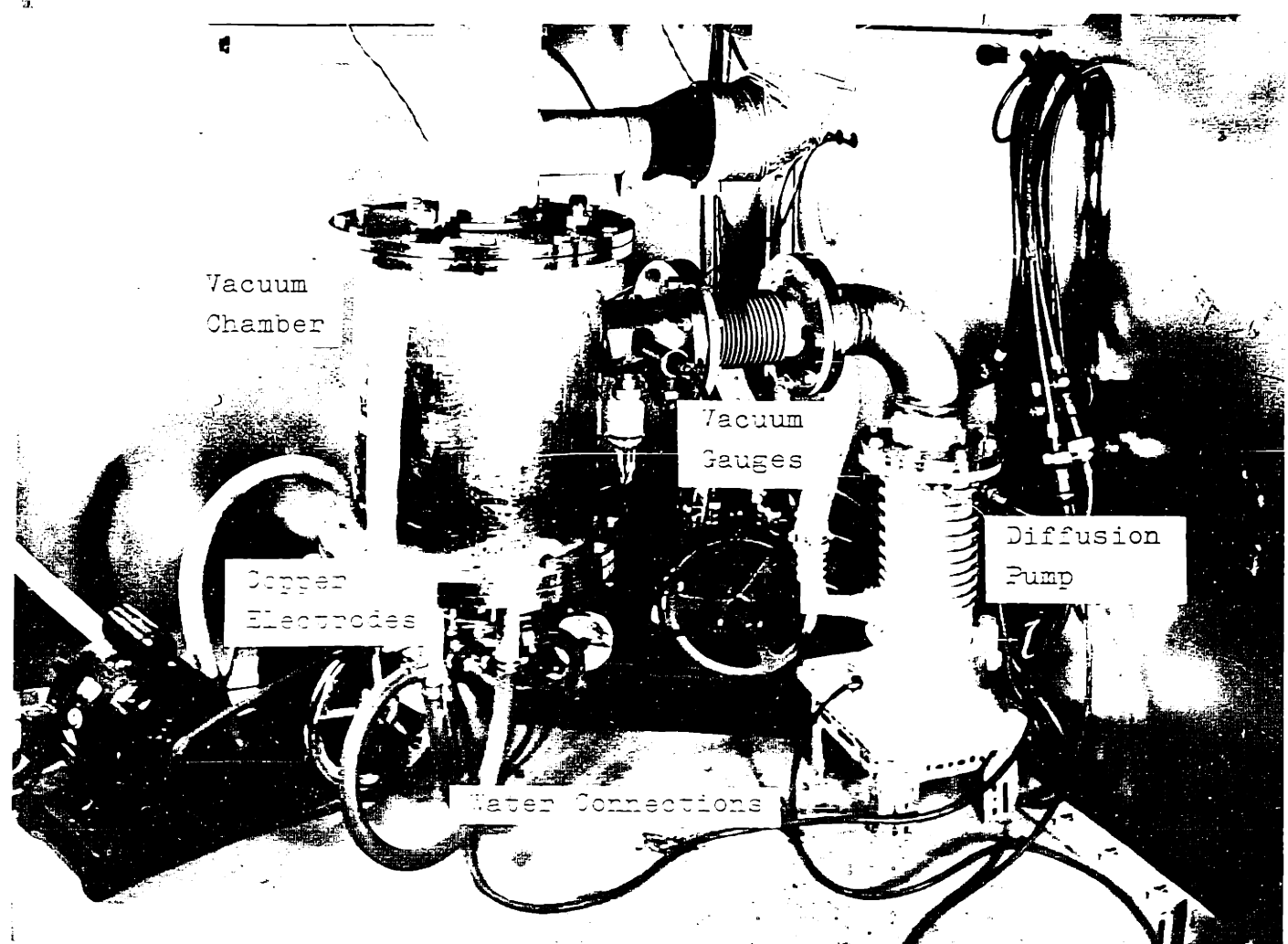
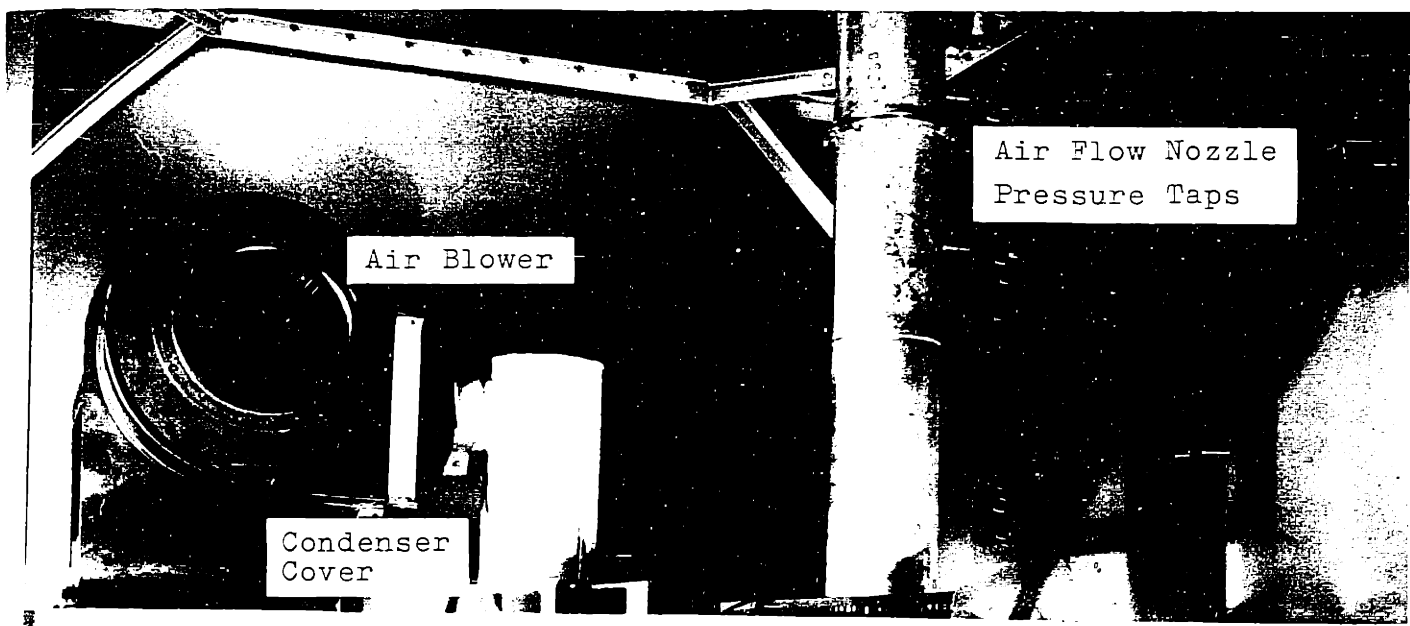


FIG. 5 PARTIAL ASSEMBLY OF EQUIPMENT

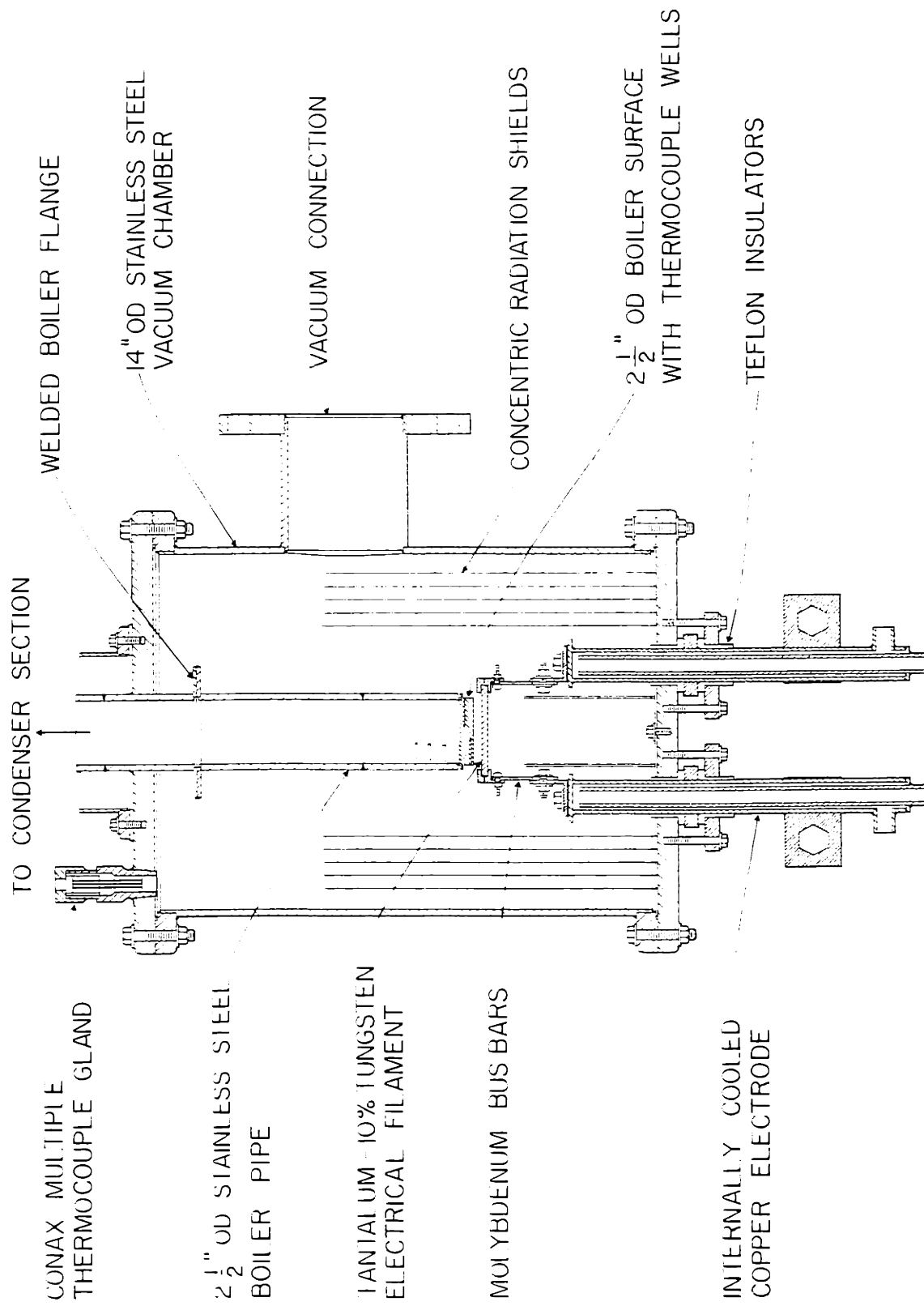
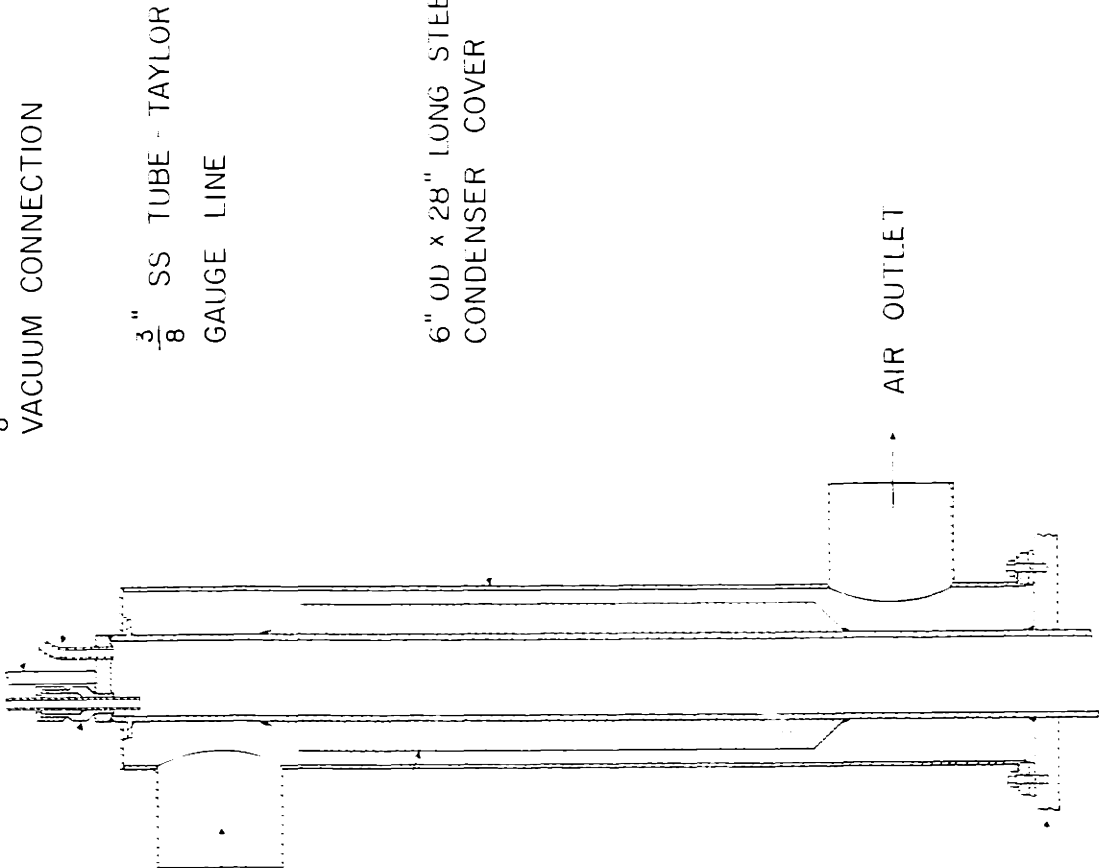


FIG 6 HEATER & BOILER SECTIONAL DRAWING

$\frac{3}{8}$ " SS CONAX PACKING GLAND
FOR SODIUM FILL LINE

$\frac{3}{8}$ " SS TUBE - PRESSURE &
VACUUM CONNECTION



AIR INLET

$\frac{1}{16}$ " x $1\frac{1}{4}$ " x 18" COPPER FINS HELIARC
TACK WELDED TO SS PIPE AT TOP
& BOTTOM AND SILVER SOLDERED
ALONG ENTIRE LENGTH

$\frac{3}{8}$ " SS TUBE - TAYLOR
GAUGE LINE

6" OD x 28" LONG STEEL
CONDENSER COVER

VACUUM CHAMBER COVER

AIR OUTLET

FIG 7 CONDENSER SECTIONAL DRAWING

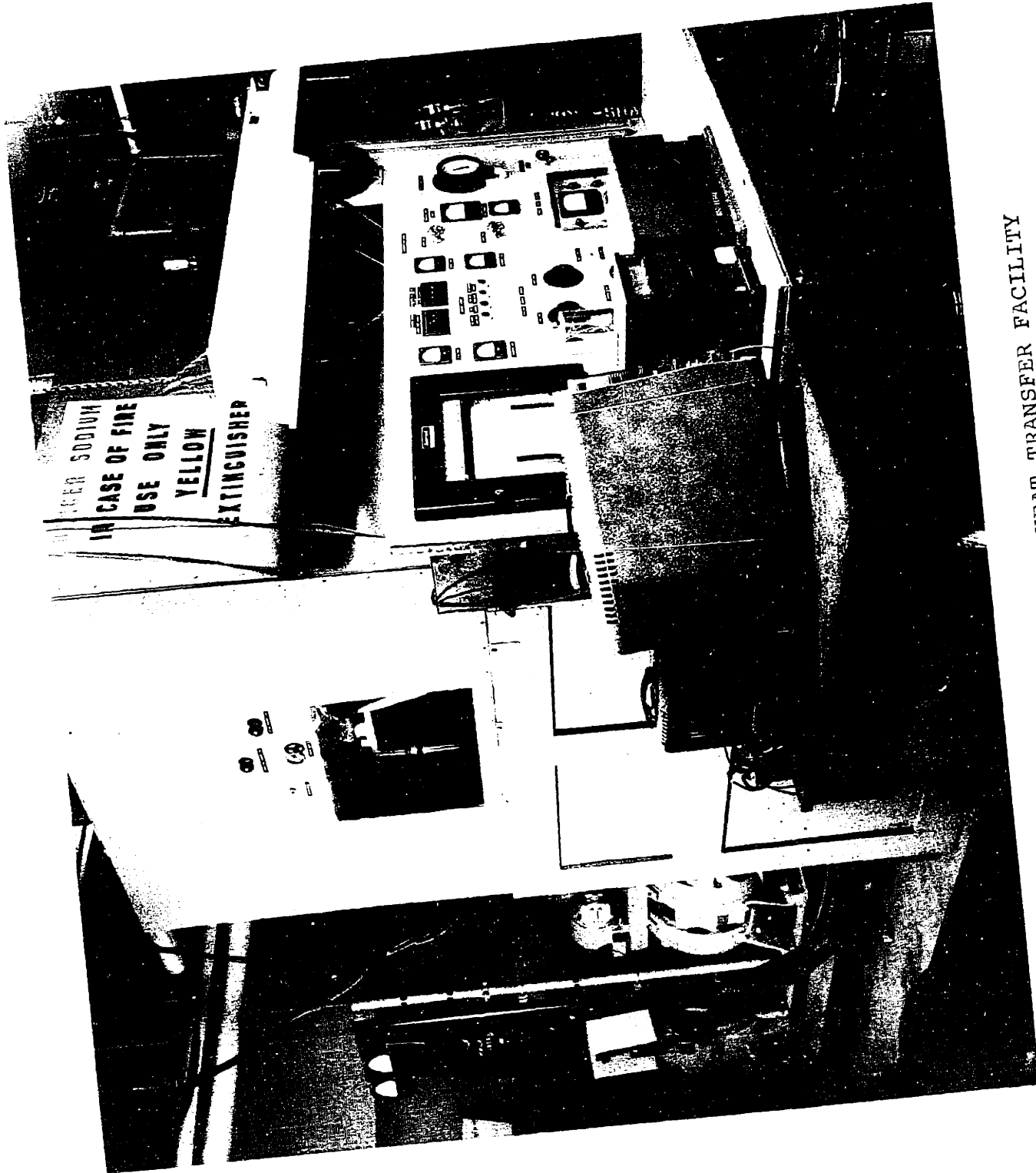


FIG. 8 GENERAL VIEW OF HEAT TRANSFER FACILITY

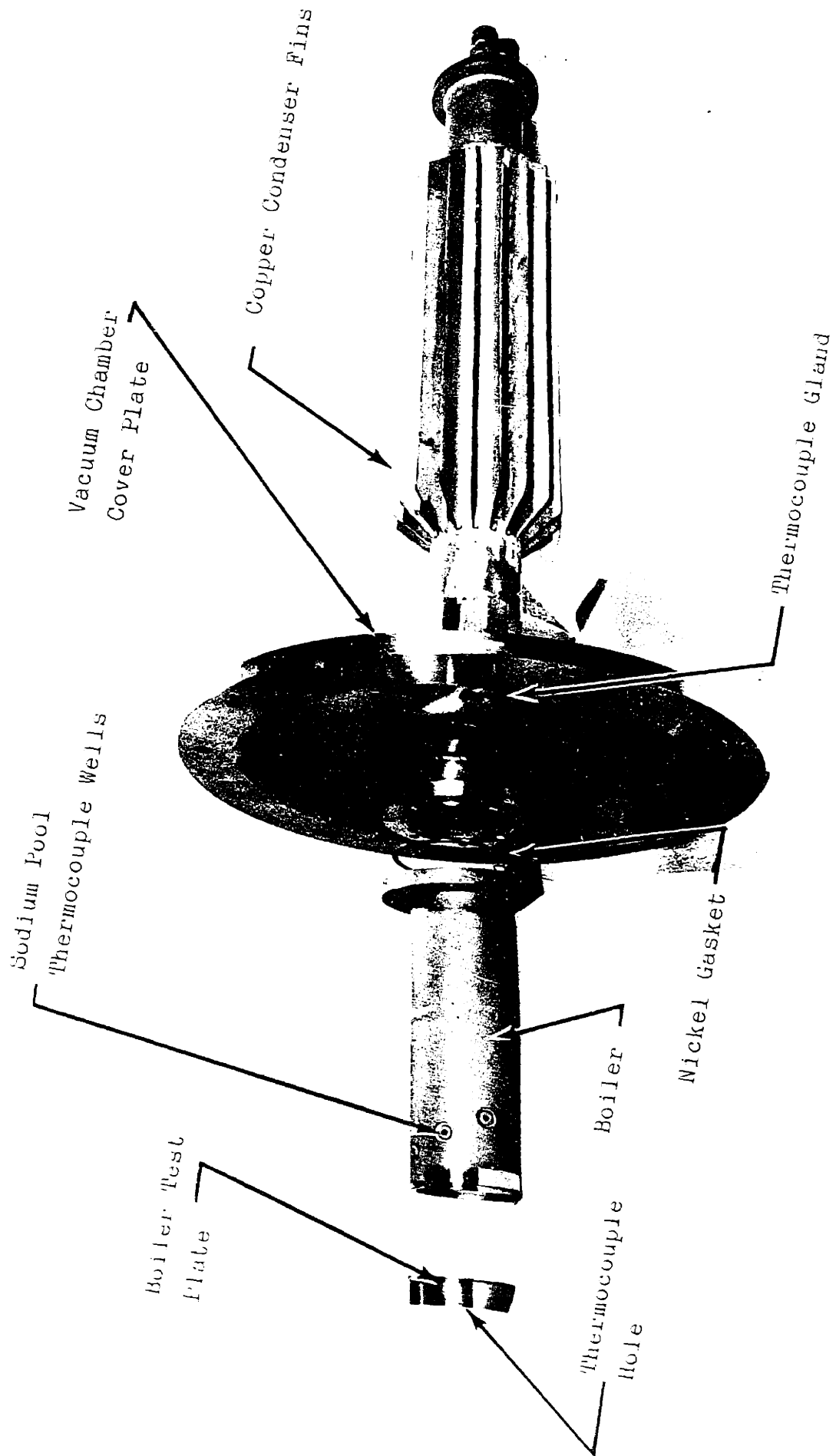
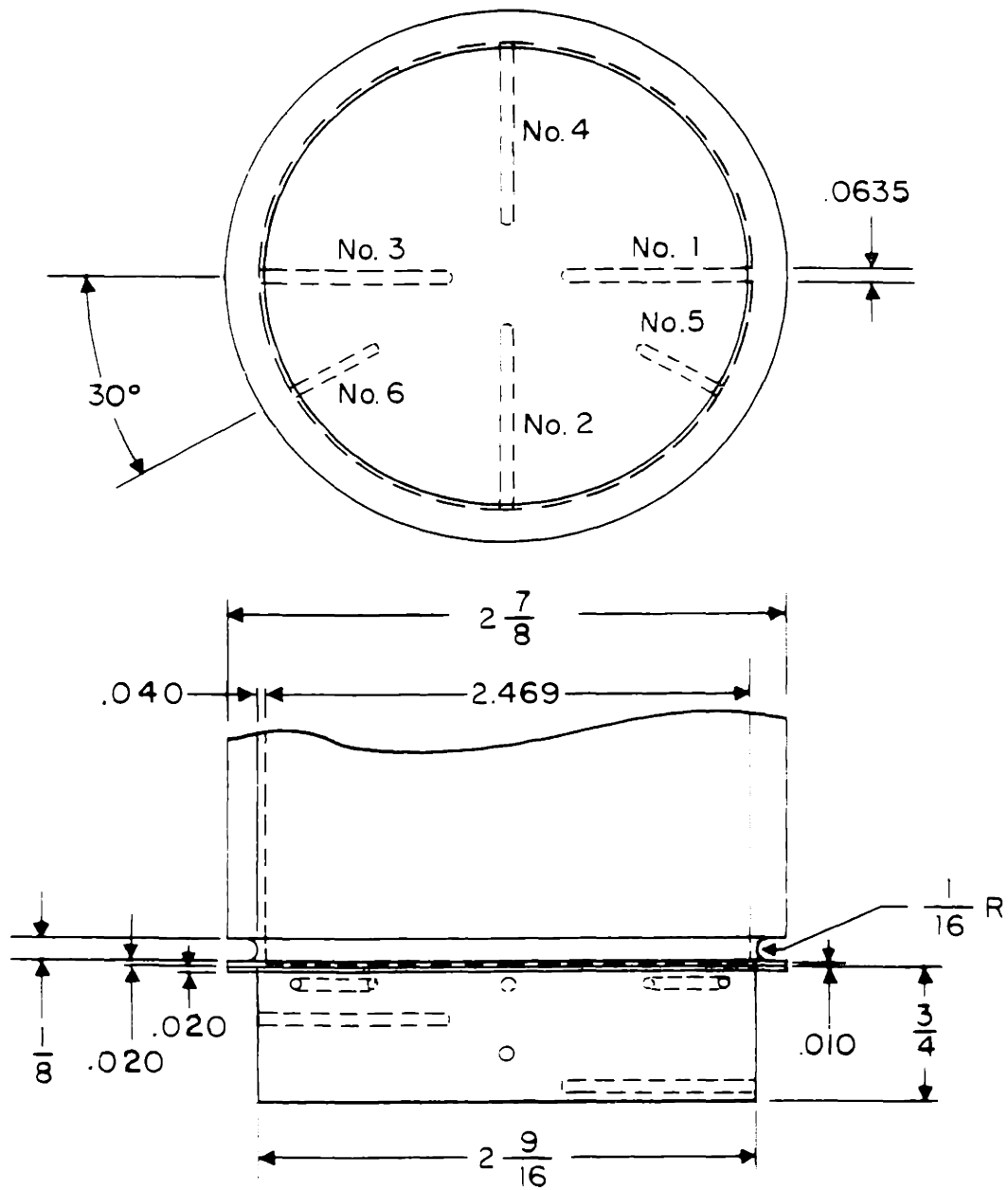


FIG. 9 EXPLODED VIEW OF BOILER-CONDENSER SECTION



T.C. NO.	IMMERSION LENGTH	☉ DISTANCE TO BOILER SURFACE
1	1.0 IN.	0.660 IN.
2	1.0 IN.	0.470 IN.
3	1.0 IN.	0.280 IN.
4	1.0 IN.	0.090 IN.
5	0.5 IN.	0.090 IN.
6	0.5 IN.	0.090 IN.

FIG. 10 DETAILS OF BOILER

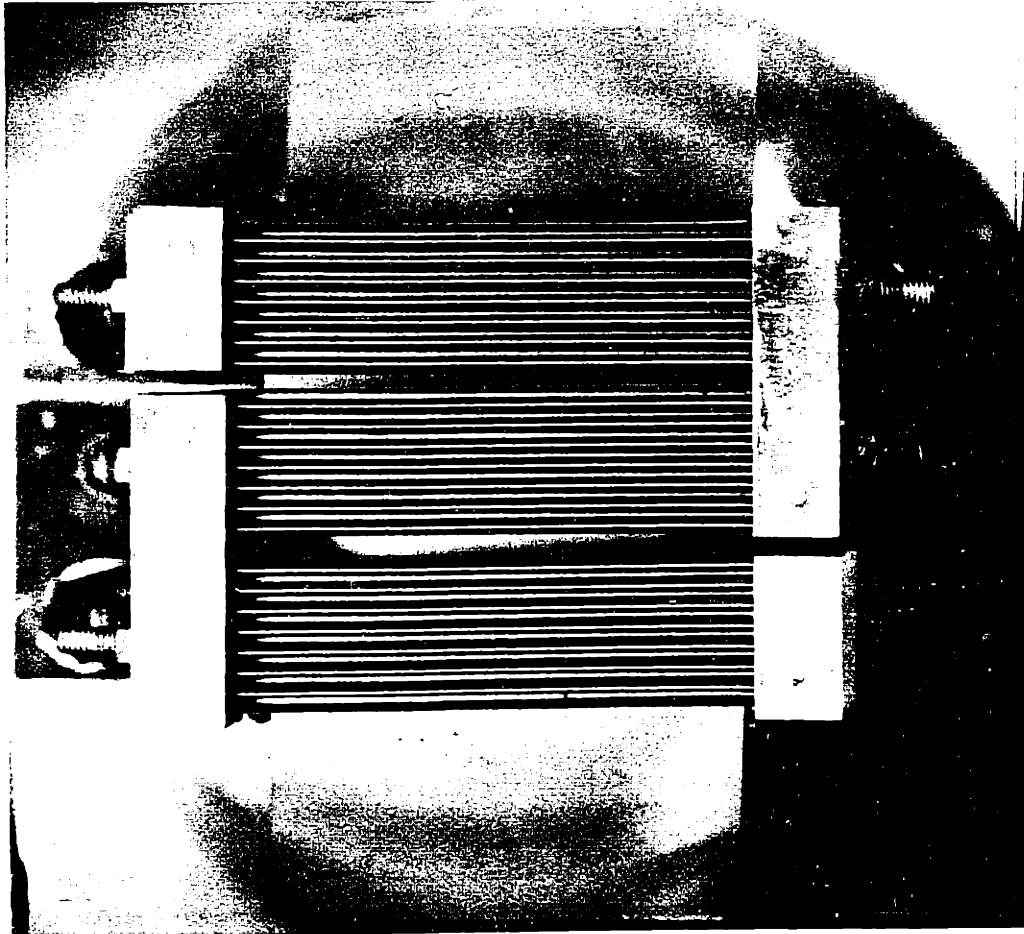


FIG. 11 OVERHEAD VIEW OF MAIN HEATER

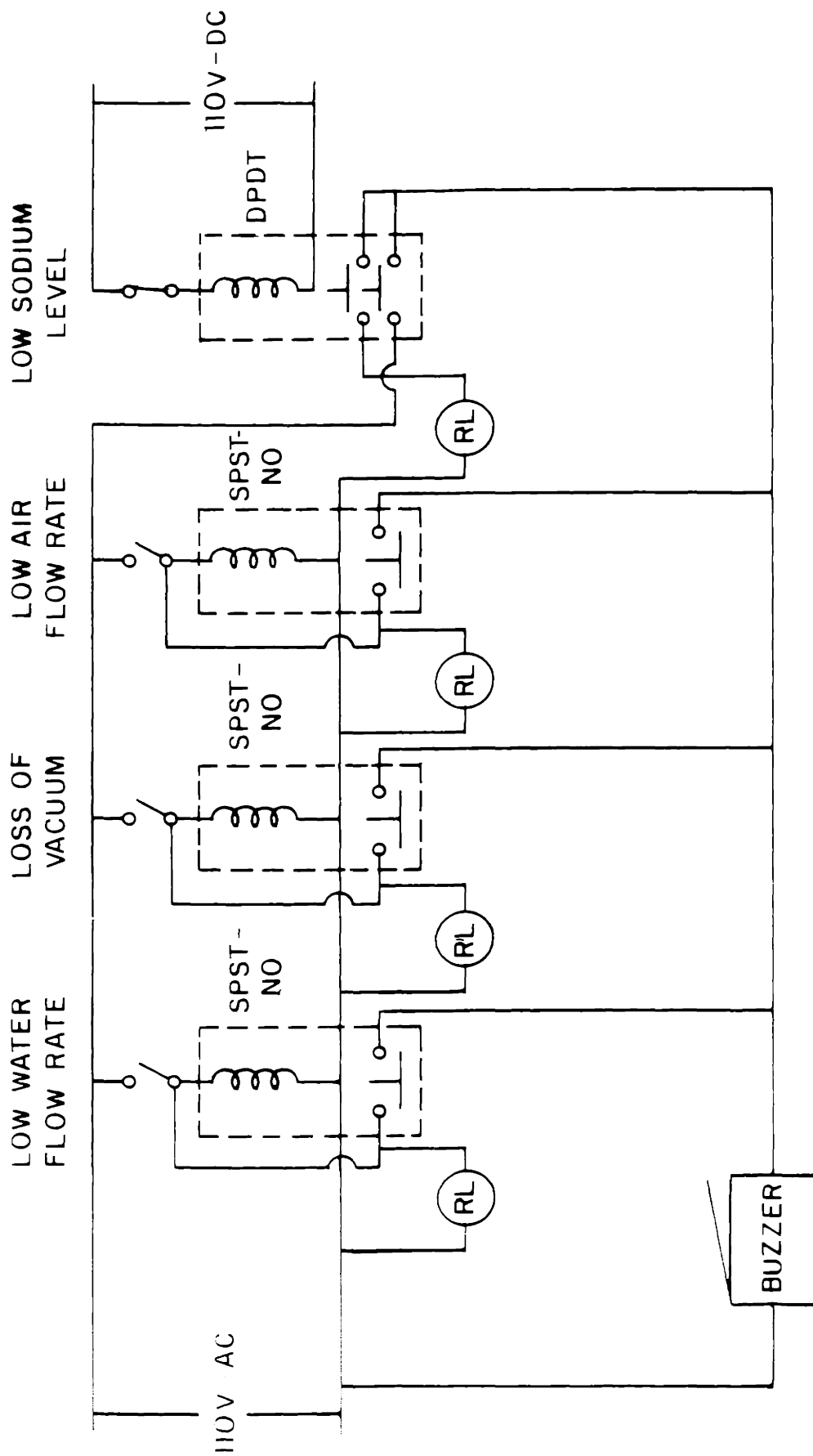
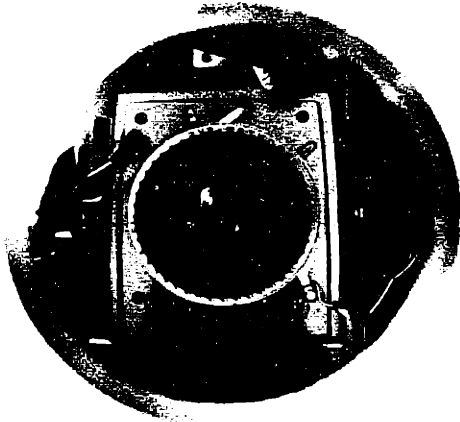
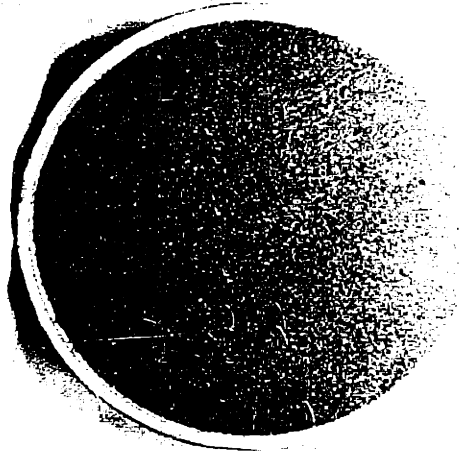


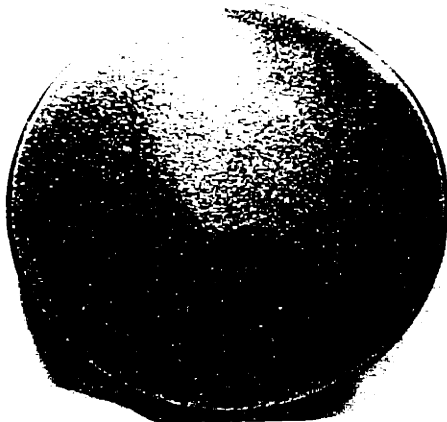
FIG. 12 ELECTRICAL WIRING DIAGRAM FOR CONTROL SYSTEM



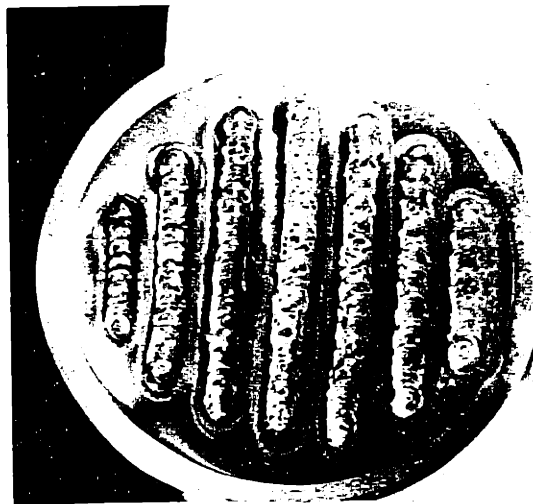
MIRROR 1



POROUS COATING



ETCHED SURFACE

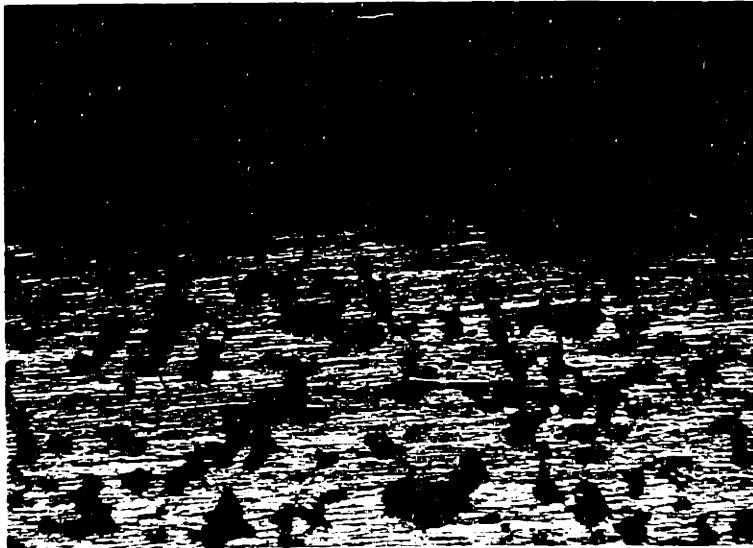


POROUS WELD

FIG. 13. OVERHEAD VIEW OF FOUR TEST SURFACES

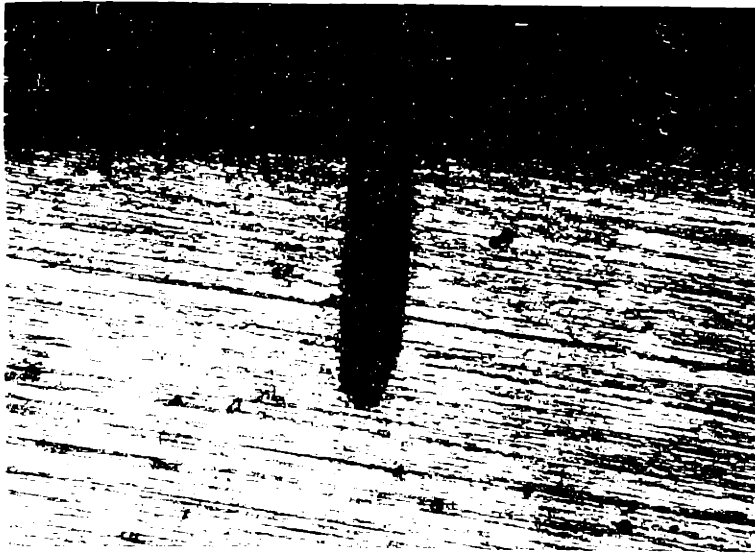


SAMPLE OF POROUS WELD

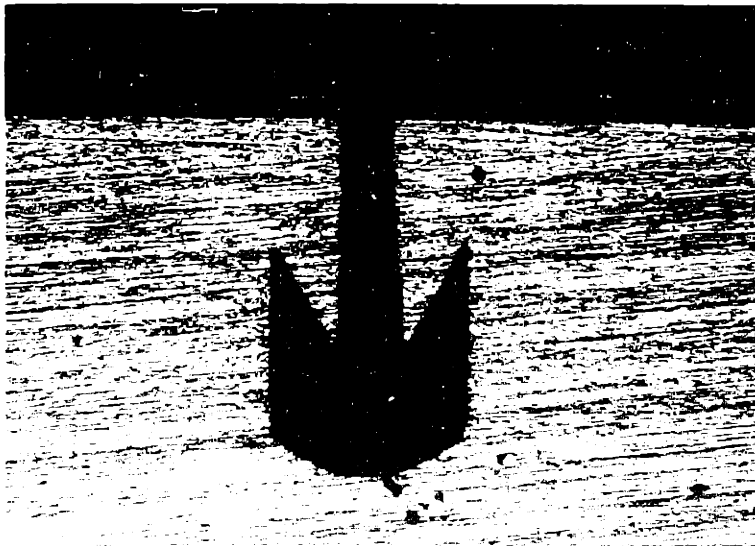


SAMPLE OF 35L POROUS PLATE

FIG. 14. PHOTOMICROGRAPHS OF CROSS-SECTIONS
OF POROUS SAMPLES (100X)



SAMPLE OF SPARKED CAVITY,
.004 IN. DIA. X .018 IN. DEEP



SAMPLE OF DOUBLY RE-ENTRANT CAVITY
.004 IN. MOUTH DIA. X .025 IN. DEEP

FIG. 15. PHOTOMICROGRAPHS OF CROSS-SECTIONS
OF ARTIFICIAL CAVITIES (75X)

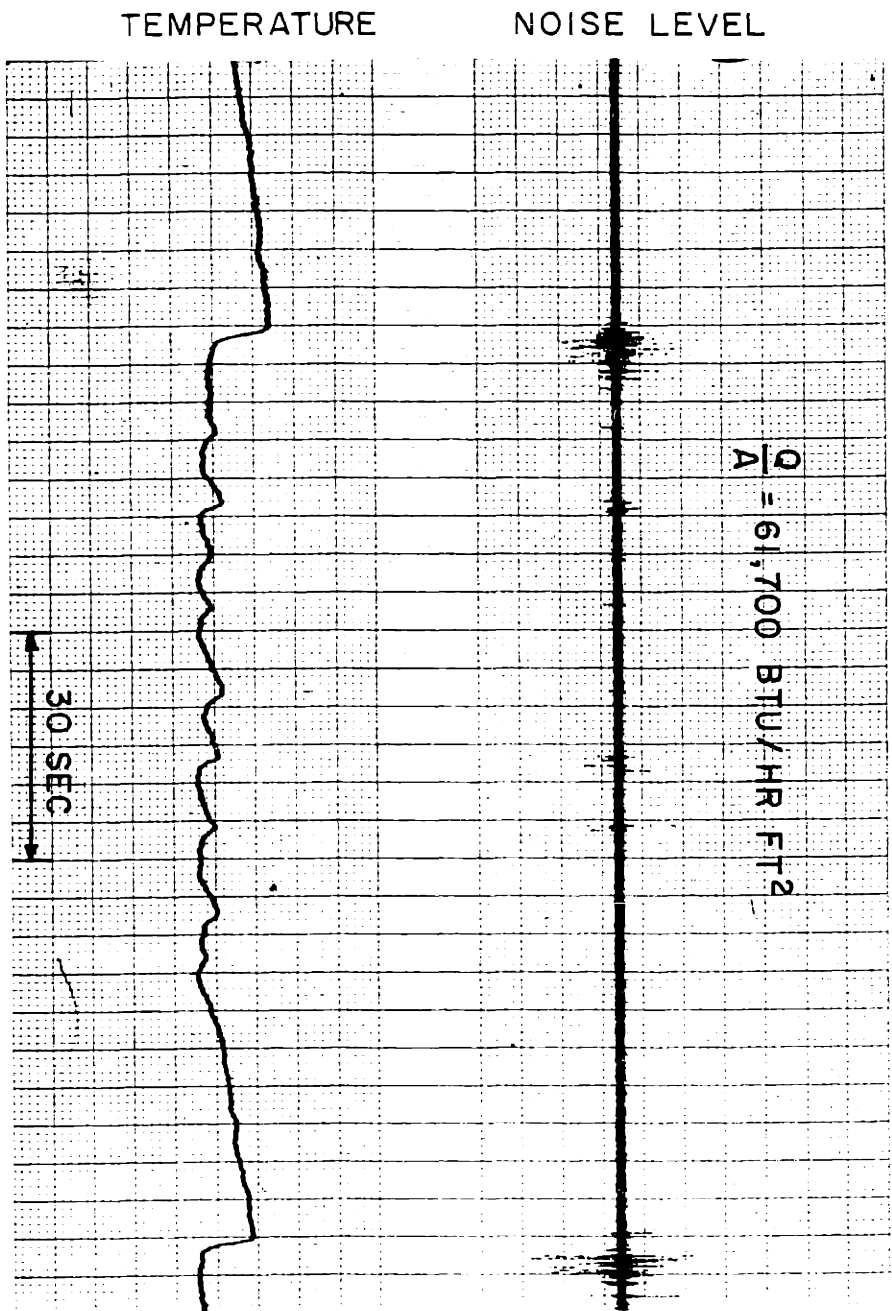


FIG. 16 COINCIDENCE OF NOISE LEVEL AND WALL TEMPERATURE DURING UNSTABLE NUCLEATE BOILING OF SODIUM AT $Q/A = 61,700 \text{ BTU/HR. FT}^2$

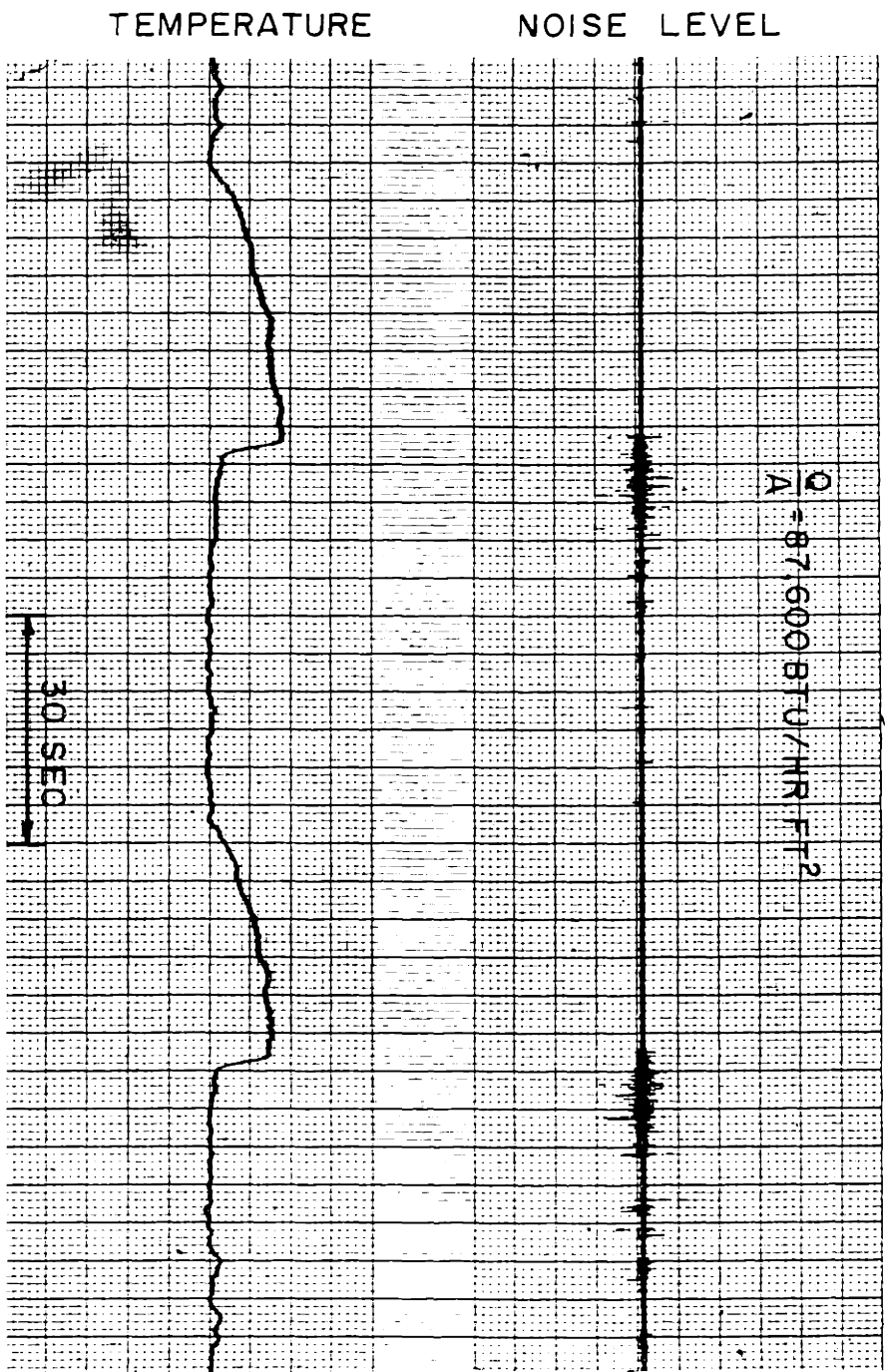


FIG 17 COINCIDENCE OF NOISE LEVEL AND WALL TEMPERATURE DURING UNSTABLE NUCLEATE BOILING OF SODIUM AT $Q/A = 87,600 \text{ BTU/HR FT}^2$

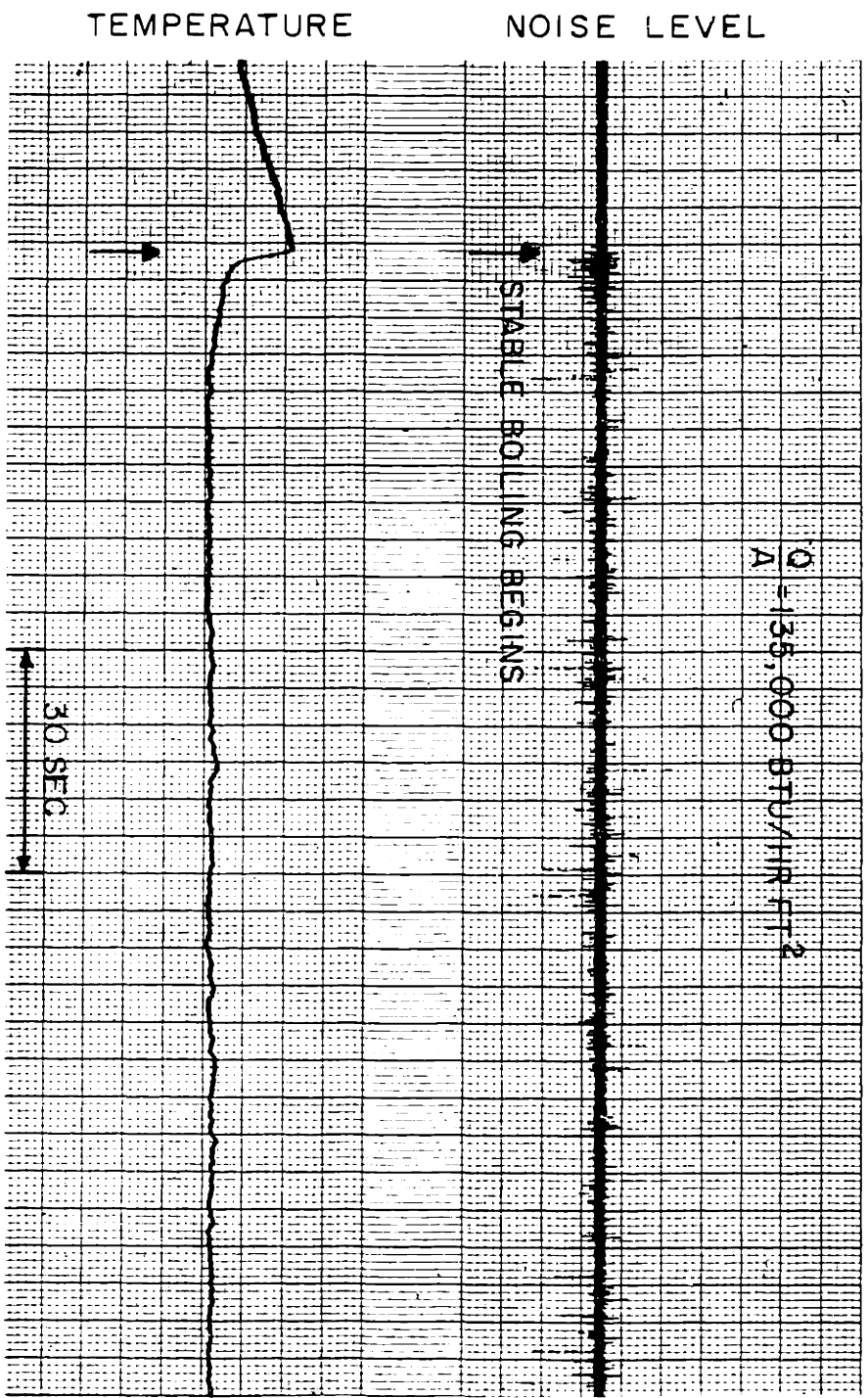


FIG 18 COINCIDENCE OF NOISE LEVEL AND WALL TEMPERATURE DURING STABLE BOILING OF SODIUM AT $Q/A = 135,000 \text{ BTU/HR FT}^2$

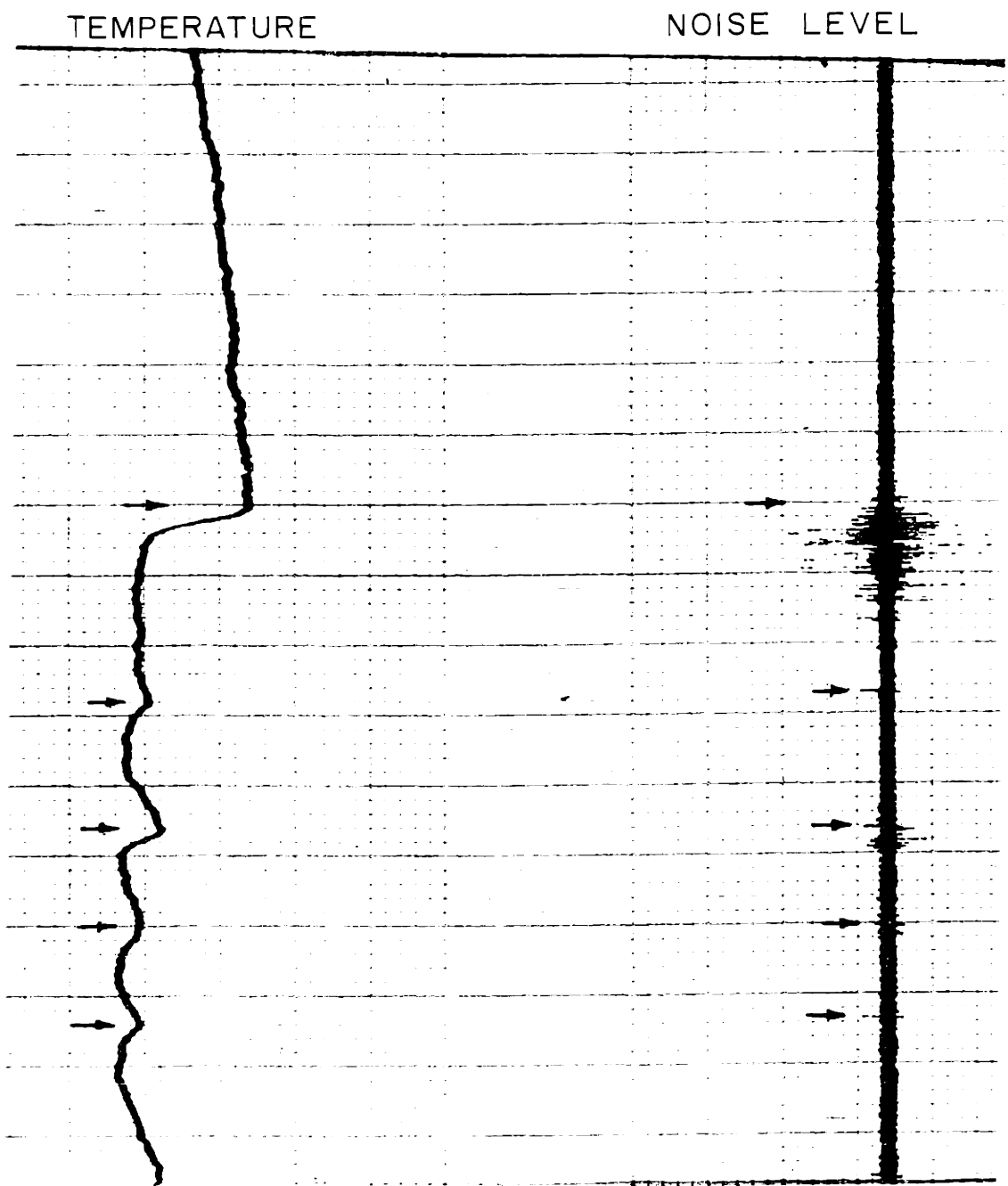


FIG. 19 ENLARGED PHOTOGRAPH SHOWING COINCIDENCE OF NOISE LEVEL AND WALL TEMPERATURE DURING "BUMPING" (2.5X)

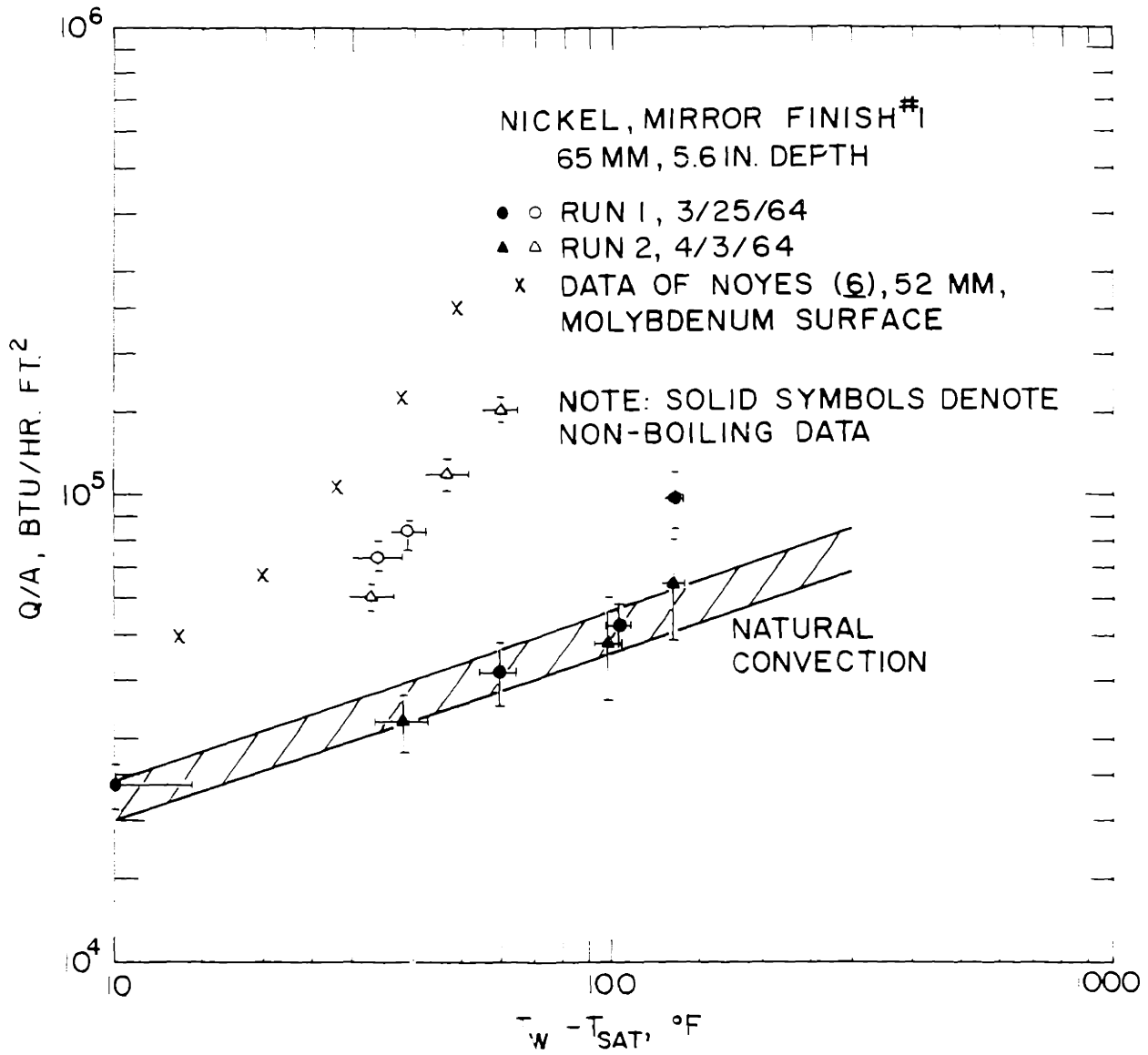


FIG. 20 SAMPLE DATA WITH EXPERIMENTAL ERROR LIMITS SHOWING DATA OF NOYES FOR COMPARISON

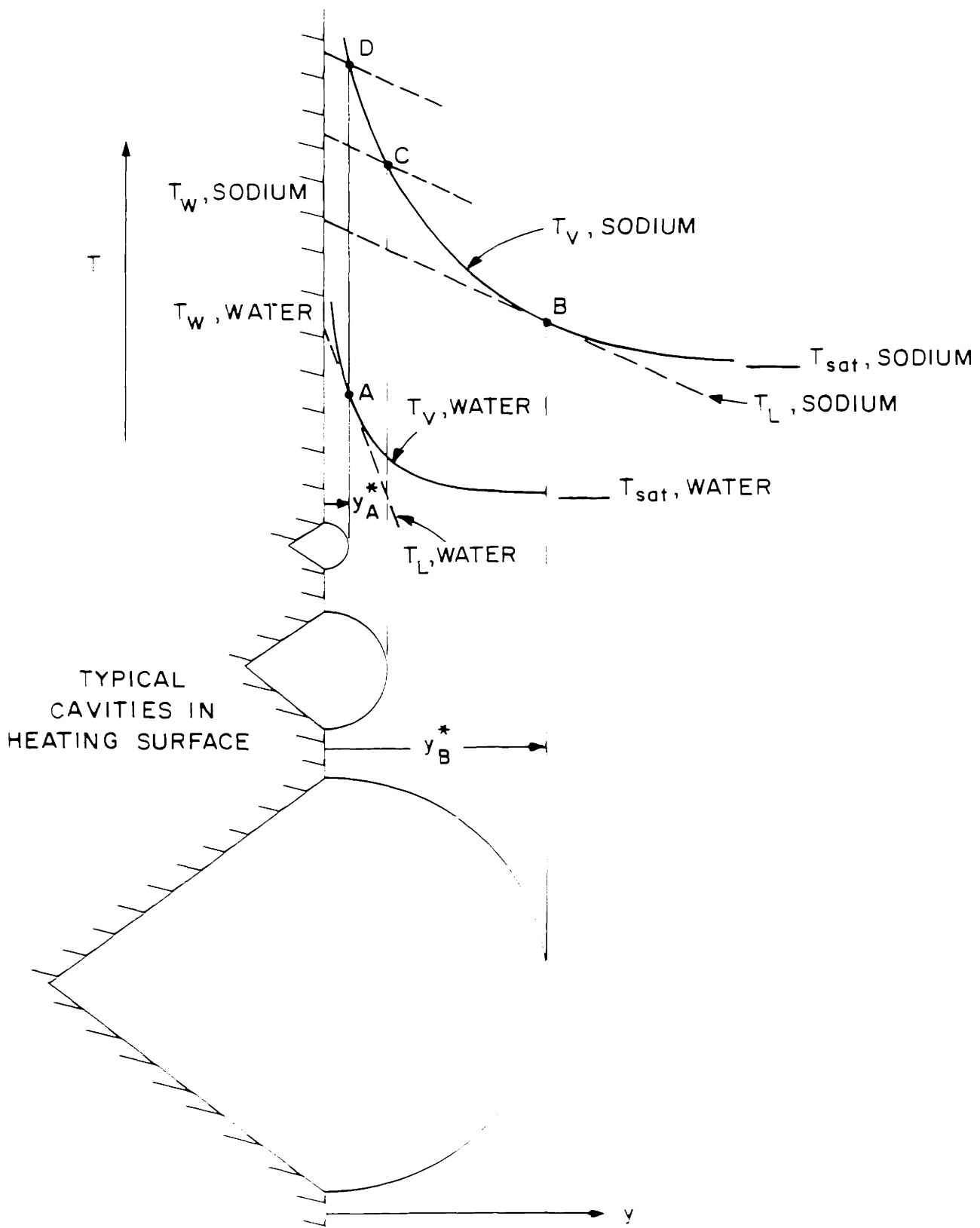


FIG. 21 INITIATION OF BUBBLE GROWTH FOR WATER AND SODIUM

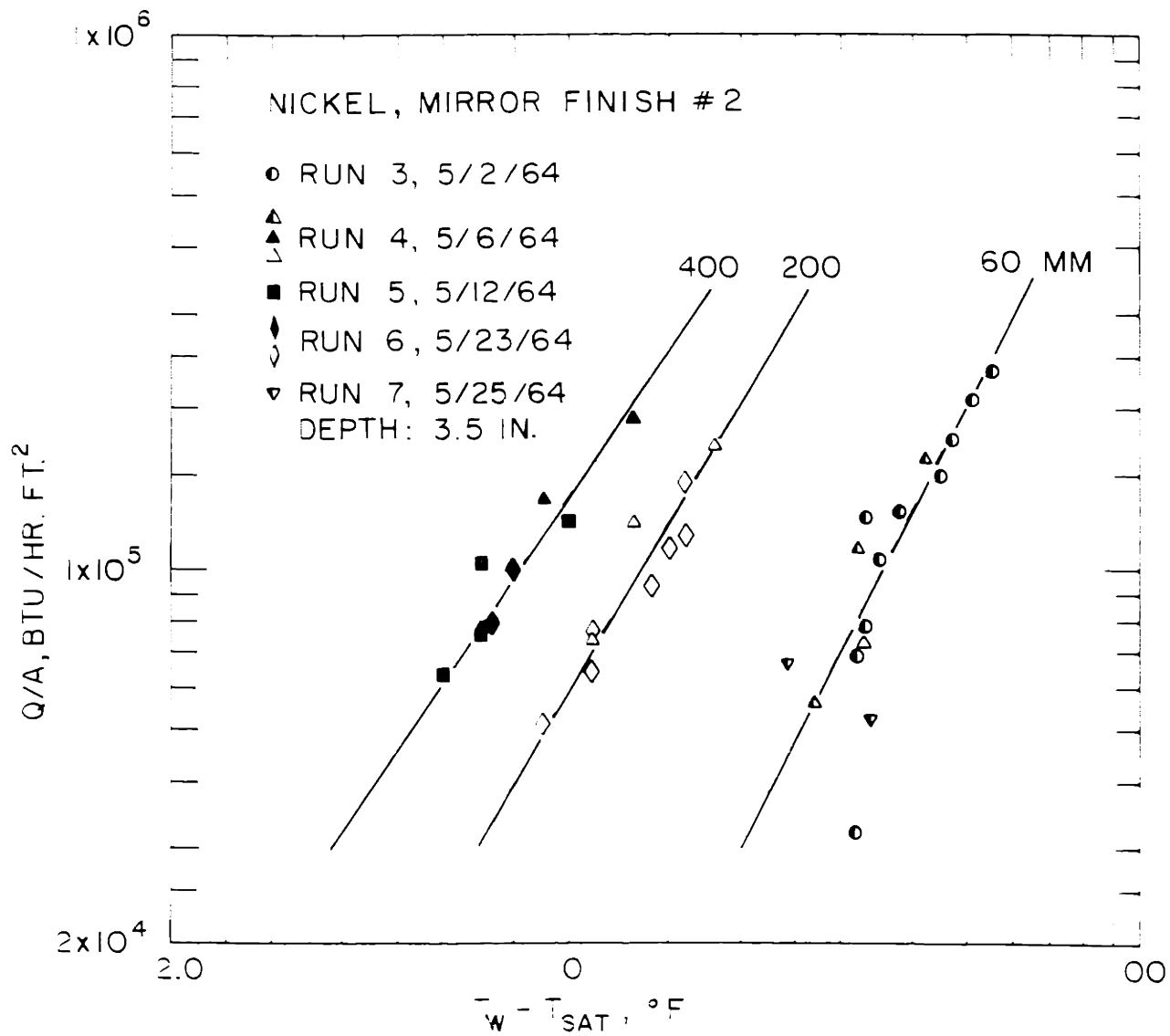


FIG. 22 EFFECT OF PRESSURE ON NUCLEATE POOL BOILING OF SODIUM

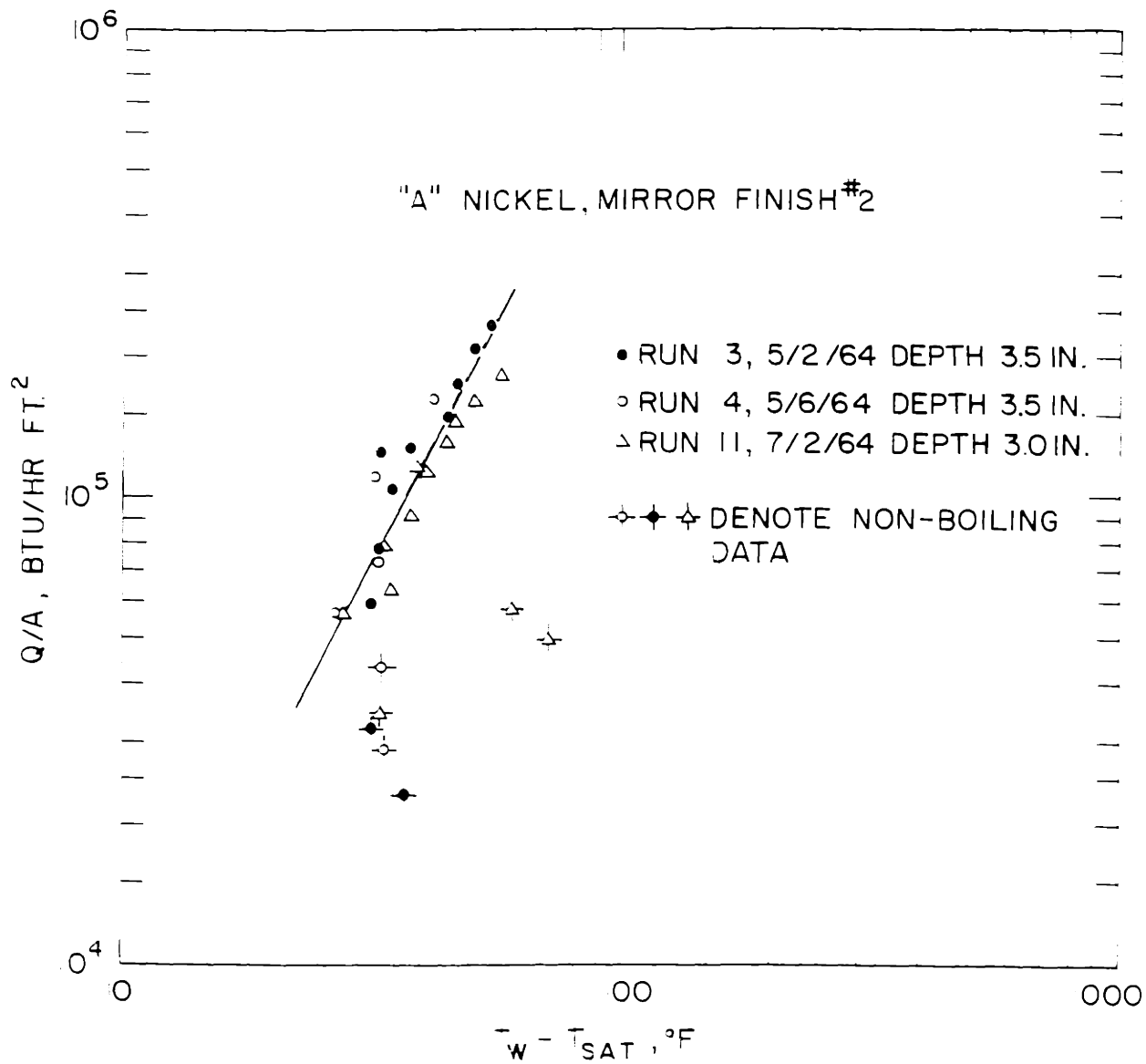


FIG. 23 REPRODUCIBILITY OF NUCLEATE BOILING RESULTS

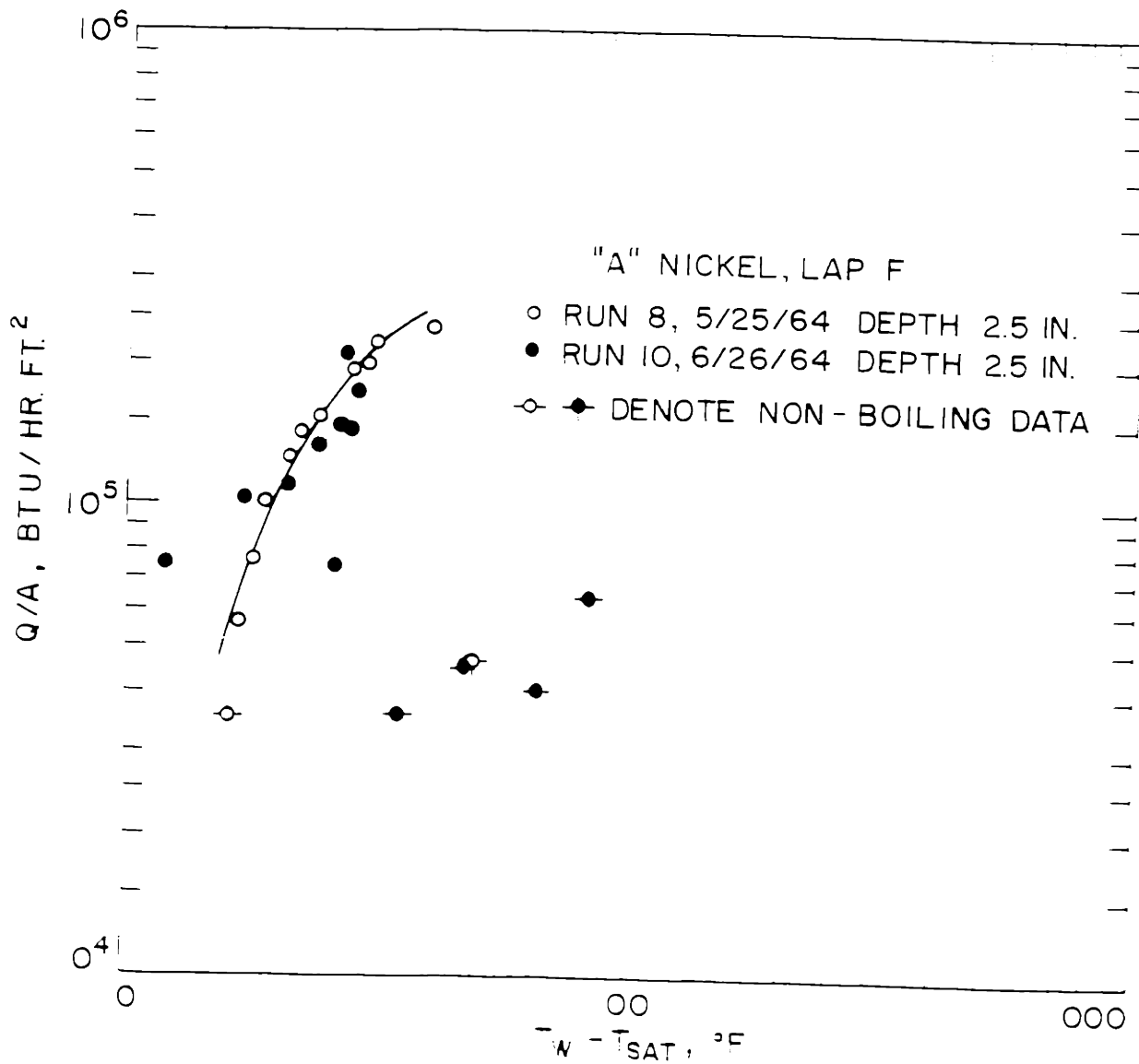


FIG. 24 REPRODUCIBILITY OF NUCLEATE BOILING RESULTS

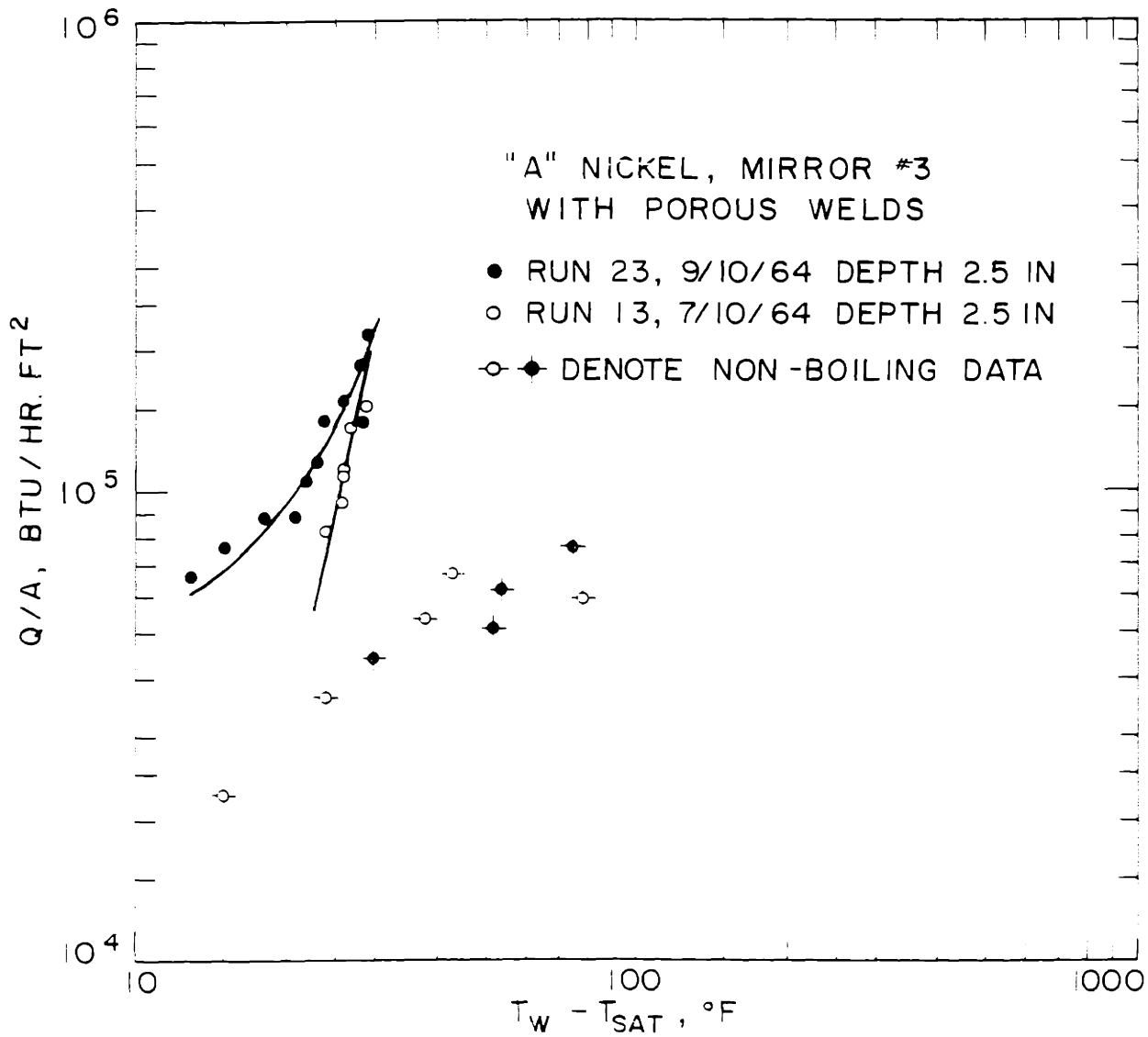


FIG. 25 REPRODUCIBILITY OF NUCLEATE BOILING RESULTS

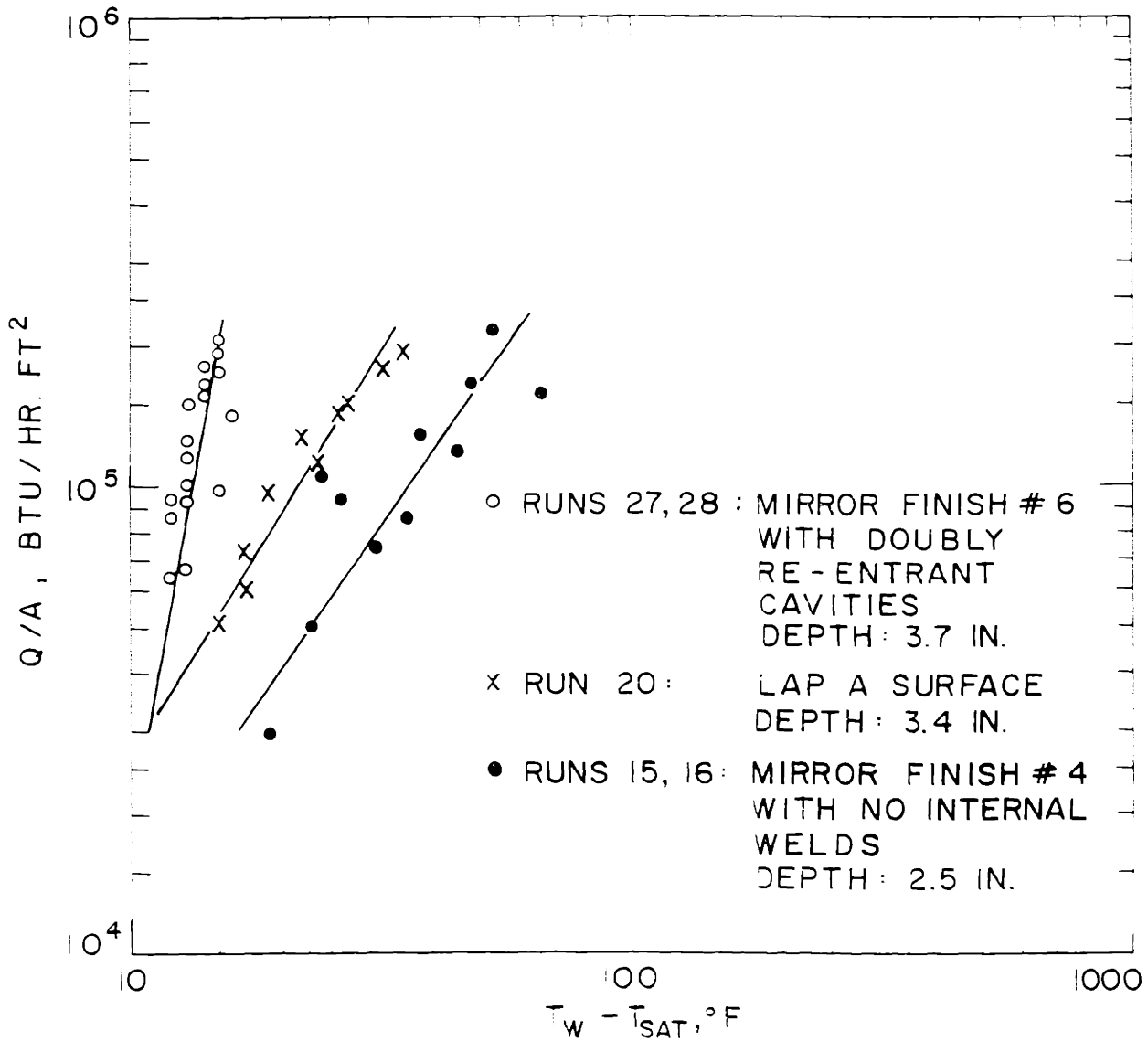


FIG. 26 EFFECT OF ROUGHNESS ON NUCLEATE POOL BOILING OF SODIUM

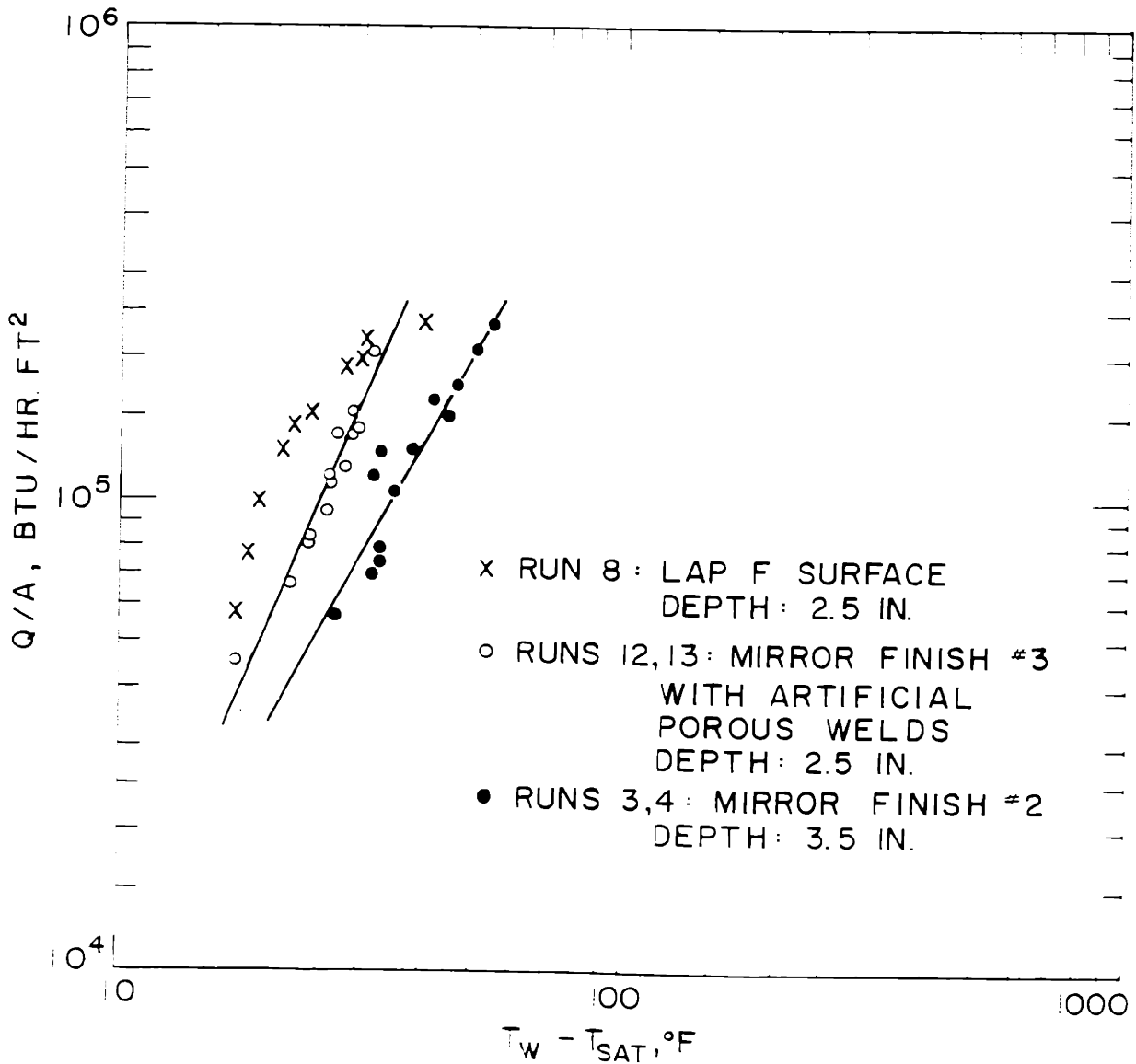


FIG. 27 EFFECT OF ROUGHNESS ON NUCLEATE POOL BOILING OF SODIUM

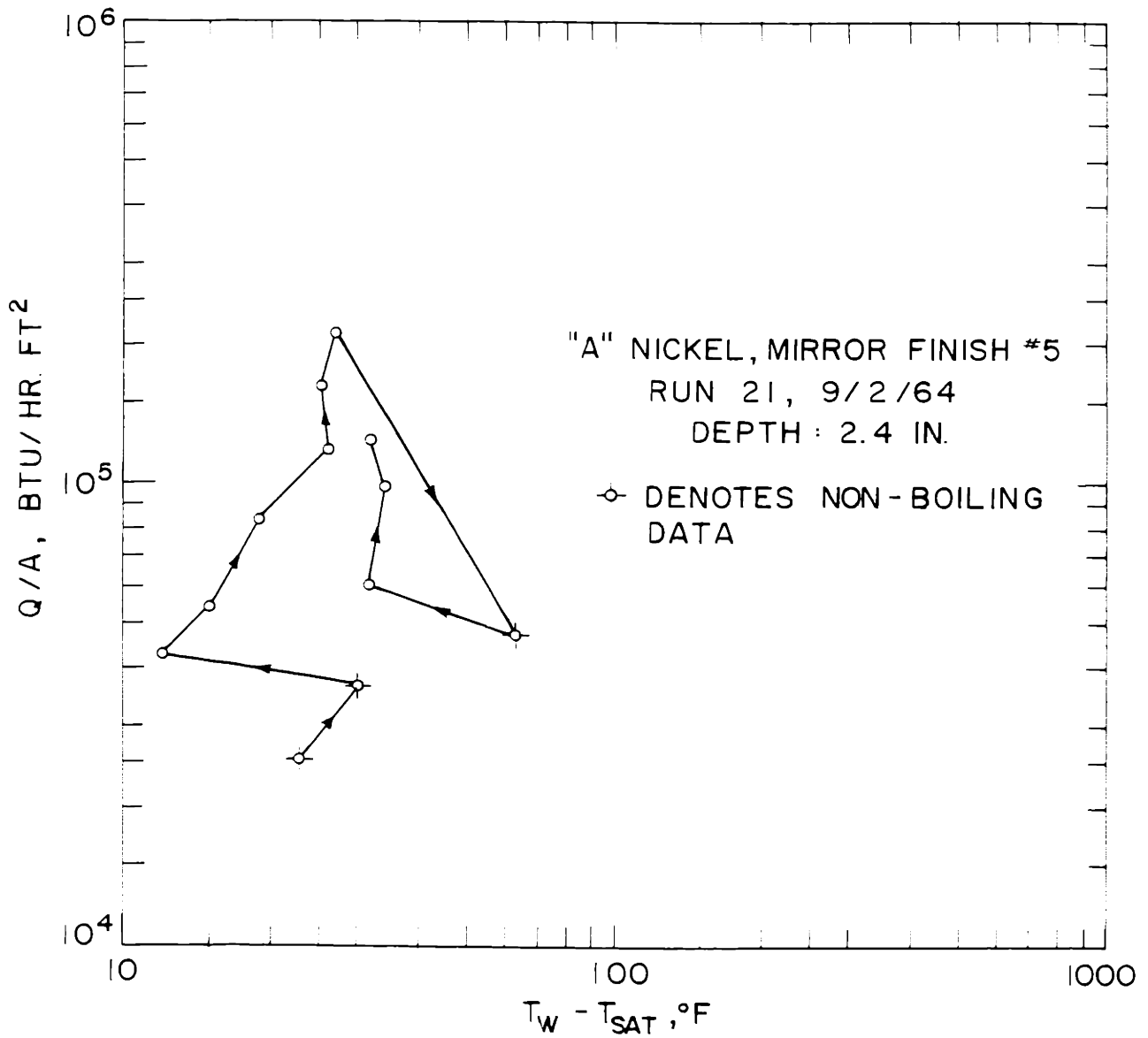


FIG. 28 EFFECT OF AGING ON THE NUCLEATE BOILING CURVE OF SODIUM

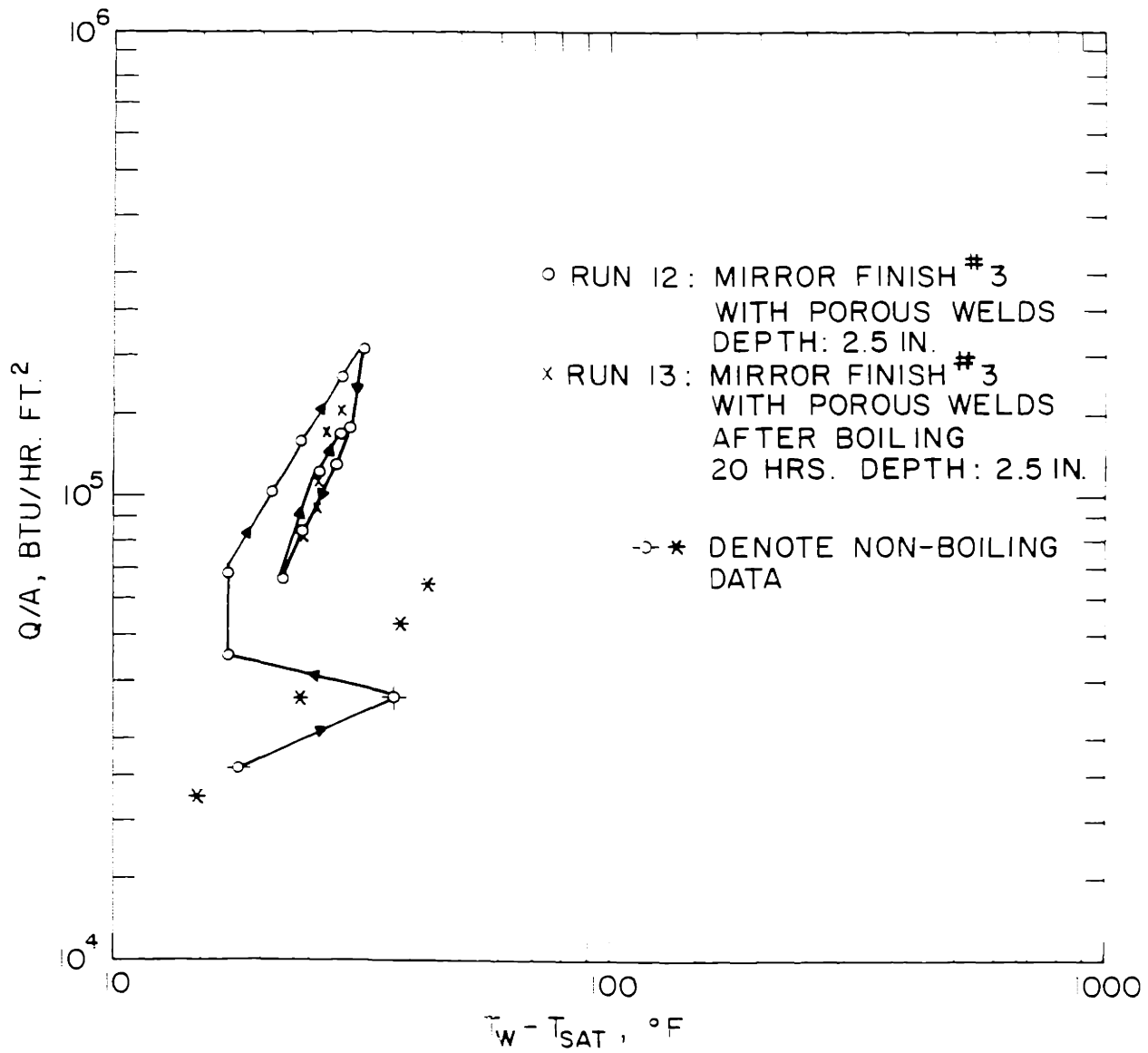


FIG. 29 EFFECT OF AGING ON THE NUCLEATE BOILING CURVE OF SODIUM

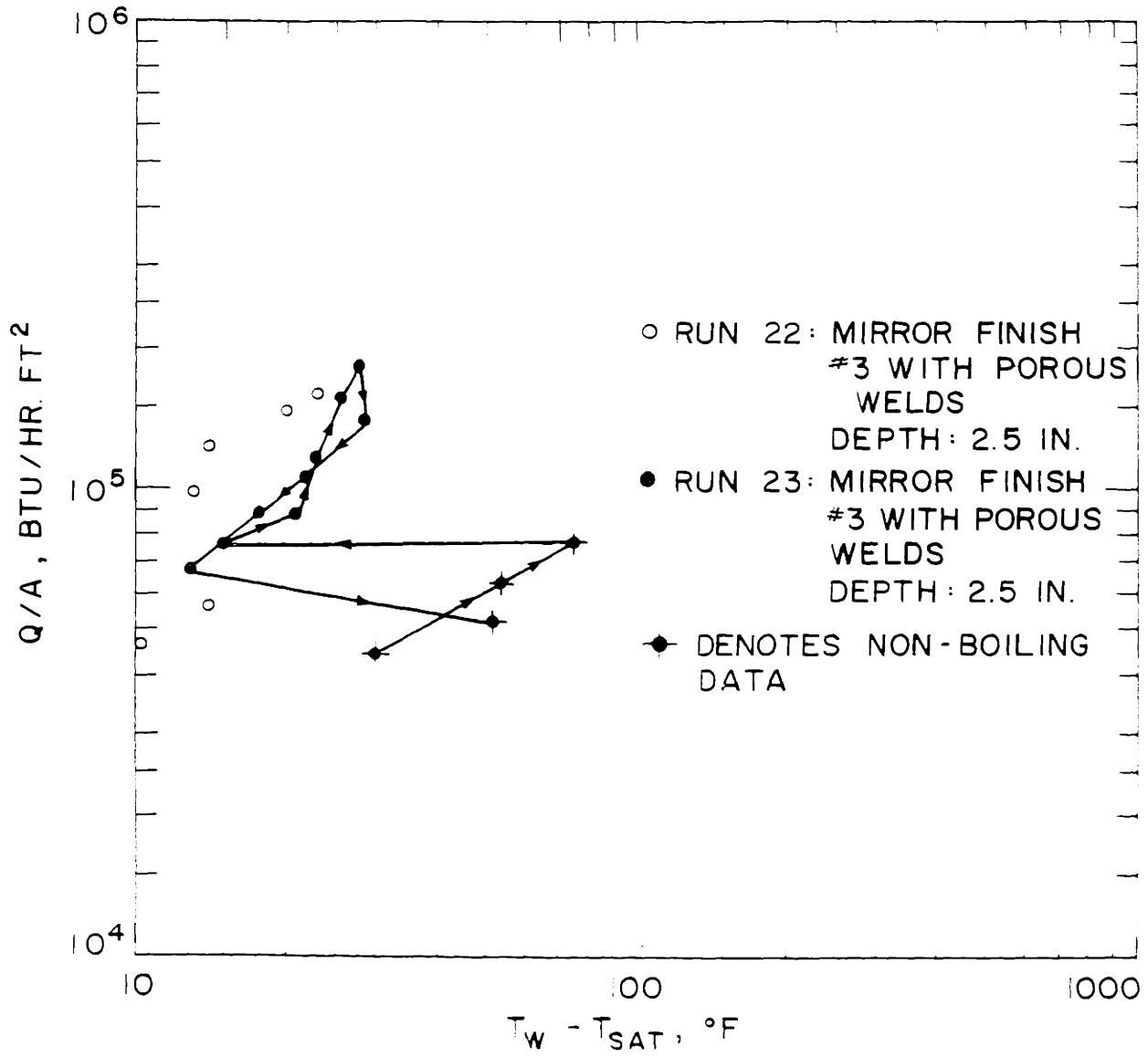


FIG. 30 EFFECT OF AGING ON THE NUCLEATE BOILING CURVE OF SODIUM

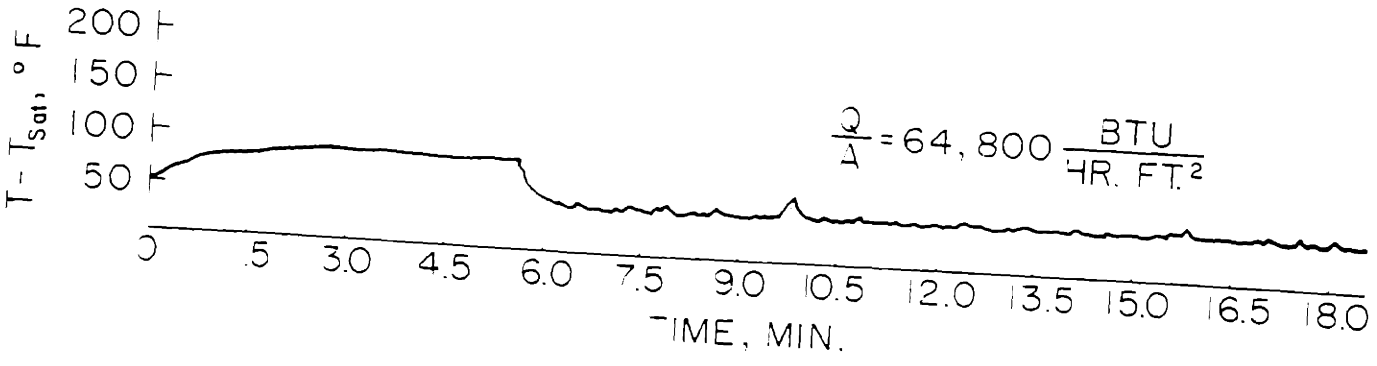
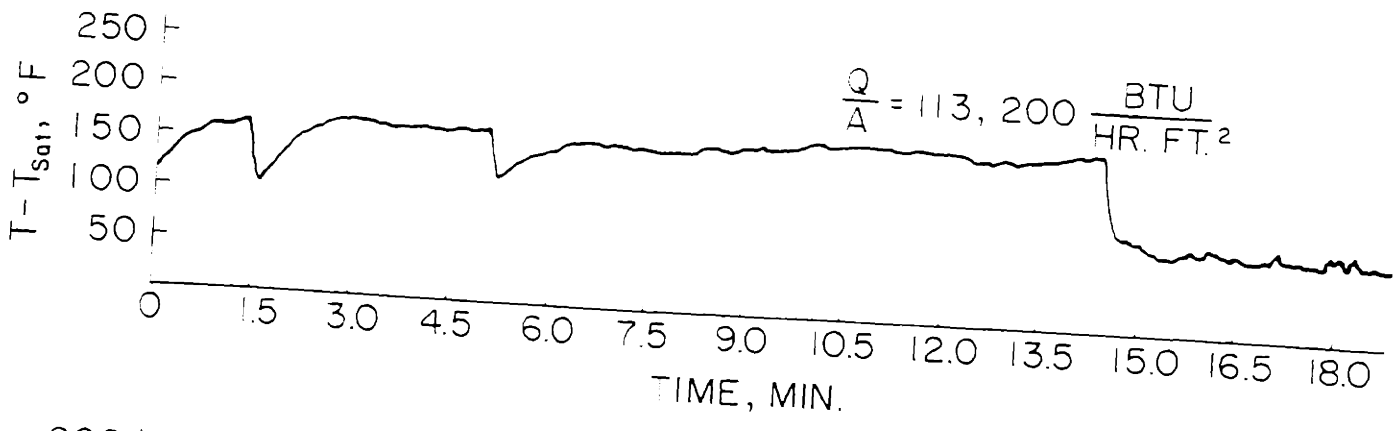
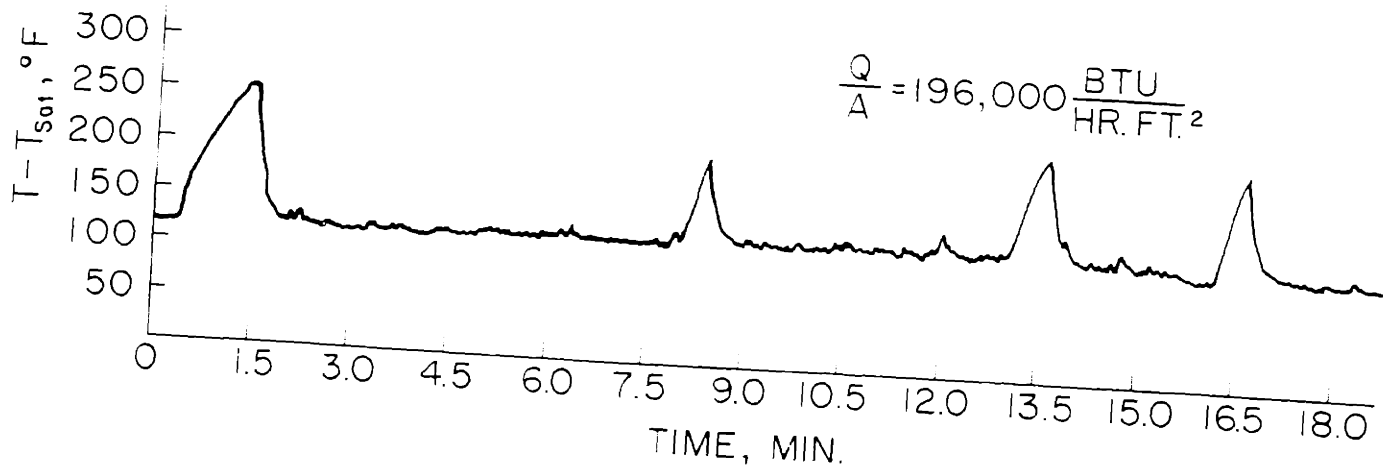


FIG. 31 TEMPERATURE TRACE OF THERMOCOUPLE NO. 4 FOR STAINLESS STEEL 316, LAP A SURFACE

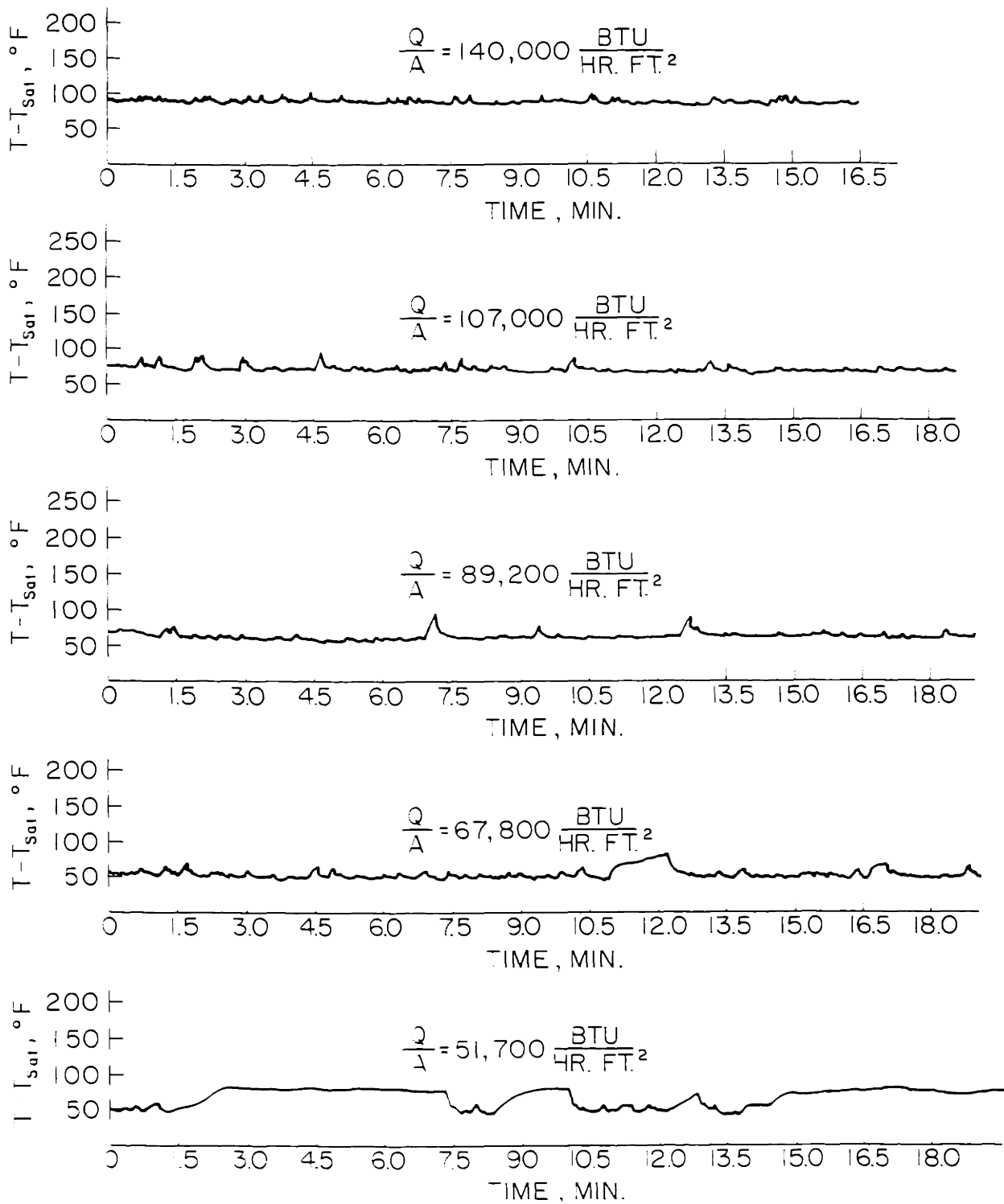


FIG. 32 TEMPERATURE TRACE OF THERMOCOUPLE NO. 6
 FOR "A" NICKEL, MIRROR SURFACE WITH ARTIFICIAL
 POROUS WELDS.

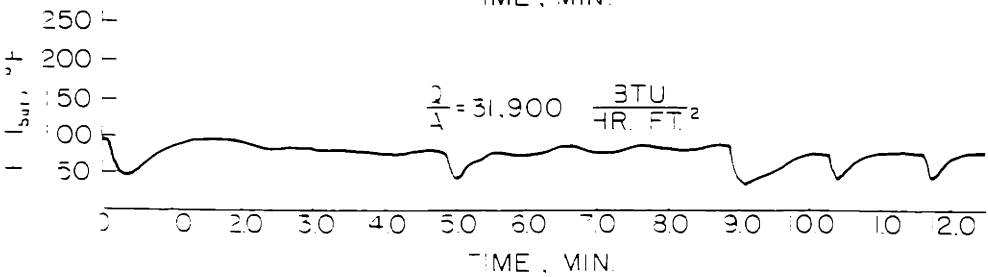
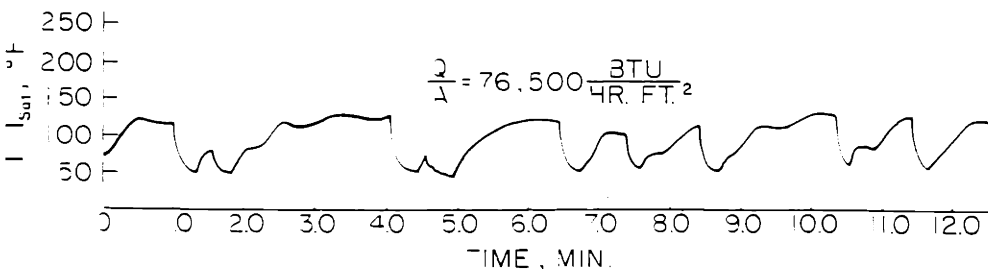
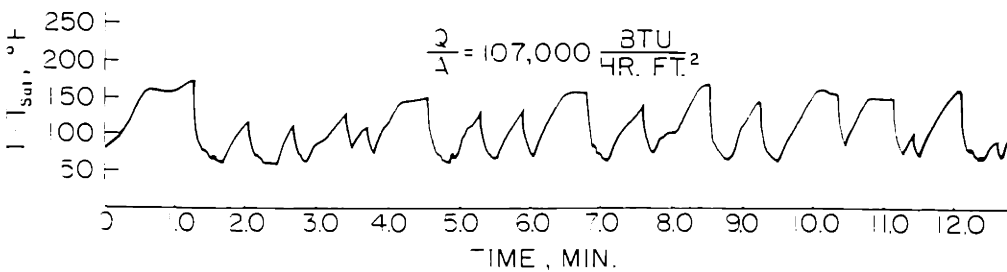
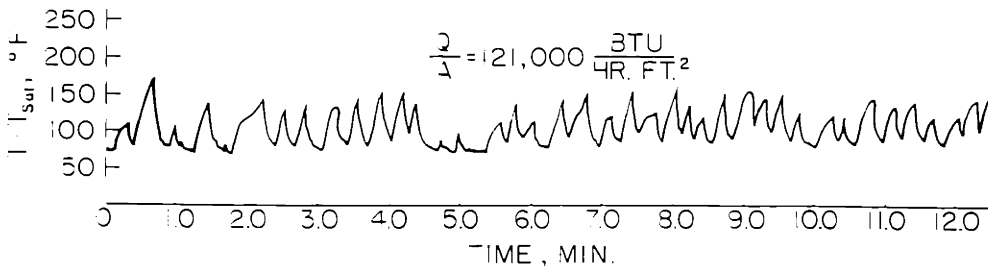
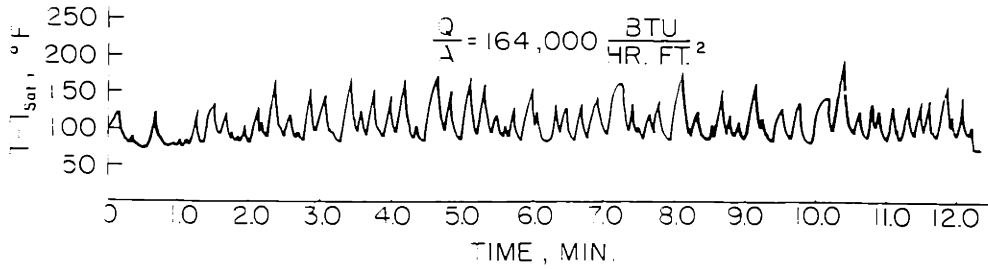
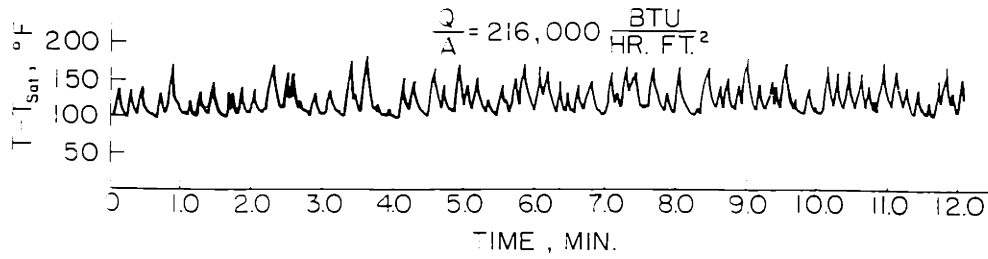


FIG. 33 TEMPERATURE TRACE OF THERMOCOUPLE NO 6 FOR "A" NICKEL, MIRROR SURFACE WITH NO INTERNAL WELDS

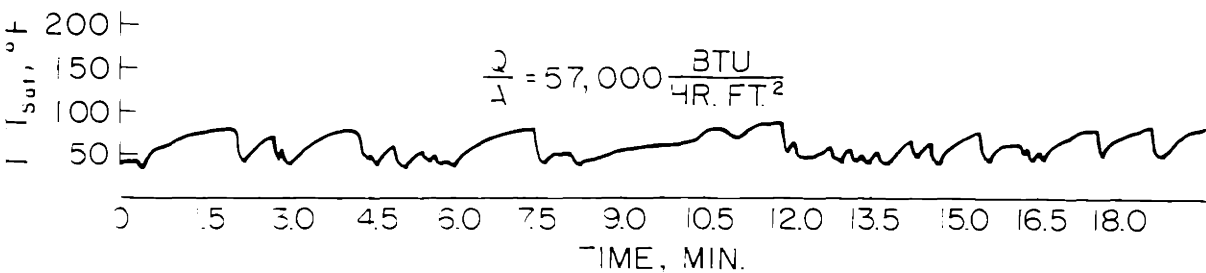
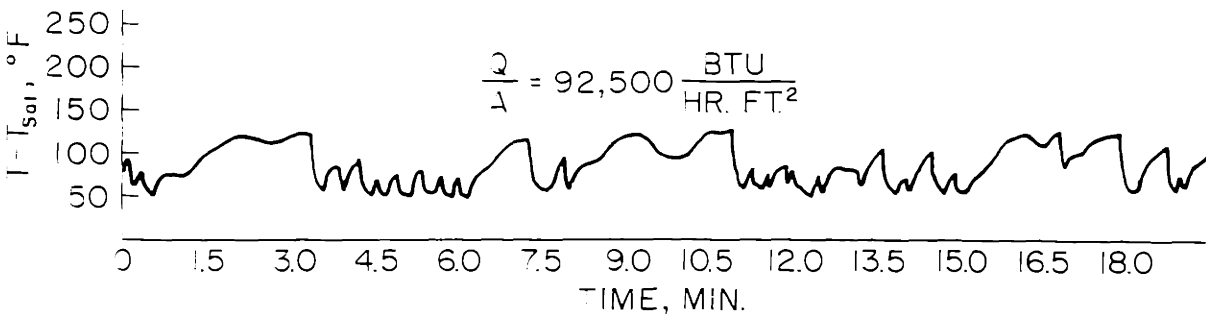
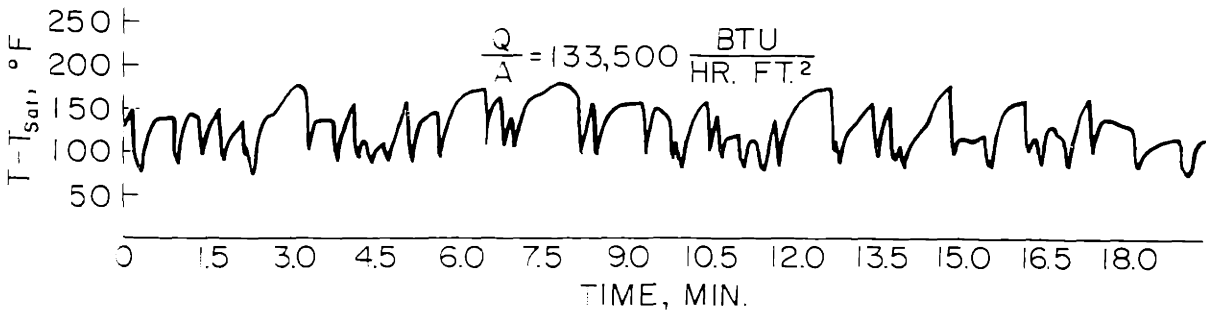
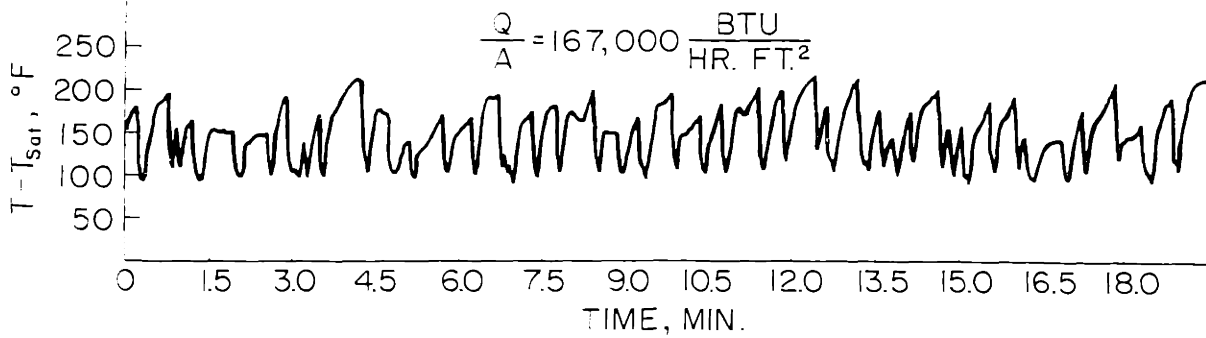


FIG. 34 TEMPERATURE TRACE OF THERMOCOUPLE NO. 6 FOR
 "A" NICKEL, MIRROR SURFACE WITH NO INTERNAL
 WELDS. PLUS TEN ARTIFICIAL CYLINDRICAL CAVITIES.

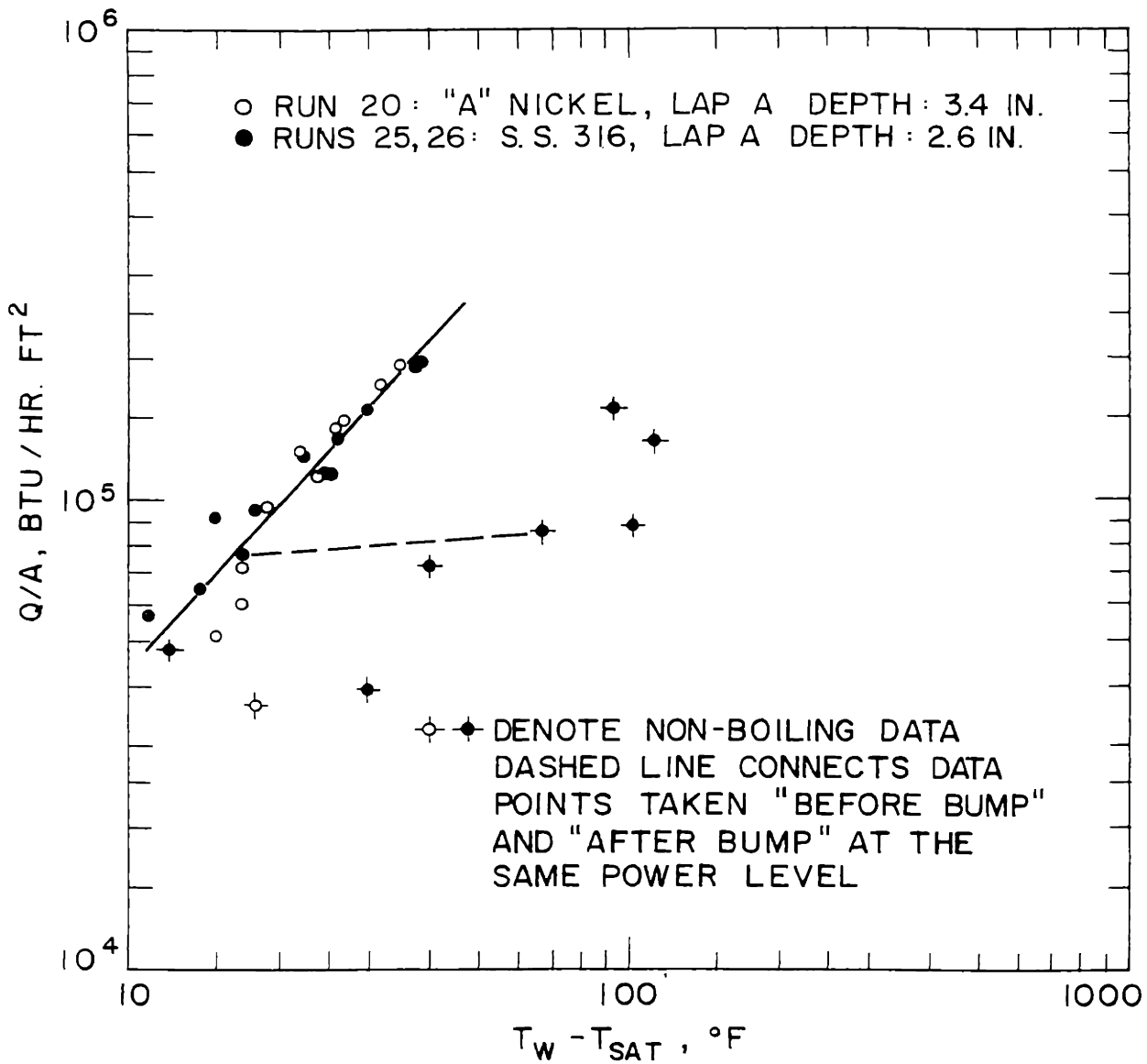


FIG. 35 EFFECT OF MATERIAL ON NUCLEATE BOILING STABILITY OF SODIUM

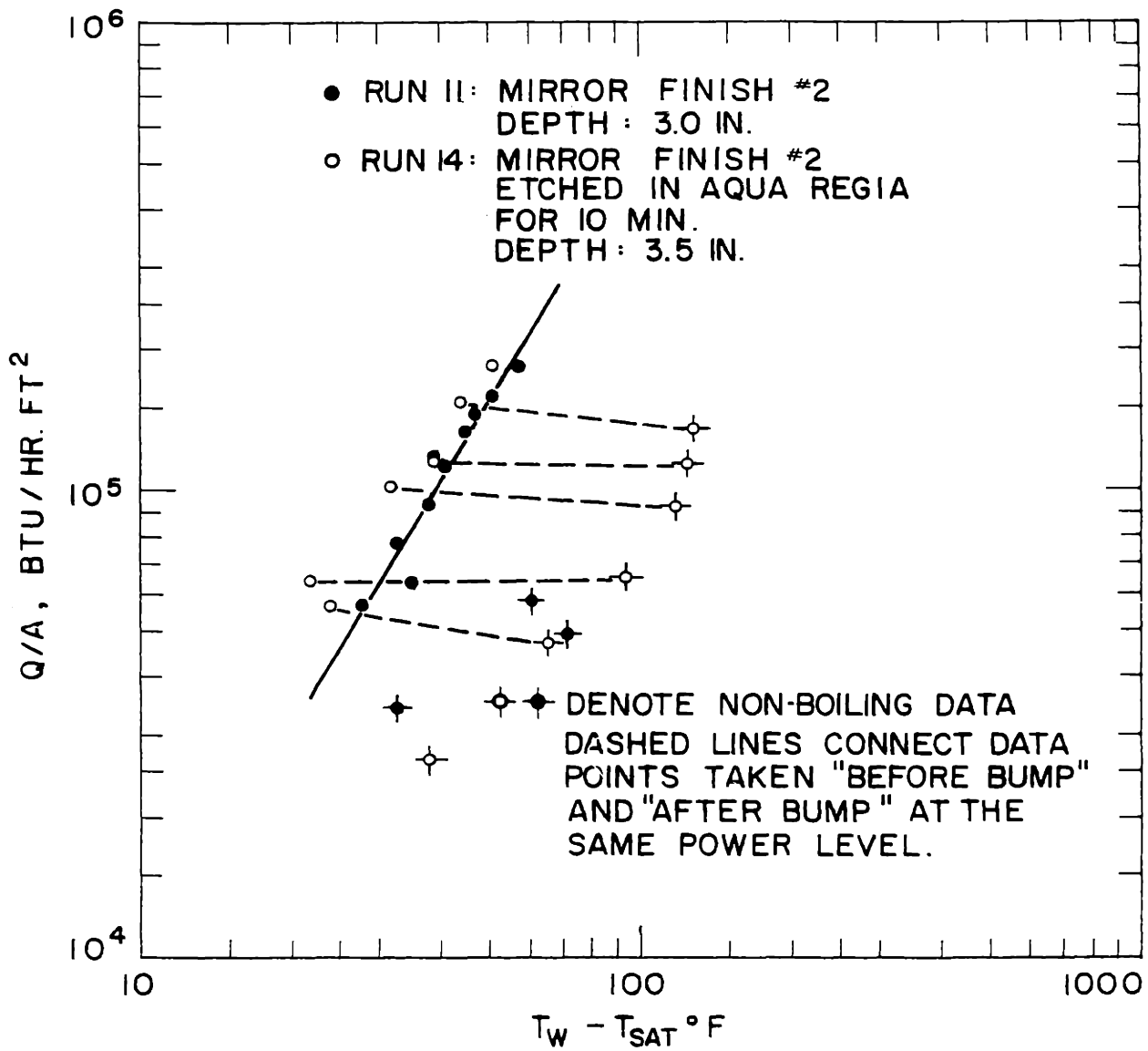


FIG. 36 EFFECT OF CHEMICAL TREATMENT ON NUCLEATE BOILING STABILITY OF SODIUM

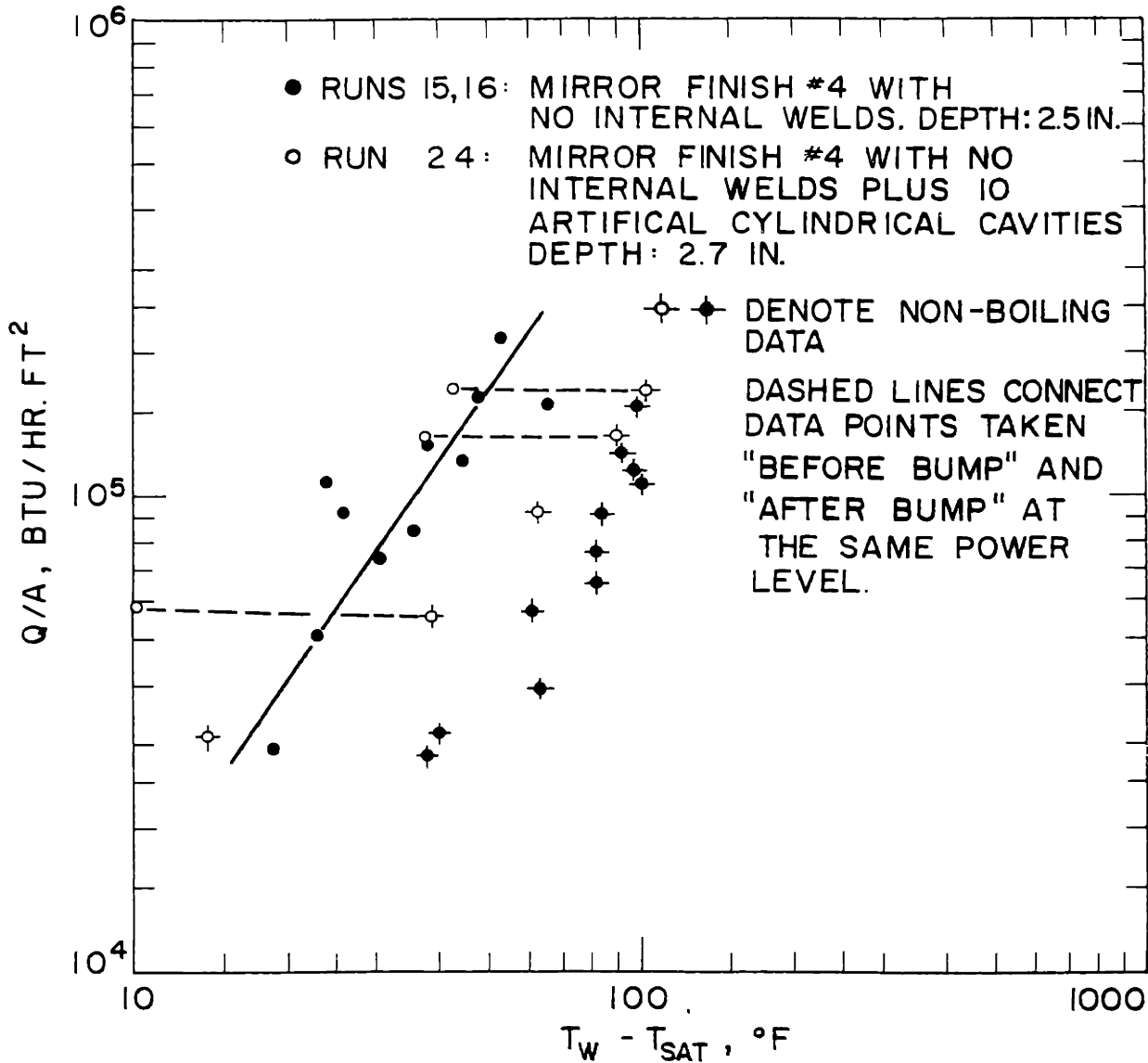


FIG. 37 EFFECT OF ARTIFICIAL CYLINDRICAL CAVITIES, .004 IN. DIAMETER, ON NUCLEATE BOILING STABILITY OF SODIUM

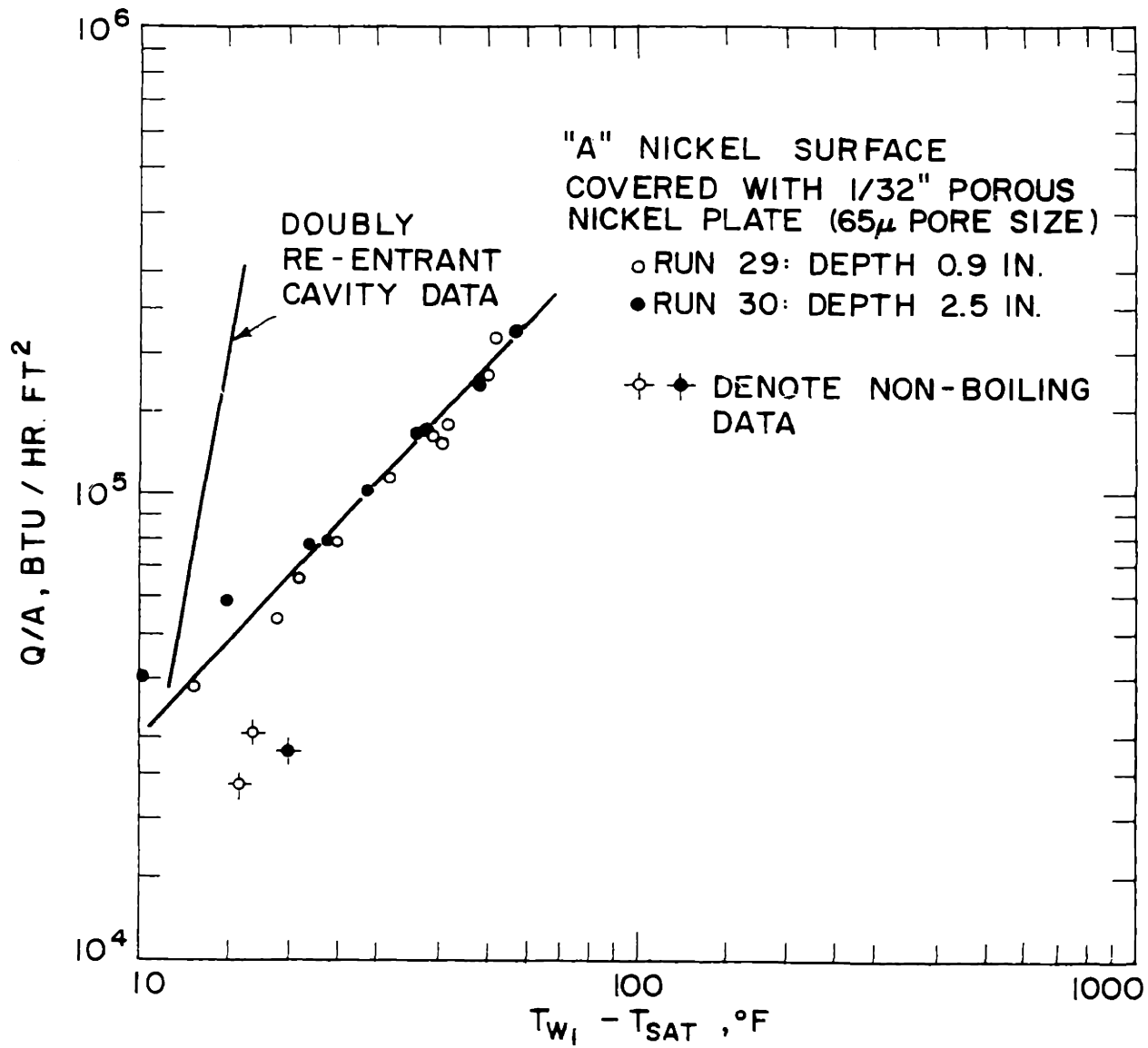


FIG. 38 EFFECT OF POROUS COATING ON NUCLEATE BOILING
 STABILITY OF SODIUM

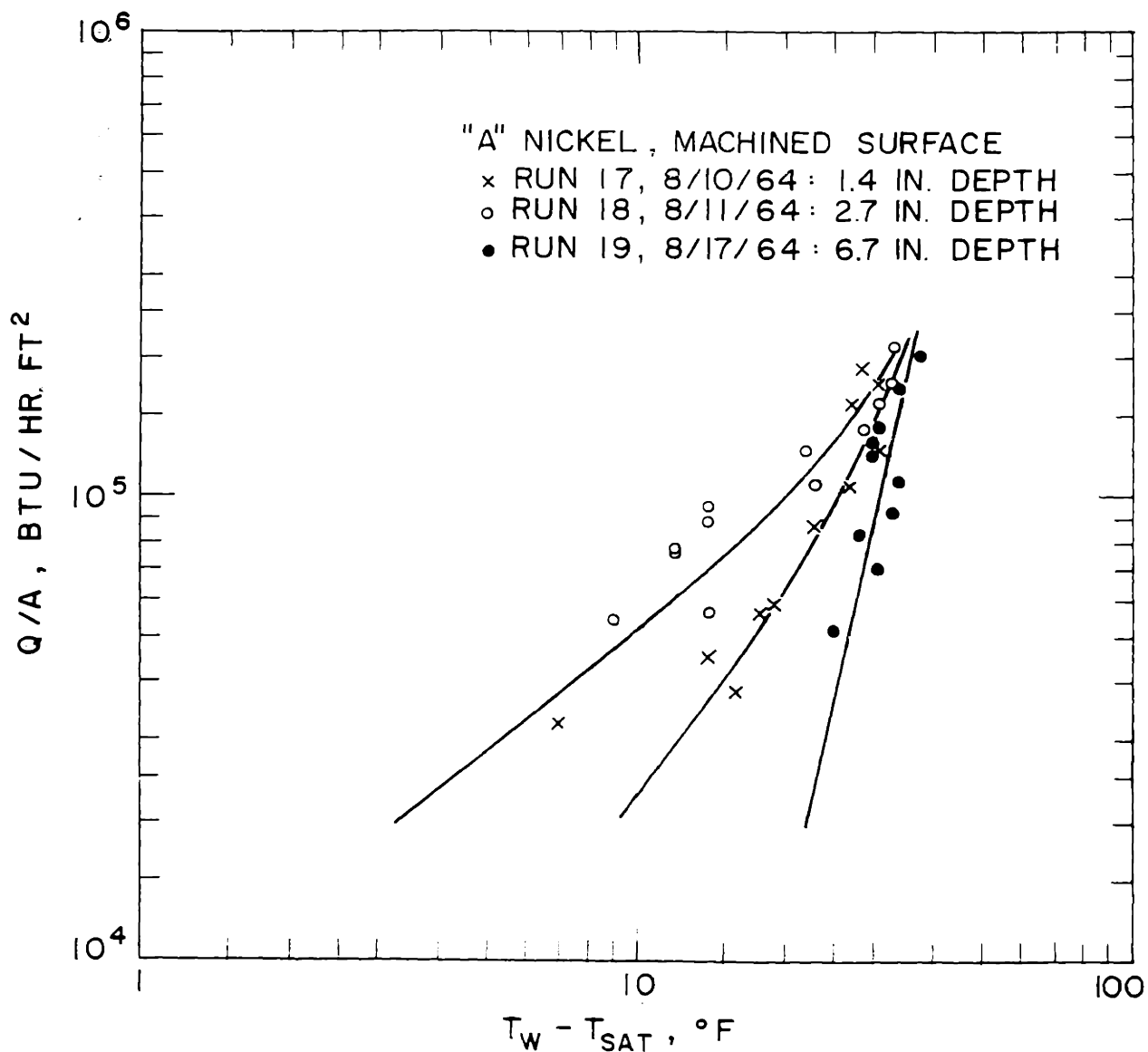


FIG. 39 EFFECT OF POOL DEPTH ON THE NUCLEATE BOILING CURVE OF SODIUM

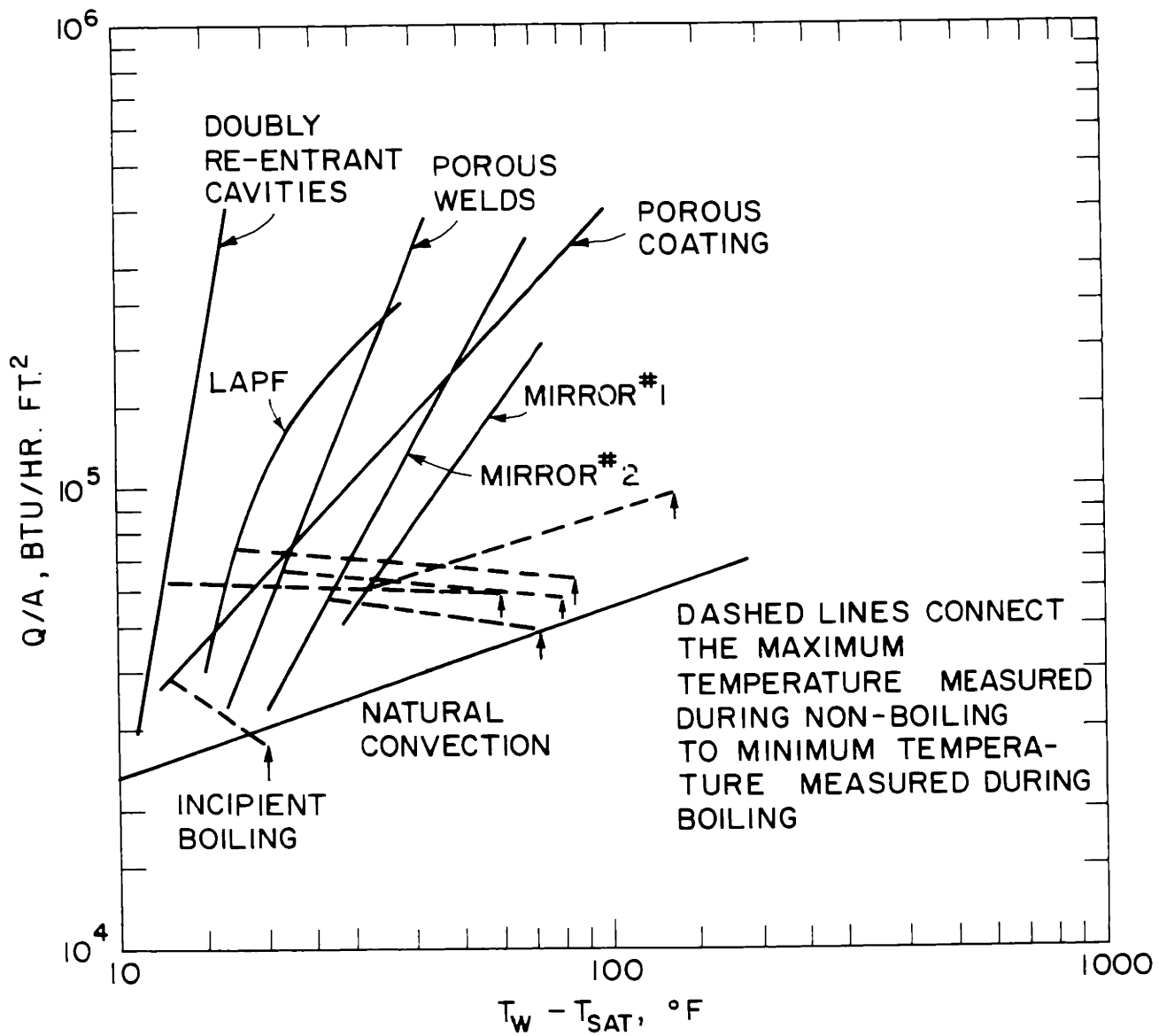


FIG. 40 COMPREHENSIVE PLOT OF SODIUM HEAT TRANSFER DATA AT AN AVERAGE PRESSURE OF 65 MM HG

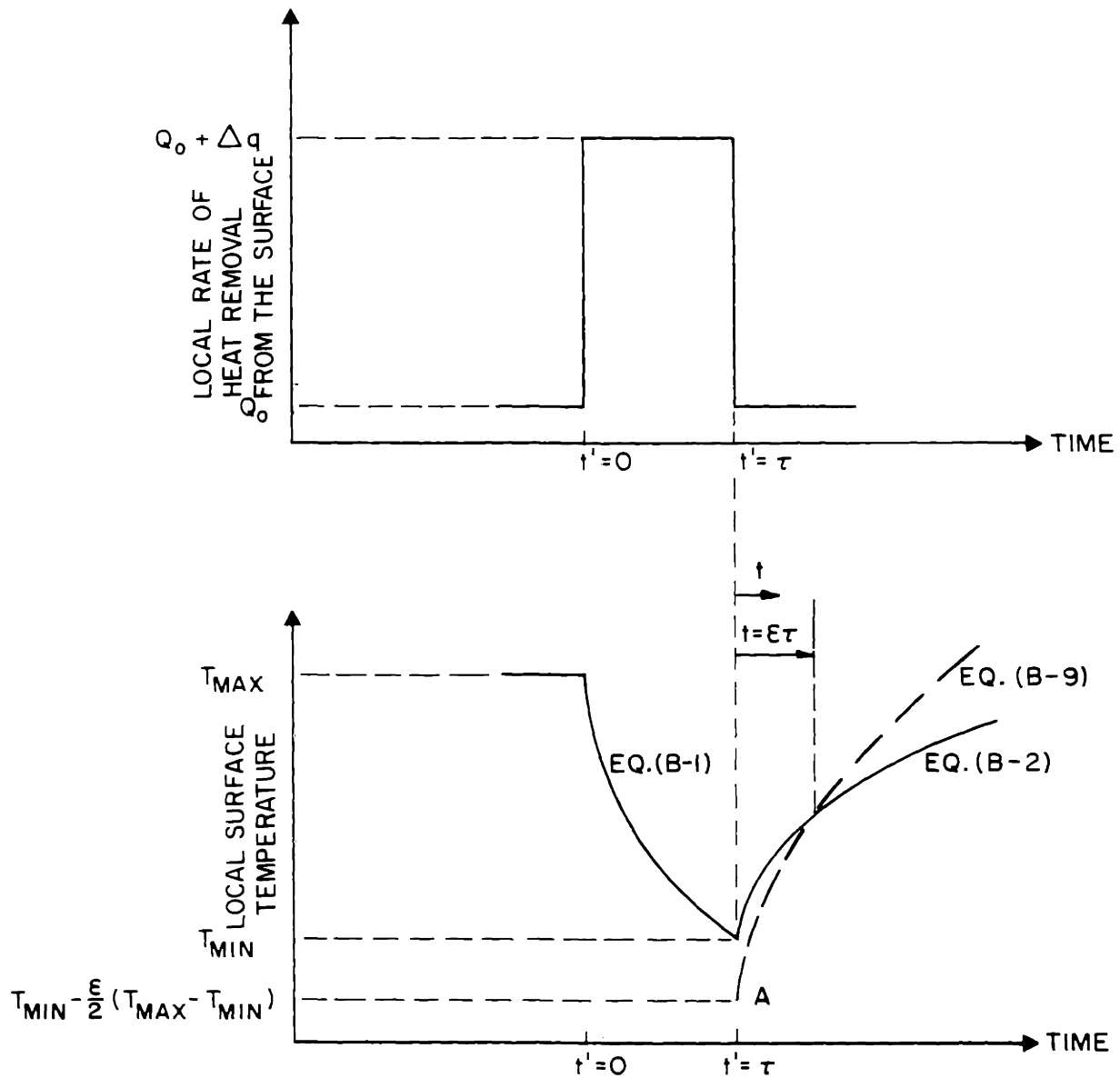


FIG. 41 SCHEMATIC REPRESENTATION OF THE LOCAL SURFACE HEAT FLUX AND LOCAL SURFACE TEMPERATURE DURING BUBBLE GROWTH FROM A CAVITY.

BIOGRAPHICAL NOTE

The author was born in Little Neck, Long Island, New York on August 15, 1938. He attended a nearby parochial school, St. Anastasia, and attended high school in New York City at St. Francis Xavier where he was graduated in 1956.

His undergraduate studies were performed at the University of Notre Dame, and he was graduated magna cum laude in June, 1960, receiving a B.S. degree in Engineering Science. He was then commissioned an ensign in the U.S. Naval Reserve.

The author was released from active duty with the Navy to attend graduate school at M.I.T. in the Nuclear Engineering Department. He received an S.M. degree in February, 1962, writing a thesis entitled "Heat transfer to a fluid flowing turbulently in a smooth pipe with walls at constant temperature" for Professor Warren M. Rohsenow.

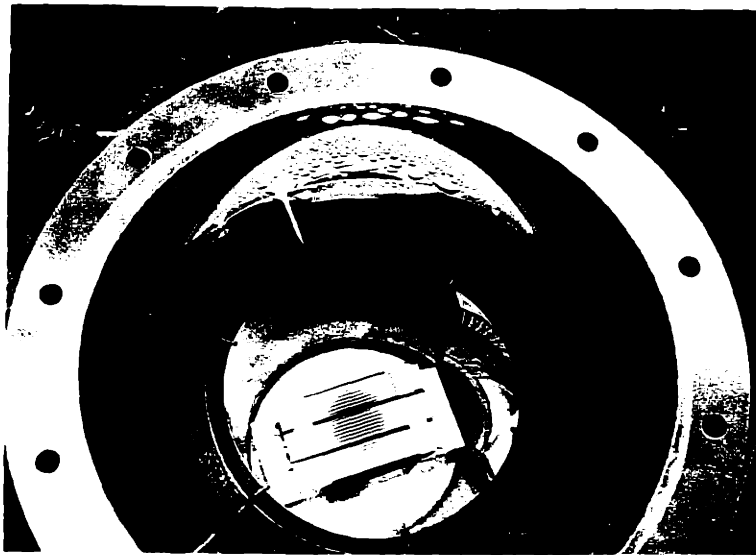
The author was employed for two summers by Gibbs and Cox, Inc. in 1958 and 1959, and for one summer by Brookhaven National Laboratory in 1960. He received an A.E.C. Special Fellowship in 1960-1961, 1961-1962 and 1962-1963, and he received a General Electric Foundation Fellowship in 1963-1964.

He married the former Mary Virginia Indence on June 10, 1961, and they have a daughter, Terese Vaughn, and a son, Paul James, Jr.

The author is a member of Tau Beta Pi and Sigma Xi. He has been assigned as an instructor at the U.S. Naval Postgraduate School, Monterey, California, beginning February, 1965.



VIEW OF BOILER FLANGE



OVERHEAD VIEW OF VACUUM CHAMBER

FIG. 42. PHOTOGRAPHS SHOWING SODIUM LEAKAGE

FILM

REWIND

R

LEAKAGE